LEIBNIZ-INSTITUT FÜR ATMOSPHÄREN PHYSIK IAP

Habilitationsschrift

am Leibniz-Institut für Atmosphärenphysik in Kühlungsborn

On the physics of polar mesosphere summer echoes

von
Markus Rapp

Abstract: Polar mesosphere summer echoes (PMSE) are very strong radar echoes primarily observed in the VHF wavelength range from altitudes close to the polar summer mesopause. Radar waves are scattered at irregularities in the radar refractive index which at mesopause altitudes is solely determined by the electron number density. For efficient scatter, the electron number density must reveal structures at the radar half wavelength (Bragg condition; ∼3 m for typical VHF radars). The question how such small scale electron number density structures are created in the mesopause region has been a longstanding open scientific question for almost ∼30 years. The current work reviews experimental and theoretical milestones on the way to an advanced understanding of PMSE. Based on new experimental results from in situ observations with sounding rockets, ground based observations with radars and lidars, numerical simulations with a microphysical model of the life cycle of mesospheric aerosol particles, and theoretical considerations regarding the diffusivity of electrons in the ice loaded complex plasma of the mesopause region, the first consistent explanation for the generation of these radar echoes is formulated. The main idea is that mesospheric neutral air turbulence in combination with a significantly reduced electron diffusivity due to the presence of heavy charged ice aerosol particles (radii ∼5-50 nm) that form in the very cold environment of the polar summer mesopause region lead to the creation of structures at spatial scales significantly smaller than the inner scale of the turbulent velocity field itself. Importantly, owing to their very low diffusivity, the plasma structures acquire a very long lifetime, i.e., 10 min to hours in the presence of particles with radii between 10 and 50 nm. This leads to a temporal decoupling of active neutral air turbulence and the existence of small scale plasma structures and PMSE and thus readily explains observations proving the absence of neutral air turbulence at PMSE altitudes. With this explanation at hand, it is shown that PMSE are a suitable tool to permanently monitor the thermal and dynamical structure of the mesopause region allowing insights into important atmospheric key parameters like temperatures, winds, gravity wave parameters, turbulence, solar cycle effects, and long term changes.

Postal address:
Schloss-Str. 6
18225 Kühlungsborn
Germany

IAP Kühlungsborn
Mai 2004
IAP Nr. 08/2004
ISSN 1615-8083

On the physics of polar mesosphere summer echoes

Habilitationsschrift
zur
Erlangung des akademischen Grades
doctor rerum naturalium habilitatus / habilitata (Dr. rer. nat. habil.)
der Mathematisch-Naturwissenschaftlichen Fakultät
der Universität Rostock

vorgelegt von
Markus Rapp, geb. am 12. Mai 1970 in Koblenz
aus Kühlungsborn

Kühlungsborn, 03. November 2003

Gutachter:

Prof. Dr. Franz-Josef Lübken
Leibniz-Institut für Atmosphärenphysik, Kühlungsborn, Deutschland

Prof. Dr. Martin Friedrich
Institut für Kommunikationsnetze und Satellitenkommunikation, Technische Universität Graz, Österreich

Prof. Dr. John D. Mitchell
Department of Electrical Engineering, Pennsylvania State University, USA

Probevorlesung:

3. Mai 2004

Contents

1 Introduction

The polar mesosphere in summer is host to a number of fascinating geophysical phenomena that are primarily caused by its extreme thermal structure. Owing to the gravity wave driven mean meridional circulation with upwelling and adiabatically expanding air masses above the summer pole, mean minimum temperatures of ∼130 K are reached at the mesopause at around 88 km [e.g., *Becker and Schmitz*, 2002; *Lübken*, 1999]. These extremely low temperatures marginally allow ice particles to form and grow at altitudes between ∼80 and 90 km, hence forming ice clouds being ∼65 km higher than ordinary clouds in the troposphere where our day to day weather takes place. Under favorite conditions the largest of these ice particles (with radii larger than ∼30 nm) can even be visually observed in the form of noctilucent clouds (=NLC) which have been discovered as early as 1883 [*Leslie*, 1885; *Jesse*, 1885]. Almost 100 years later it was then found that also the smaller ice particles that have not yet grown to a large enough size to be visually observed lead to measurable signatures in the form of strong radar echoes, nowadays known as polar mesosphere summer echoes or PMSE [*Czechowsky et al.*, 1979; *Ecklund and Balsley*, 1981; *Röttger et al.*, 1988; *Hoppe et al.*, 1988].

In recent years, these high atmospheric ice clouds have reached a considerable scientific interest since it was suspected that the mesopause environment should change due to anthropogenic activity. For example, models showed that the increase of atmospheric carbon dioxide concentrations should lead to a temperature decrease in the mesopause region [*Roble and Dickinson*, 1989] and it was also argued that increasing atmospheric concentrations of methane should lead to enhanced water vapor at mesopause altitudes [*Thomas et al.*, 1989]. For recent reviews of trends in the middle atmosphere see *Ramaswamy et al.* [2001] and *Beig et al.* [2003]. Since ice particles around the mesopause are sensitive to both temperature and water vapor, it was suspected that properties like their brightness should change [*Thomas et al.*, 1989]. *Thomas* [1996] even went as far as to promote these changes as a suitable tool to identify climate changes in the polar mesosphere earlier than in the much more complex troposphere.

At the current stage the discussion if we already observe long term changes of mesospheric ice particle properties is controversial [*von Zahn*, 2003; *Thomas et al.*, 2003]. However, it is evident that for a scientifically based judgement about these issues we require a detailed and rigorous understanding of the physical processes involved. While the basic physics of noctilucent clouds has been quite well understood [e.g., *Thomas*, 1991; *Gadsden and Schröder*, 1989], the understanding of polar mesosphere summer echoes has bothered the scientific community until only recently [*Cho and Röttger*, 1997; *Rapp and Lübken*, 2003a; *Rapp et al.*, 2003b].

The current manuscript summarizes 12 of the candidate's publications that have led to the first consistent description of the physics of PMSE (see appendix A and B for a list and copies of these papers). This summary starts with a section describing the most important observational characteristics of PMSE and our theoretical understanding prior to this work. Then, we discuss supporting and contradicting evidence for and against the so far 'standard'-theory by *Cho et al.* [1992] in the scope of our own and other new experimental and theoretical contributions and show that it has to be revised (papers 2, 3, 4, 5, 6, 10, 11). Subsequently, we describe our new physical understanding both including model simulations leading to an empirical formula for PMSE signal strength (papers 1, 4, 12) as well as the new rigorous theoretical treatment of electron diffusion in the vicinity of charged aerosol particles (paper 7). Together, these results lead to the conclusion that neutral air turbulence in combination with

the details of turbulent electron-advection in the complex ice-loaded plasma environment of the mesopause region are identified as the main physical processes underlying PMSE (papers 7, 8). Subsequently, some predictions of the new theory are tested based on available high resolution plasma measurements obtained during a sounding rocket flight and the new theory is applied to explain observed layering characteristics of the radar echoes (papers 9, 12). Finally, we close with a summary and discussion of remaining open physical questions that should be addressed in future investigations.

2 PMSE: Experimental facts and first theoretical approaches

At the end of the 1970s, VHF radars operating at frequencies of $\sim$ 50 MHz discovered very strong radar echoes from around the summer mesopause region at altitudes between $\sim$80 and 90 km [*Czechowsky et al.*, 1979; *Ecklund and Balsley*, 1981]. The first long term data set covering observations at Poker Flat, Alaska (65° N) between February 1979 and December 1980 was presented by *Ecklund and Balsley* [1981] revealing a strong seasonal variation of both the observed echo power and the altitude range where the echoes were observed. Figure 1 shows the time averaged altitude profiles of signal to noise ratio (SNR) for typical summer and winter periods taken from this study. Evidently, during the summer months the average

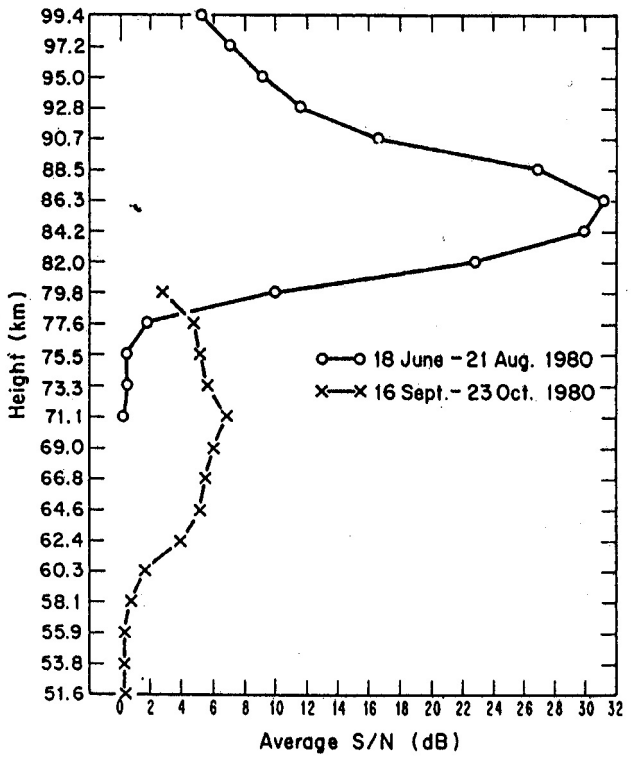

Figure 1: Time averaged profiles of signal to noise ratio (in decibels) for typical summer and winter periods. This Figure is reproduced from *Ecklund and Balsley* [1981], copyright by the American Geophysical Union.

signal peak is located considerably higher (i.e., at $\sim$86 km) than during winter time, where only weak echoes (average SNR ratios $\sim$ 5 dB) are received from altitudes below $\sim$ 75 km. During summer time, however, the echoes are extremely strong reaching an average maximum SNR of $\sim$30 dB. Due to their predominant appearance in the polar regions these strong echoes

are commonly called polar mesosphere summer echoes or PMSE [*Röttger et al.*, 1988; *Hoppe et al.*, 1988].
Radar waves are scattered by irregularities in the refractive index which at altitudes around 85 km is solely determined by the electron number density. In general, one distinguishes between incoherent scatter (or Thompson scatter) which is due to the thermal random motion of the electrons and coherent scatter, i.e., the scatter at ordered structures in the electron density distribution. Coherent scatter only occurs when the refractive index irregularity spectrum possesses significant spectral power at scales around the radar half wavelength (=Bragg condition) which is 3 m for a 50 MHz radar [*Tatarskii*, 1971]. The irregularities leading to the weak radar backscatter outside the polar summer season at altitudes below say ∼75 km have been traced back to neutral air turbulence [*Woodman and Guillen*, 1974; *Balsley et al.*, 1983; *Røyrvik and Smith*, 1984] which in turn is generated by breaking gravity waves propagating upwards from the troposphere (note though that recent experimental evidence of so called 'polar mesosphere winter echoes' indicates that at least some of these echoes at lower altitudes may not be understandable in the scope of pure turbulent activity [*Kirkwood et al.*, 2002, 2003]). However, early efforts to explain the significantly stronger echoes from the summer polar mesopause region by neutral air turbulence led to a paradox that was already identified in the early work on the subject [*Balsley et al.*, 1983]: in order to satisfy the Bragg criterium the radar half wavelength must be located in the inertial subrange of the turbulent power spectrum since for smaller scales, i.e., in the viscous subrange, irregularities are quickly dissipated due to molecular diffusion [e.g., *Heisenberg*, 1948]. A minimum necessary turbulent energy dissipation rate ϵ can be easily estimated by equating the inner scale $l_0^H = 9.9 \cdot (\nu^3/\epsilon)^{\frac{1}{4}}$ (=the transition scale between the inertial and the viscous subrange; see also *Lübken et al.* [1993a]) and the radar Bragg scale. Using a typical kinematic viscosity ν for an altitude of 85 km of 1 m^2/s, this estimate yields $\epsilon \approx$100 W/kg equivalent to a heating rate of dT/dt =86400 K/d. This heating rate is three orders of magnitude larger than all other relevant heating and cooling rates at the same altitudes and is clearly unrealistic [e.g., *Mlynczak*, 2000; *Lübken*, 1997].
Ever since the initial observations, it has hence been a major goal of both experimental and theoretical investigations on PMSE to resolve this paradox and identify the physical processes responsible for the creation of structures in the electron number density where under normal conditions they should not exist. In this section, we present an overview of the milestones regarding the available observational and theoretical work on PMSE forming the background of our current knowledge. Note that given the wealth particular of experimental investigations we are aware of the fact that the results presented can only be a selection of some of the relevant work in the field. For further reading we also refer to the previous review articles by *Cho and Kelley* [1993] and *Cho and Röttger* [1997].

2.1 Overview: Experimental facts

2.1.1 Climatology

Seasonal variation
As already evident from the pioneer work by *Ecklund and Balsley* [1981], PMSE reveal a pronounced seasonal variation. Figure 2 shows the seasonal variation of the occurrence rate of PMSE as observed with the 53 MHz ALWIN radar (ALWIN=ALOMAR Wind radar) on the North-Norwegian island Andøya (69.3°N, 16.0°E) during the years 1999, 2000, and 2001 [*Bremer et al.*, 2003; *Latteck et al.*, 1999a]. The main characteristics are the steep increase during end of May/beginning of June, a rather high level near 90 % in the middle of June until the middle/end of July, and a more gradual decrease during August. The observations

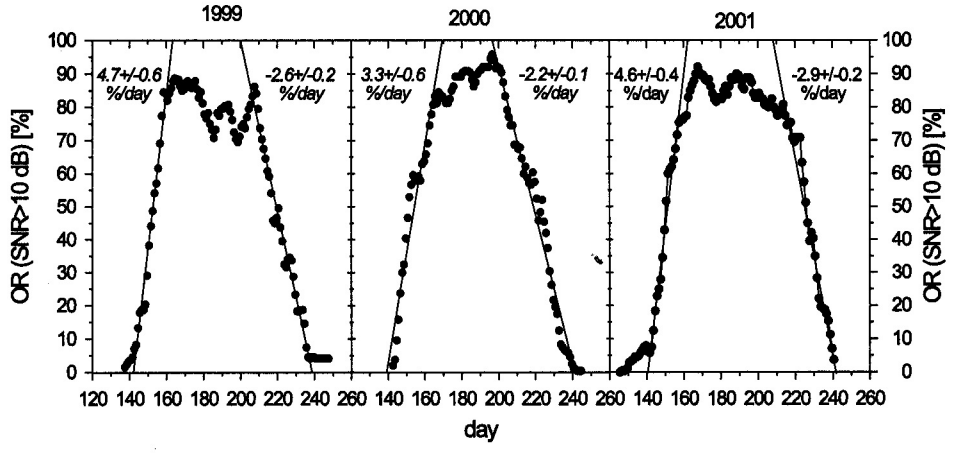

Figure 2: Seasonal variation of the occurrence rate of PMSE with a SNR ratio larger than 10 dB after observations with the ALWIN radar on the North-Norwegian island Andøya during the years 1999, 2000, and 2001. This Figure is reproduced from *Bremer et al.* [2003], copyright by the American Geophysical Union.

shown in Figure 2 are in general agreement with independent observations from different radars located at about the same geographical latitude [e.g., *Balsley and Huaman*, 1997; *Kirkwood et al.*, 1998]. Intrigued by the fact that the seasonal variation of the NLC occurrence rate is very similar [*Gadsden*, 1998], several authors have tried to relate the occurrence of PMSE to the occurrence of ice particles that may form in the period from end of May until the end of August because of the very low temperatures of the mesopause region [e.g., *Lübken*, 1999]. Figure 3 shows a comparison of the NLC- and PMSE-occurrence rate as a function of season and the time and altitude range during which the degree of water ice saturation S is larger than 1 [*Lübken*, 1999]. S is the ratio between the actual water vapor partial pressure and the saturation vapor pressure over ice which *Lübken* [1999] derived from a climatology of temperatures and air densities obtained with the falling sphere technique and water vapor mixing ratios from model simulations [*Garcia and Solomon*, 1994]. The saturation water vapor pressure over ice was derived from the empirical formula of *Marti and Mauersberger* [1993]. It is evident from this comparison that PMSE occur in exactly the height and time interval where ice particles can exist in the mesopause region and confirms earlier considerations that ice particles may play a decisive role in the creation of the radar echoes [*Cho and Kelley*, 1993; *Cho and Röttger*, 1997]. Note that since the work of *Lübken* [1999] better data on both water vapor in the mesopause region and an updated empirical formula for the saturation vapor pressure have become available [*Seele and Hartogh*, 1999; *Körner and Sonnemann*, 2001; *McHugh et al.*, 2003; *Mauersberger and Krankowsky*, 2003]. However, including this new information does not change the general conclusion that the PMSE- and ice particle- existence period and altitude region are identical.

Latitudinal variation

Apart from the aforementioned measurements at ~65-69°N, PMSE have also been observed as far North as 75°N and 78°N [*Huaman et al.*, 2001; *Rüster et al.*, 2001] and as far South as 52-54°N where the echoes are then consequently called 'mesosphere summer echoes' or MSE [*Czechowsky et al.*, 1979; *Reid et al.*, 1989; *Thomas et al.*, 1992; *Latteck et al.*, 1999b; *Zecha et al.*, 2003]. While a lot of general features like the typical echo strengths and the

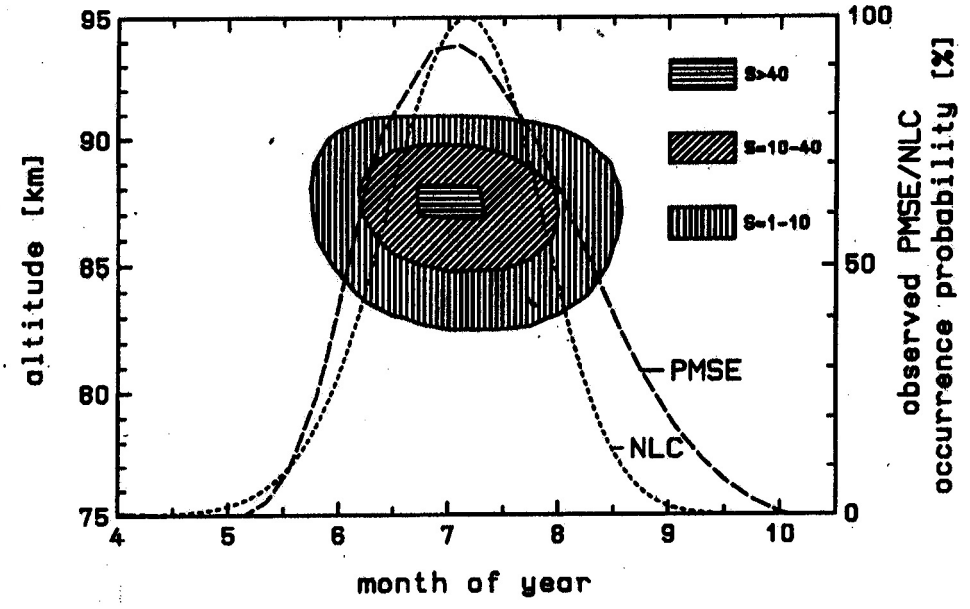

Figure 3: Contour plot of the degree of saturation S as a function of season and altitude (shaded areas) derived from a falling sphere temperature and density climatology and model water vapor mixing ratios from *Garcia and Solomon* [1994]. In addition, relative occurrence probabilities are shown (normalized to 100% at the maximum) for PMSE (dashed line) and NLC (dotted line). This Figure is reproduced from *Lübken* [1999], copyright by the American Geophysical Union.

altitude region of occurrence are independent of the geographic latitude, it has been found that the occurrence rate shows a pronounced gradient with latitude (all values for July, 1): the occurrence rate drops from almost 100 % at 78°N [*Lübken et al.*, 2003], ~90 % at 69°N [*Bremer et al.*, 2003], to only ~10-20 % at 54°N [*Zecha et al.*, 2003]. This general picture is in line with recent 3d-model results of the thermal and dynamical structure of the mesosphere suggesting colder temperatures closer to the pole and hence a more favorable environment for the formation of ice particles [*von Zahn and Berger*, 2003]. This picture is only 'disturbed' by the observations at Resolut Bay (75°N) where low occurrence frequencies of less than ~50 % have been reported [*Huaman et al.*, 2001]. Note though that occurrence frequencies reported from different stations and radars must be considered with some caution since the radars are not identical in design and hence do not have the same absolute sensitivity. Unfortunately, absolutely calibrated volume reflectivities from these radars are only available for some selected case studies (see section 2.1.2).
PMSE have also been observed at Southern latitudes even though significantly less frequent than in the Northern hemisphere [*Balsley et al.*, 1993, 1995; *Woodman et al.*, 1999]. Possible hemispheric differences in the thermal and dynamical structure have been discussed [*Dowdy et al.*, 2001; *Becker and Schmitz*, 2003; *Siskind et al.*, 2003; *Chu et al.*, 2003], however, the experimental data base is scarce such that the reason for the observed hemispheric asymmetry remains to be identified [*Lübken et al.*, 1999].

Long term and short term variations
Recently, first results on long term changes of PMSE properties have been reported. *Bremer*

et al. [2003] considered mean PMSE occurrence frequencies for the years 1994 through 2001 and found a significant positive correlation with the solar Ly-α radiation (the Ly-α flux varies by about a factor of 2 during one 11-year solar cycle). The authors concluded that the observed variation is due to changes in the background ionization that is mainly controlled by the ionization of NO due to Ly-α. These arguments are in line with considerations by *Rapp et al.* [2002a] who argued that moderate changes of ionization should lead to a positive correlation with the PMSE signal strength.
On shorter time scales a variety of other physical processes altering PMSE properties have been identified. *Hoffmann et al.* [1999] reported a strong semidiurnal variation of both the SNR and the altitude where the maximum SNR was observed. This variation is in phase with similar semidiurnal variations in NLC properties (like centroid altitude and brightness) and has been traced back to the action of the semidiurnal tide with minor contributions from the diurnal variation of ionization [*von Zahn et al.*, 1998; *von Zahn and Bremer*, 1999; *Klostermeyer*, 1999a]. Other reasons for short term variability have been identified as solar and geomagnetic activity [*Bremer et al.*, 1996a, 2001] as well as dynamical phenomena like e.g. gravity waves that mainly move the PMSE layers up and down and lead to substantial vertical velocities in PMSE reaching values of $\sim \pm 5$ m/s [e.g., *Hoppe and Fritts*, 1994, 1995; *Rüster et al.*, 1996].

2.1.2 Properties of PMSE layers

Radar frequency dependence
One of the most striking properties of PMSE is the pronounced dependence of the absolute observed volume reflectivity (= the backscattering cross section per unit volume) on the radar frequency: since the first observations at 50 MHz, PMSE have been observed at a variety of frequencies between 2.78 MHz and 1.29 GHz. Table 1 gives an overview of different studies published to date together with some of the most important results, including reported absolute volume reflectivities: Even though the different measurements of volume reflectivities were not performed at the same location and time (and must hence be compared with a cautionary note in mind since the geopyhsical situation is certainly different), it is evident from Table 1 that the volume reflectivity shows a tremendous decrease with increasing frequency (or decreasing Bragg scale). For example, from 50 MHz to 500 MHz, the Bragg scale changes by only one order of magnitude, i.e., from 3 m to 30 cm, but the corresponding reflectivities change by as much as 6 orders of magnitude. This frequency dependence certainly poses severe constraints on any physical explanation of PMSE - we will come back to this issue when we discuss possible physical explanations (see section 3.1).

Spectral width
Further information on the physical mechanism responsible for the creation of the electron irregularities leading to PMSE is obtained from the Doppler-broadened spectra of the received signals. As explained in detail for example in *Hocking* [1989], the Doppler spectral width yields information on the velocity variance of the detected scatterers in the radial direction (=the pointing direction of the radar beam). The highest precision data on PMSE spectral widths obtained so far have been measured with the EISCAT VHF radar operating at 224 MHz [*Röttger et al.*, 1988]. This radar possesses the advantage of a narrow beam (i.e., only 2 km horizontal extent at $\sim$85 km) such that the spectra are not significantly affected by effects like beam- or shear-broadening [*Hocking*, 1989]. Figure 4 shows a comparison of the spectra of incoherent signals from the ionosphere (left panel) and coherent signals from a PMSE (right panel) after *Röttger and LaHoz* [1990]. Figure 4 shows several interesting

Frequency (Bragg scale) [MHz (m)]	Location	Reference	Reflectivity $[m^{-1}]$
2.78 (53.9)	Tromsø, (69°N)	*Bremer et al.* [1996b]	
8-9 (18.8)	Vasil'surk, Russia (56°N)	*Karashtin et al.* [1997]	
3.3, 4.9, 7.6	Gakona, Alaska, (62°N)	*Kelley et al.* [2002]	
49.6 (3.0)	Tromsø, (69°N)	*Röttger et al.* [1990]	$2.0 \cdot 10^{-12}$
50.0 (3.0)	Poker Flat (65°N)	*Ecklund and Balsley* [1981]	
		Kelley and Ulwick [1988]	$9.0 \cdot 10^{-15}$
51.5 (2.9)	Resolut Bay (75°N)	*Huaman et al.* [2001]	
53.5 (2.8)	Andøya, (69°N)	*Inhester et al.* [1990]	$4.0 \cdot 10^{-12}$
53.5 (2.8)	Svalbard, (78°N)	*Röttger* [2001]	$2.2 \cdot 10^{-14}$
224 (0.67)	Tromsø, (69°N)	*Hoppe et al.* [1988]	$1.5 \cdot 10^{-16}$
		Röttger et al. [1988]	
		Hocking and Röttger [1997]	$1.3 \cdot 10^{-15}$
500 (0.3)	Svalbard, (78°N)	*Röttger* [2001]	$5.3 \cdot 10^{-19}$
933 (0.16)	Tromsø, (69°N)	*Röttger et al.* [1990]	$1.2 \cdot 10^{-18}$
1290 (0.12)	Sondrestrom, (67°N)	*Cho and Kelley* [1992]	

Table 1: PMSE studies at different frequencies

features: First of all, the comparison of the absolute spectral widths of incoherent and coherent spectra clearly demonstrates the completely different physics underlying the spectra: while the incoherent scatter spectra (being due to the Brownian motion of the electrons) show a typical width on the order of ∼100 Hz at 83.6 km, corresponding spectra from the coherent echoes are much narrower, i.e., the broadest spectra only yield widths of 10-15 Hz and can be as narrow as ∼1 Hz. Following *Hocking* [1985], *Röttger et al.* [1988] related these widths to turbulent rms-velocity fluctuations with corresponding values between 0.5-10 m/s. These very small rms-fluctuations underline the paradox already mentioned above: according to *Hocking* [1985] and *Gibson-Wilde et al.* [2000] the rms-velocity fluctuations w_{rms} may be converted to a turbulent energy dissipation rate by $\epsilon = 2 \cdot \omega_B \cdot w_{rms}^2$ where ω_B is the Brunt frequency. Using a typical value of $\omega_B = 10^{-2}$ 1/s we see that w_{rms}=0.5 m/s corresponds to $\epsilon = 5 \times 10^{-3}$ W/kg. On the other hand, to have the inner scale of turbulence equal to the Bragg scale (which is 67 cm in the case of the EISCAT 224 MHz radar), $\epsilon = 5 \times 10^4$ W/kg would be required. Hence, there is a discrepancy of seven orders of magnitude (!) between the required turbulent energy dissipation rate to explain the scatter as being due to pure neutral air turbulence and the value derived from the spectral width of the radar signal.
In addition, *Röttger and LaHoz* [1990] pointed out that also the spectral shape of the PMSE is significantly different from the usually Gaussian or Lorentzian shape of incoherent spectra. Rather, the PMSE spectra appear as a superposition of several narrow band spectra (Figure 4, spectra for July, 2, 1987) or as a single high amplitude spike superimposed on a weaker and wider spectral background (Figure 4, spectra for July, 9, 1987). *Röttger and LaHoz* hypothesized that these signatures were due to fairly small and localized refractive index

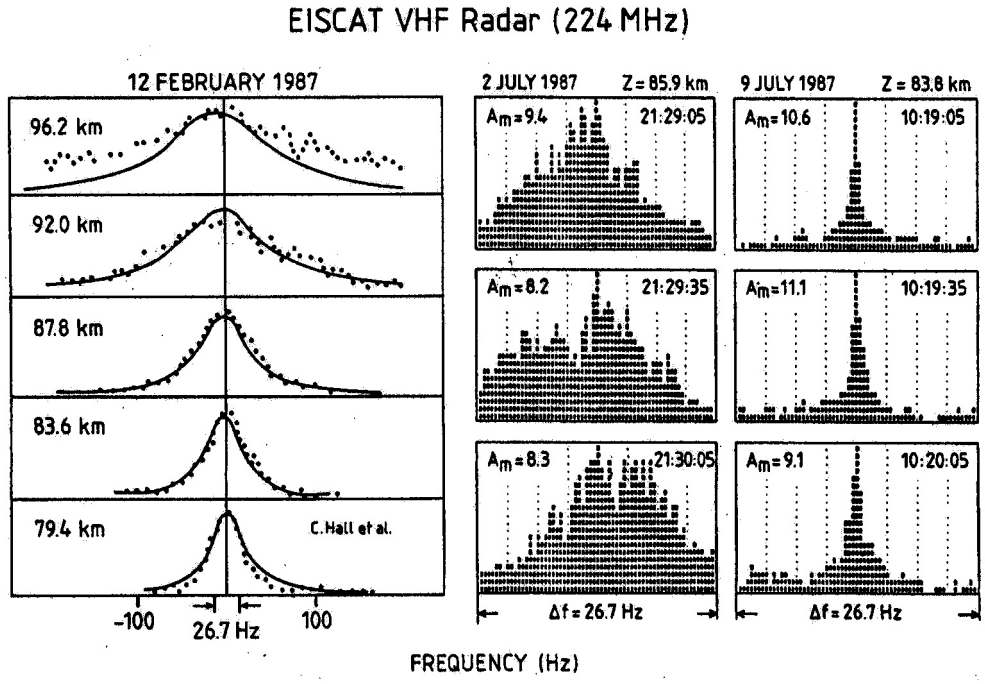

Figure 4: Spectra of incoherent scatter signals (left panel) and of coherent-scatter polar mesosphere summer echoes measured with the EISCAT 224 MHz radar in Tromsø. This Figure is reproduced from [*Röttger and LaHoz*, 1990].

structures coexisting within the radar beam (i.e, within a volume of 1 km in vertical and 2 km in horizontal extent) which move with different velocities. This would further imply that the structures causing PMSE are unlikely to be filling the scattering volume homogeneously.

Aspect sensitivity

A further property of the radar echoes that can potentially teach us a lot about the physics of the scattering process and the nature of the scatterers is the so called aspect sensitivity. The aspect sensitivity describes the radar signal dependence when the beam is tilted from the vertical direction. In general, a strong signal decrease with increasing beam tilting angle implies that the observed scatterers are specular (like in the case of Fresnel scatter), whereas no signal dependence on the tilting angle is usually identified with isotropically oriented scattering structures as they would be expected in the case of three-dimensionally isotropic turbulence.

Quantitatively, the aspect sensitivity is usually expressed as the half width, θ_S, of the angular polar diagram of the backscatter [*Hocking et al.*, 1986]. Hence, large values of θ_S imply a small aspect sensitivity and vice versa. *Czechowsky et al.* [1988] reported the first measurements of the aspect sensitivity of PMSE and found indeed a significant aspect sensitivity with θ_s between 2 and 10°. Interestingly, the results of *Czechowsky et al.* [1988] show large aspect sensitivities (small θ_s) in the lower part of the PMSE layer coincident with rather small values of the observed spectral width and small aspect sensitivities (large θ_s) in the upper part of the layer together with a considerably larger spectral width (see Figure 5). This morphology of aspect sensitivity and spectral width suggests that in the upper part of the PMSE the scatterers are more isotropic ('turbulent') whereas they appear to be strongly stratified (specular or 'non-turbulent') in the lower part of the layer. *Czechowsky and Rüster* [1997]

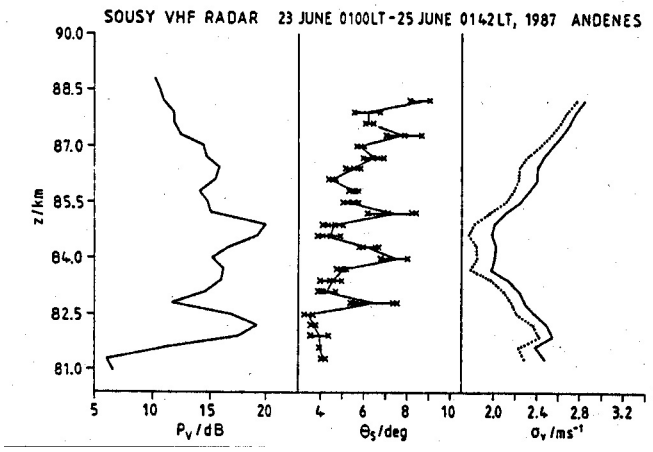

Figure 5: (a) Mean power (P_V) measured in the vertical beam direction for a two day period, (b) aspect sensitivity parameter (θ_s), and (c) mean spectral width for the vertical beam uncorrected (solid line) and corrected (dashed line) for beam broadening. This Figure is reproduced from *Czechowsky et al.* [1988], copyright by the American Geophysical Union.

report that in 90 % of their observations PMSE appear to have narrow spectral width and strong aspect sensitivity, whereas in 10 % of their measurements they found cells of enhanced turbulence characterized by extremely broad spectral width that appear predominantly in the upper part of the PMSE-region, i.e., above 86 km. Similar features were later confirmed by several independent investigators [e.g., *Zecha et al.*, 2001, 2003; *Chilson et al.*, 2002].

Layering characteristics

One final property of PMSE that requires particular attention is the fact that the echoes often occur in several well distinguishable layers that often persist for several ten minutes to hours and can be as thin as only ∼85 m [e.g., *Franke et al.*, 1992; *Rüster et al.*, 2001]. A physical explanation of this extremely stable layering has been missing until recently and will be discussed below (see section 4.2).

2.1.3 Rocket borne observations

Apart from the wealth of radar studies, PMSE have been investigated during several sounding rocket campaigns. In Table 2 we state a list of the campaigns conducted to date together with suitable references. The most important results derived from these measurements are summarized below.

Campaign	Location	Date	Reference
STATE	Poker Flat, Alaska	June 1983	*Ulwick et al.* [1988]
MAC/SINE	Andøya, Norway	July 1987	*Inhester et al.* [1990]
NLC91	Kiruna, Sweden	July/August 1991	*Goldberg et al.* [1993]
SCALE	Andøya, Norway	July/August 1993	*Blix* [1999]
ECHO	Andøya, Norway	July/August 1994	*Havnes et al.* [1996b]
DROPPS	Andøya, Norway	July 1999	*Goldberg et al.* [2001]
SOLSTICE	Andøya, Norway	June 2001	*Smiley et al.* [2003]
MIDAS/MACWAVE	Andøya, Norway	July 2002	*Blix et al.* [2003a]

Table 2: Sounding rocket campaigns dedicated to the study of PMSE

Electron biteouts and small scale structures
One of the most prominent features of the PMSE environment is the fact that the electron number density appears to be frequently disturbed in the altitude region of the radar echoes. Figure 6 shows one of the earliest observations from the STATE campaign in 1983 [*Ulwick et al.*, 1988]. Figure 6 shows that the electron number density is depleted by as much as a factor of ten in the altitude region where strong echoes were observed from the Poker Flat VHF radar. Ever since the STATE observations, similar depletions of the electron number density, also called 'biteouts', were observed in almost all rocket borne electron number density measurements in the vicinity of PMSE (see Table 2 for suitable references) and must hence be considered as a typical feature of the PMSE environment. In section 2.2 we address our understanding of this feature in detail and show that the electron biteouts are direct evidence for the presence of charged ice aerosol particles at PMSE altitudes. Note also that such biteouts were observed much earlier than PMSE itself [e.g., *Pedersen et al.*, 1969] - see *Lübken and Rapp* [2001] and *Friedrich et al.* [1994] for overviews of plasma measurements in the high latitude summer mesopause region.
Apart from this large scale characteristics of the electron number density in the PMSE altitude range, *Ulwick et al.* [1988] further showed that the observed radar echoes are quantitatively characterized by the structure of the electron profile at the radar Bragg scale: following the work of *Røyrvik and Smith* [1984] (who made similar rocket measurements in order to explain VHF echoes at ∼70 km altitude observed at Jicarmarca, Peru) they directly computed the radar signal to noise ratio from the power spectral density of the measured electron number density irregularities at the Bragg scale and found a very good quantitative agreement. These results were later confirmed by several independent investigators [*Inhester et al.*, 1990; *Lübken et al.*, 1993b; *Blix et al.*, 2003c] and hence showed that PMSE are due to volume scattering from electron number density irregularities and not from specular reflections from single steep gradients as they appear for example at the edges of the electron biteouts [see also *Hocking and Röttger*, 1997, for a discussion of the feasibility of specular reflection to explain PMSE].

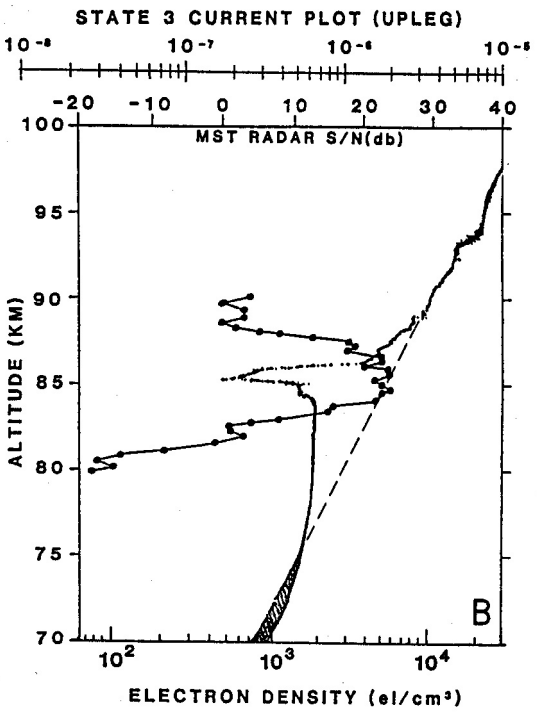

Figure 6: Height profiles of rocket borne DC probe measurements of the electron number density (solid line) and VHF radar echoes (solid circles) for the STATE-3 rocket flight conducted on June, 17, 1983 from Poker Flat, Alaska. The dashed line illustrates a more typical D-region electron number density. This Figure is reproduced from *Ulwick et al.* [1988], copyright by the American Geophysical Union.

First neutral air turbulence measurements

As described above, the first attempts to explain PMSE also considered neutral air turbulence as a possible mechanism to create the fluctuations in the electron number density in one or the other way (see also section 2.2). During the NLC91 campaign, *Lübken et al.* [1993b] performed the first direct measurements of the turbulent energy dissipation rate in a PMSE layer. *Lübken et al.* [1993b] measured fluctuations of neutral air density as a conservative and passive tracer for neutral air turbulence [see *Lübken*, 1992, for details on this technique] and identified turbulent fluctuations only in the upper part of the altitude range where the CUPRI radar (CUPRI=Cornell University Portable Radar Interferometer, see *Swartz et al.*, 1993) observed strong PMSE and concluded that processes different from neutral air turbulence must be responsible for the creation of at least the lower PMSE layer. These findings were further supported by different spectral shapes of electron irregularities in the upper and lower part of the PMSE as well as different spectral width of the radar signals in the two altitude parts [*Ulwick et al.*, 1993; *Cho et al.*, 1993]. A thorough discussion of more recent experimental results on the morphology of neutral air turbulence and PMSE is presented in section 3.2.

Observation of charged particles

While the observation of electron biteouts, the occurrence of PMSE in the vicinity of noctilucent clouds (see below), and the tight coupling of the seasonal dependence of PMSE and NLC occurrence provided strong evidence that PMSE are closely related to aerosol particles, the first direct in situ measurement of (charged) ice particles in an PMSE environment must

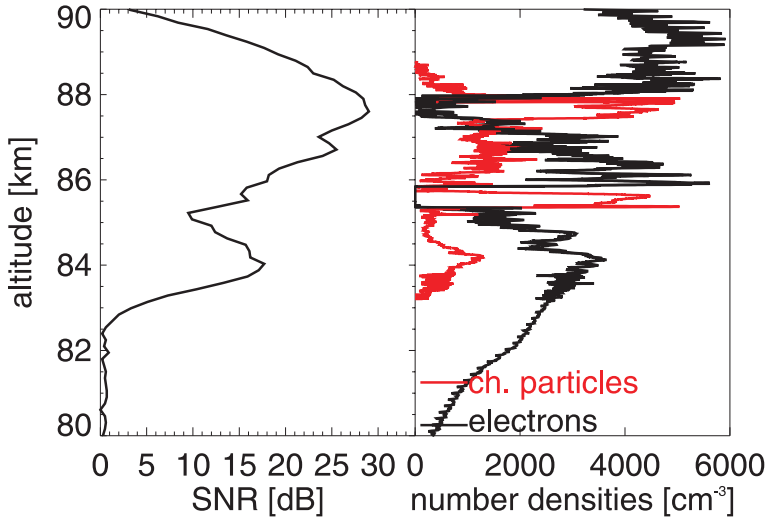

Figure 7: Left panel: Profile of the radar signal to noise ratio (SNR) measured with the ALOMAR-SOUSY VHF radar during sounding rocket flight ECT02. Right panel: profiles of electron number densities (black line) and aerosol charge number densities (red line) measured during sounding rocket flight ECT02. These data are taken from *Havnes et al.* [1996b] and *Lübken et al.* [1998].

be considered as one of the major steps towards an understanding of PMSE. The pioneering work was done by *Havnes et al.* [1996b] who applied a sophisticated Faraday-cup-like instrument (the 'DUSTY'-detector) to measure the charge number density associated with the particles. Figure 7 shows the first altitude profile of charged aerosol particles measured during the ECHO sounding rocket campaign from the Norwegian Andøya Rocket Range on July, 28, 1994. *Havnes et al.* [1996b] observed negatively charged particles in two distinct layers, one centered at 87.5 km and the other centered at 85.5 km altitude. Most interestingly, the electron number density measurement made on the same sounding rocket revealed two distinct electron biteouts exactly at the same altitudes indicating that biteouts form because the aerosol particles act as an efficient sink for electrons (and hence acquire a net negative charge; see section 2.2). During the same campaign, *Havnes et al.* [1996b] also observed a layer of positively charged aerosol particles collocated with an electron enhancement (instead of the more common biteout) in the altitude range where a noctilucent cloud was observed by a ground based lidar. These measurements are however much more difficult to explain than the observations of negatively charged particles. In subsequent campaigns, several investigations have provided further evidence for the existence of negatively charged aerosol particles in PMSE [*Havnes et al.*, 2001; *Mitchell et al.*, 2001, 2003; *Smiley et al.*, 2003]. Concerning positively charged particles there seem to be further indications that they do exist [*Mitchell et al.*, 2001, 2003; *Smiley et al.*, 2003], however, our current understanding of these measurements is far from being conclusive.

Electric field measurements in PMSE

Electric field measurements in PMSE layers have proven to be extremely difficult to perform because of the severe interaction of the charged aerosol particles with the supersonically moving sounding rocket payload. *Zadorozhny et al.* [1993] reported strong electric fields on the order of ∼1 V/m in a PMSE layer, however, based on laboratory investigations on the impact of supersonic water clusters on their electric field mill, they later published corrections

with values of about the same order of magnitude [*Zadorozhny et al.*, 1997]. In a more recent investigation, *Holzworth et al.* [2001], applying a different technique, also found strong V/m perturbations at PMSE altitudes. However, *Holzworth et al.* [2001] also showed that these signatures were artificially created by payload/charged particle flow interactions during the traverse of the PMSE layer and concluded that if there was any DC-electric field, it was smaller than just a few ten mV/m. *Pfaff et al.* [2001] analyzed the same data set for small scale irregularities and identified small scale structures with amplitudes of ∼10 mV/m that they claimed were not artificially created but geophysical. In summary, electric field measurements conducted to date do not yield a conclusive picture such that further experimental efforts are needed to obtain quantitative results on the strength of large and small scale electric fields at PMSE altitudes.

2.1.4 Common volume observations with NLCs

Finally, also common volume observations of noctilucent clouds and PMSE confirmed the close relationship between the radar echoes and ice particles in the mesopause region. *Nussbaumer et al.* [1996] presented the first common volume observation of a noctilucent cloud with the ALOMAR RMR-lidar and a PMSE with the ALOMAR SOUSY radar at the Andøya Rocket Range [*von Zahn et al.*, 2000; *Singer et al.*, 1995]. These authors found a close relationship between the two phenomena with the NLC layer being located at the lower edge of the PMSE layer in most of the cases. *von Zahn and Bremer* [1999] significantly expanded the data base presented in this first study by analyzing a total of 22 joint NLC/PMSE observations and basically confirmed the close relationship between NLC and PMSE. One typical example of common volume radar and lidar measurements is presented in Figure 8. Altogether, *von Zahn and Bremer* [1999] identified three distinct types of PMSE/NLC obser-

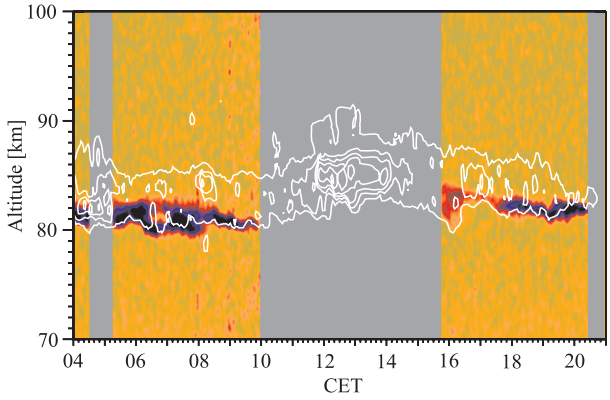

Figure 8: Contour lines of radar signal to noise ratio (white lines) as a function of altitude and time. The blue shaded area marks the noctilucent cloud detected by the ALOMA RMR lidar in the same volume where the radar measurements were taken [*von Zahn and Bremer*, 1999]. This Figure was featured on the cover page of *Geophysical Research Letters*, volume 26, number 11, 1999, copyright by the American Geophysical Union.

vations: in the standard case (=type 1; in 66% of all observations), NLC and PMSE occurred simultaneously in the same volume, with the NLC layer being located in the lower part of the PMSE layer and with identical lower edges. Type 2 allowed for temporal differences between the layers, i.e., at times there were NLC present but no PMSE (in 16% of all observations), and type 3 allowed for spatial differences between the layers, i.e., at times the NLC was not located at the lower edge of the PMSE (in 21% of all observations). The close coupling of

NLC and PMSE is further strong evidence that ice particles play a substantial role for the creation of the radar echoes. In particular, the frequent occurrence of type 1 observations leads to the conclusion that NLC are evidence of the particles that have grown large enough to be visually observable whereas PMSE are related to both large (i.e., when they coincide with NLC) but also the smaller ice particles that are not yet visually observable. These conclusions are in line with the standard growth and sedimentation scenario of mesospheric ice particles where it is considered that the ice particles nucleate at the altitude with largest supersaturation (i.e., close to the mesopause) and then grow by further condensation of water vapor onto their surface, sediment down due to gravity, and gain further size until they are large enough to be visually observed as NLC [see also *Turco et al.*, 1982, and section 4.1].

2.2 Overview: Theoretical understanding

2.2.1 Aerosol charging

As seen above, there is a wealth of observations suggesting that ice aerosol particles play a substantial role for the creation of PMSE. In particular the observations of strong depletions in the electron number density also suggests that the aerosol particles act as a sink for the electrons and hence become negatively charged [*Pedersen et al.*, 1969]. *Reid* [1990] was the first to consider this process quantitatively: based on the electron and positive ion capture rates due to *Natanson* [1960] (see also *Rapp* [2000] for a discussion of these capture rates) he studied the concentration of singly and doubly charged ice particles and the feedback of their charging on the background electron and positive ion number density as a function of the number density of available ice particles. Keeping also the ice-equivalent water vapor content inside reasonable limits, *Reid* [1990] concluded that several thousand ice particles per cubic-centimeter with a radius of ∼10 nm were the most likely candidate to explain the observed electron biteouts. Consequently, most of the ice particles should be singly negatively charged. The drawback of this study, however, was its restriction to singly and doubly charged particles such that *Jensen and Thomas* [1991] developed this model further by allowing for an arbitrary negative particle charge and derived the statistical charge distribution as a function of particle radius for standard background conditions of the D-region (production rate of electrons and positive ions Q=10 $cm^{-3}s^{-1}$ and electron-positive ion recombination rate $\alpha = 10^{-6}cm^3s^{-1}$, corresponding to an undisturbed plasma density of $\sqrt{Q/\alpha}$ ≈3000 cm^{-3} which is a reasonable value for the polar D-region [*Friedrich and Torkar*, 2001]). *Jensen and Thomas* [1991] found an average aerosol charge of -1e for particles with radii between 1 and 10 nm, and then a linear increase of the aerosol charge, i.e., ∼-2e for 30 nm particles and -3e for particles with a radius of 50 nm (with e being the elementary charge). These results were then further generalized by *Rapp and Lübken* [2001] who also systematically considered the dependence of the aerosol charge on the background plasma conditions and studied the expected response not only of the electron number density but also the positive ion number density. Figure 9 shows the change of the electron and positive ion number density relative to a background where no particles (i.e.,$\sqrt{Q/\alpha}$) are present as a function of both particle number density N_A and particle radius r_A. *Rapp and Lübken* [2001] pointed out that the ice particles leave a characteristic 'fingerprint' in the plasma if the effect on both electrons and ions is considered: while the electron number density is expected to be depleted for all aerosol particle parameters considered, the positive ion number density can be either depleted (when being controlled by the capture on the ice particles) or even enhanced (when being controlled by the recombination with electrons). Hence, *Rapp and Lübken* [2001] showed that the combined measurement of the disturbance in the electrons and ions allows for a characterization of the aerosol particles themselves. This idea was then successfully applied

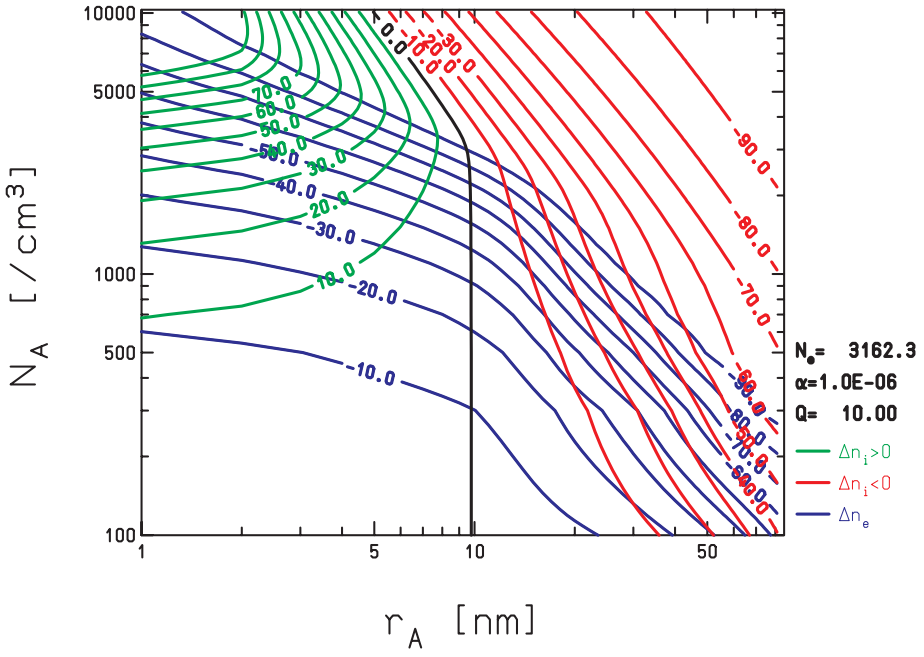

Figure 9: Relative disturbance of electron (blue lines) and positive ion number density (green and red lines), Δn_e and Δn_i, as a function of the particle radius, r_A, and number density, N_A. The calculations have been perfomed for an electron/ion production rate Q=10/(cm^{3}s) and a recombination coefficient α=10^{-6}cm^3/s [*Rapp and Lübken*, 2001].

by *Lübken and Rapp* [2001] who derived aerosol parameters like radii and number densities from the observation of positive ion and electron disturbances under PMSE and/or NLC conditions. In summary, the interaction of the electrons and positive ions with mesospheric aerosol particles appears to be quantitatively understood. Nevertheless, it must be noted that so far there is no physical explanation for the occasional observation of positively charged aerosol particles (see section 2.1.3). It has been proposed that photo emission of 'dirty' ice particles may be involved [*Havnes et al.*, 1990], however, quantitative calculations of the charging of ice aerosol particles by photo emission are hampered by the fact that the details of the complex index of refraction of such 'dirty' ice particles are not yet available [*Rapp and Lübken*, 1999].

2.2.2 Turbulence with high Schmidt number

The first breakthrough in our understanding of PMSE was achieved through the work of *Kelley et al.* [1987] who proposed that the electrons around the polar summer mesopause region could be low diffusivity tracers due to the presence of large positive ion clusters and the ambipolar coupling of the electrons to these ions. If the tracer diffusivity D is considerably smaller than the kinematic viscosity of air ν, or in other words, if the Schmidt number Sc=ν/D is considerably larger than 1 then fluctuations in the tracer field can extend to much smaller scales than the fluctuations of the turbulent velocity field. This basic result of the theory of turbulent tracer advection goes back to *Batchelor* [1959] who demonstrated that tracer structures at scales around the inner scale are compressed by a pure strain motion due to the velocity gradient ($\sim \sqrt{\epsilon/\nu}$) acting on scales around the inner scale l_0^H (=the transition scale between the inertial and the viscous subrange, see above). This strain leads to the creation of structures significantly smaller than l_0^H which subsequently can only be erased by

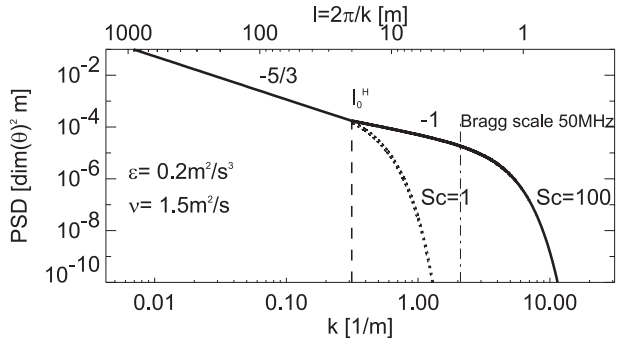

Figure 10: Power spectral densities (PSD) of a passive tracer θ for two different Schmidt numbers of Sc=1 and Sc=100, respectively. The upper ordinate converts wavenumbers to lengths. The numbers '-5/3' and '-1' indicate the wavenumber power law at the scales shown. The vertical dashed line indicates the inner scale (see text for details) and the vertical dashed dotted line indicates the Bragg scale of a 50 MHz radar.

the action of molecular diffusion. If, however, the diffusion coefficient of the tracer is much smaller than the kinematic viscosity of air (being responsible for the damping of the velocity fluctuations) tracer structures can persist at scales $\ll l_0^H$ (see Figure 10). *Batchelor* [1959] further estimated the shape of the tracer spectrum beyond l_0^H and found that the spectrum should reveal a so called viscous convective subrange characterized by a k^{-1} dependence (where k is the wavenumber). Note that indeed this spectral behaviour has been verified by laboratory investigations on high Schmidt number tracers [*Gibson and Schwartz*, 1963] and by direct numerical simulation methods [*Bogucki et al.*, 1997]. Quantitative considerations based on *Kelley et al.* [1987]'s ideas and the available experimental knowledge on proton hydrates in the polar summer mesopause region [*Johannessen and Krankowsky*, 1972; *Kopp et al.*, 1985] showed, however, that the mass of the positive ions was far too small in order to lead to an electron Schmidt number $\gg$1 required to explain the PMSE observations. Subsequently, *Cho et al.* [1992] considered larger particles, namely charged ice particles. *Cho et al.* [1992] applied the multipolar diffusion theory of *Hill* [1978] to a diffusion system consisting of electrons, positive ions and charged aerosol particles. They found that if somewhat more than 50% of the overall negative charge is bound on the aerosol particles, i.e., $|Z_A|N_A/N_e > 1.2$ ($|Z_A|$: number of charges per particle, N_A: particle number density, N_e: electron number density), the electron diffusivity should drop down by several orders of magnitude to the value of the aerosol diffusivity (see Figure 11).
Thus at the time of *Cho et al.* [1992]'s work the picture of our understanding of PMSE seemed to be complete: The presence of neutral air turbulence in combination with a reduced diffusivity of electrons due to the presence of a considerable amount of charged aerosol particles seemed to be sufficient to explain the existence of the electron irregularities at the Bragg scale and subsequently this concept was further elaborated and applied by several authors [*Klostermeyer*, 1997, 1999b; *Chaxel*, 1997; *Hill et al.*, 1999]. However, the observation by *Lübken et al.* [1993b] (see section 2.1.3) that soon followed the publication of the theory created a big dilemma since they showed that one of the crucial requirements of the *Cho et al.* [1992]-theory, i.e., the presence of neutral air turbulence, was not fulfilled. This dilemma triggered a variety of approaches that tried to explain PMSE in the complete absence of neutral air turbulence. These 'non-turbulent' theories will be shortly summarized and discussed in the following subsection before we return to a more thorough discussion of the *Cho et al.* [1992]-theory.

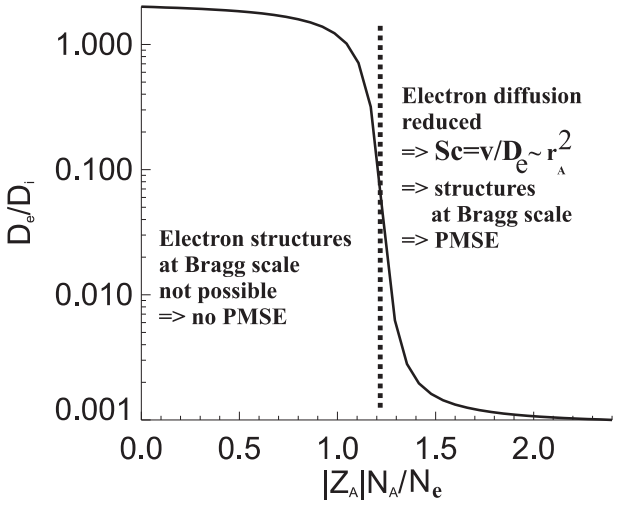

Figure 11: Electron diffusion coefficient D_e in units of the positive ion diffusion coefficient D_i as a function of the ratio between the aerosol charge number density $|Z_A|N_A$ and the free electron number density N_e according to *Cho et al.* [1992], copyright by the American Geophysical Union.

2.2.3 'Non-turbulent' theories

As described above, the proven absence of neutral air turbulence in an altitude range where PMSE was simultaneously observed triggered the formulation of a couple of 'non-turbulent' theories for PMSE in the VHF wavelength range. The dust hole scatter theory by *Havnes et al.* [1992], the opalescence theory by *Trakhtengerts and Demekhov* [1995] and *Trakhtengerts* [1994], and the consideration of charged dust diffusive waves [*Hocking et al.*, 1991] were reviewed in some detail in the article by *Cho and Röttger* [1997] so that we restrict ourselves to a short discussion of these approaches. In short, the dust hole scatter theory assumes the presence of vortices in the neutral gas that prevent sedimenting charged aerosol particles from entering into the interior of the vortex. Hence, a considerable gradient in charged particle and the electron number density along this vortex edge develops that leads to considerable radar scattering. However, this idea must be discarded since it requires structures in the neutral gas that should certainly be seen by in situ measurements like the ones described in *Lübken et al.* [1993b]. The opalescence theory basically considers relative motions of charged aerosol particles, electrons and positive ions that lead to the excitation of unstable plasma waves. However, for the instability to be excited the theory requires very large charging states of the aerosol particles ($|Z_A| > 1000$) which is in contradiction to all available experimental and theoretical evidence (see above). Finally, the charged dust diffusive wave approach suggests that viscosity waves in the neutral gas created for example by infrasound impinging on a region of a rapidly changing temperature gradient (like e.g. at the mesopause) lead to similar waves in the charged aerosol particle distribution that consequently mirror in the electron number density and lead to considerable radar backscattering. Similar to the 'turbulence with large Schmidt-number'-approach the viscosity waves in the aerosol particle distribution decay much slowlier because their diffusion is considerably smaller than that of the neutral gas. However, it must again be stated that there is no experimental evidence available for viscosity waves in the mesosphere even though a considerable number of neutral density measurements have been performed in situ in the PMSE environment [*Lübken et al.*, 1993b, 2002].

Apart from these theories for the explanation of PMSE in the VHF wavelength range it has also been suggested that at least the PMSE observations in the UHF wavelength range, i.e., at frequencies larger than 224 MHz, can be explained by a mechanism called 'dressed aerosol scatter' [*Havnes et al.*, 1990; *Cho and Kelley*, 1992; *Hagfors*, 1992]. The basic idea is that the charged aerosol particles attract a cloud of electrons (if they are positively charged; if they are negatively charged it is thought that they lead to a clustering of electrons in between the charged aerosol particles) with a typical cloud radius given by the Debye-length. Consequently, if the radar wavelength is larger than the Debye-length, then these electron clouds should lead to coherent scatter, i.e., under certain conditions the cross section is expected to be larger than the incoherent Thompson scattering cross section.[1] The most rigorous treatment of this process has so far been presented by *Hagfors* [1992]. Figure 12 shows the scattering cross-section of the charged dust component relative to the Thompson scattering cross section as a function of $f = |Z_A|N_A/N_e$, with an electron number density N_e=1000 cm^{-3} for three values of the dust charge (Z_A=Z=1,10,100) for the radar frequencies 224 MHz and 933 MHz [*Hagfors*, 1992]. Figure 12 shows that also this approach to explain

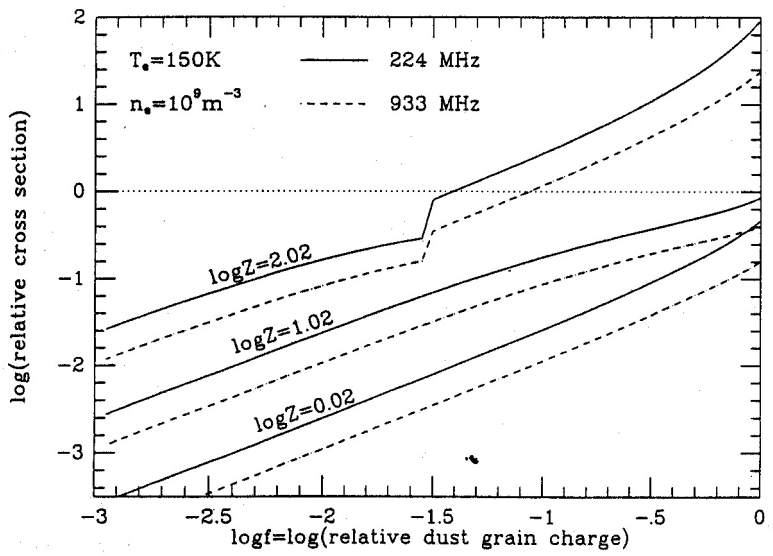

Figure 12: Scattering cross-section of the charged dust component relative to the Thompson scattering cross section as a function of $f = |Z_A|N_A/N_e$, with N_e=1000 cm^{-3} and and an electron temperature T_e=150 K for three values of the dust charge (Z_A=Z=1,10,100) for the radar frequencies 224 MHz and 933 MHz [*Hagfors*, 1992].

PMSE in the UHF wavelength range is highly problematic: first of all, it becomes clear that the dressed aerosol scattering cross section only becomes larger than the cross section for Thompson scatter if either the aerosol particle charge becomes very high (i.e., $Z_A = Z > 100$) or if $f = |Z_A|N_A/N_e \gg 1$, i.e., when the overall charge balance is completely dominated by the particle charge number density. While the first possibility (i.e., large Z_A) contradicts the available experimental and theoretical evidence on aerosol particle charging, the second possibility might at least in some cases be fulfilled (although we will present further contradicting experimental evidence against this idea in section 3.2). However, even if indeed $f = |Z_A|N_A/N_e \gg 1$, it is clear that the dressed aerosol approach cannot explain the observed

[1]The Thompson scattering cross section due to one electron is given by $2\pi r_e^2$ where r_e is the classical electron radius.

reflectivity dependence on the radar frequency (see Table 1) since the observations show that the scattering cross section at 224 MHz is $\sim$ 2-3 orders of magnitude larger than the one at 933 MHz whereas the dressed aerosol scatter theory only predicts a factor $<$10. Taken together, the dressed aerosol scatter approach must also be considered as problematic and can only explain a small part of the available PMSE observations, i.e., those at the very largest frequencies. In section 3.1 we will come back to this issue and discuss if indeed such a mechanism is necessary for the understanding of UHF PMSE.

Finally, most recently *Gumbel and Witt* [2002] have proposed a new mechanism for the creation of small scale irregularities in the charged particle number density and hence also in the electron number density. These authors studied the feasibility of ice particle nucleation on large proton hydrate cluster ions (i.e., $H^+(H_2O)_n$) and identified a positive feedback between the presence of ice particles on the one hand and the growth of cluster ions on the other hand. The basic idea of this positive feedback is depicted in Figure 13. For positive ion nucleation

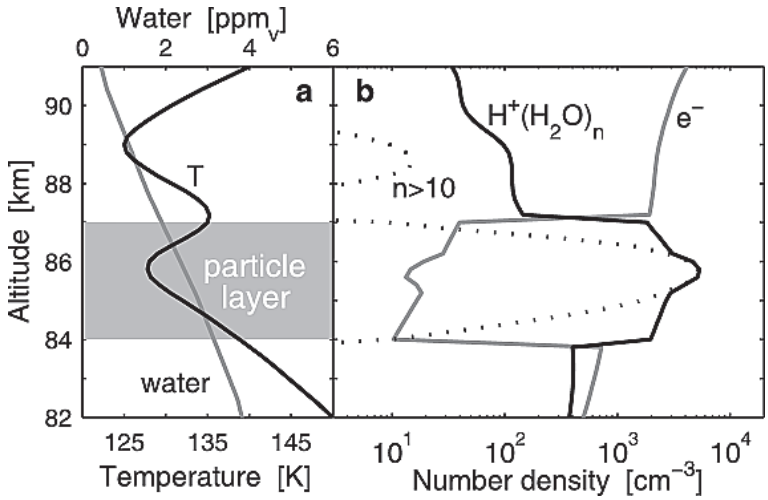

Figure 13: (a) Input temperature and water vapor mixing ratio profiles for the model simulations by *Gumbel and Witt* [2002]. The grey shaded area indicates the altitude range of an ice particle layer with 10^4 cm^{-3} particles of radius 5 nm. (b) Resulting profiles of electron number density and total proton hydrate density. The dashed line denotes the contribution of larger proton hydrates (i.e., with more than 10 H_2O-ligands). This Figure is reproduced from *Gumbel and Witt* [2002], copyright by the American Geophysical Union.

to become feasible, the clusters need to grow to a sufficient size in order to overcome the free energy barrier after which further growth is thermodynamically favored (also known as Kelvin-effect; see *Gumbel et al.* [2003] for a concise discussion of the thermodynamics of particle nucleation at around the mesopause). However, growth to sufficient size is governed by a competition between clustering reactions and recombination of the positive ion clusters with free electrons. Since the abundance of free electrons can be strongly reduced by capture to ice particles (see section 2.2.1 and Figure 13), the presence of ice particles may enhance the growth of cluster ions. This leads to a positive feedback mechanism with particle nucleation being favored in altitude regions where particles already exist. *Gumbel and Witt* [2002] further pointed out that this mechanism may potentially amplify irregularities in the ionospheric particle and charge distribution and might hence be of relevance for our understanding of PMSE. While the general picture discussed by *Gumbel and Witt* [2002] has indeed been experimentally verified, i.e., large scale ($\sim$ kilometer) enhancements of the positive ion number

density at altitudes with the presence of ice particles were indeed observed [*Lübken and Rapp*, 2001], a more detailed analysis of the feasibility of this process for the creation of small scale structures proves the approach to be problematic: as discussed in *Gumbel and Witt* [2002], even under optimum conditions (i.e., deep temperatures, many particles, and sufficient water vapor) nucleation rates can not exceed $\sim 10cm^{-3}s^{-1}$ such that it takes at least several minutes to produce 1000 cm^{-3} new particles with radii larger than 3-5 nm. This time scale needs to be compared to the diffusion time of ice particles at 3-5 nm size which is of about the same order of magnitude [*Cho et al.*, 1992]. Hence, only under optimum conditions can the particle/cluster feedback provide structure amplification that is sufficient for PMSE generation. If such optimum conditions do exist regularly must however be doubted since for example recent in situ observations have shown PMSE at altitudes where no considerable electron biteouts have been observed (such that particle growth is not favored; see *Blix et al.* [2003c] and section 3.2). In addition, also the demand for sufficient water vapor is problematic since the freeze drying effect is expected to significantly reduce the available water vapor in the presence of ice particles [*Inhester et al.*, 1994; *Rapp et al.*, 2002b; *von Zahn and Berger*, 2003]. All these caveats led *Gumbel and Witt* [2002] themselves to conclude that 'the particle/cluster feedback to be only a weak candidate for an explanation of PMSE generation.'

3 Pros and cons of the turbulence with large Schmidt-number approach

We have shown in the previous section that the *Cho et al.* [1992]-theory so far provided the most plausible attempt to explain PMSE as a consequence of mesospheric neutral air turbulence in conjunction with a large Schmidt-number of the electrons. However, in situ observations of mesospheric neutral air turbulence by *Lübken et al.* [1993b] casted a shadow of doubt on this explanation since it showed that PMSE existed at altitudes where no neutral air turbulence was present. This observation triggered the formulation of several alternative approaches which, however, have proven to be either completely unrealistic or at least problematic (see section 2.2.3). In this section, we return to the approach by *Cho et al.* [1992] and gather all available favoring and contradicting evidence in order to potentially identify critical points where the theory can be further developed and finally yield a consistent explanation for PMSE.

3.1 Supporting evidence

Further evidence for ice particles causing PMSE

While satellite measurements have recently proven that the particles forming NLC are indeed made of water ice [*Hervig et al.*, 2001] a similar direct confirmation is missing so far for PMSE. However, very strong indirect evidence that PMSE are created through the involvement of water ice particles comes from in situ temperature measurements during the simultaneous observation of PMSE. *Inhester et al.* [1994] reported a first systematic comparison of 22 temperature profiles measured with so called falling spheres and radar observations of PMSE [see e.g. *Schmidlin*, 1991, for a detailed discussion of the falling sphere technique]. *Inhester et al.* [1994] found that the PMSE occurred in exactly the altitude range where the temperatures allowed the ice particles to exist. Recently, *Lübken et al.* [2002] have provided an update of this data base and compared additional falling sphere temperature measurements and temperature measurements that were performed with active ionization gauges with simultaneously measured PMSE profiles. The significant advantage of the ionization gauge measurements is their much better altitude resolution which is only 200 m independent of

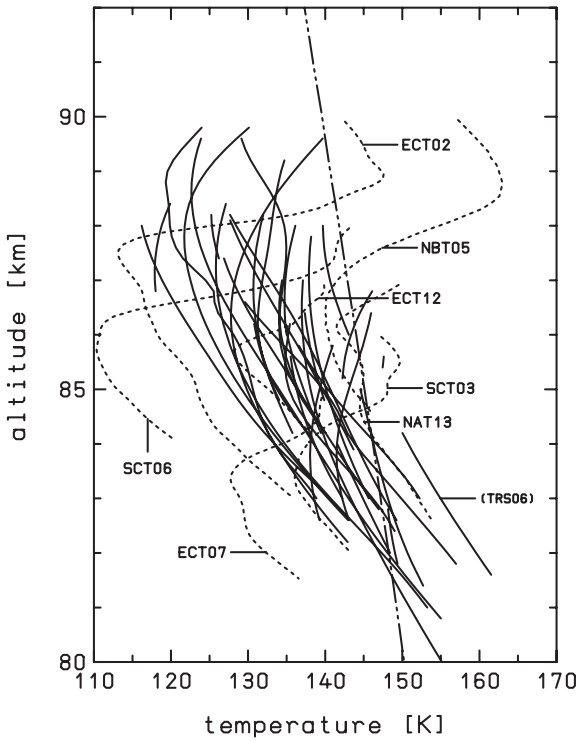

Figure 14: Temperature profiles measured within PMSE layers. Measurements by the falling sphere technique (solid lines) and by the TOTAL/CONE ionization gauges (dotted lines) are shown. The dotted-dashed line presents the frost point temperature profile using the model H_2O values from *Körner and Sonnemann* [2001]. This Figure is reproduced from *Lübken et al.* [2002], copyright by the American Geophysical Union.

altitude and their high accuracy of better than ∼2 % [*Rapp et al.*, 2001, 2002b]. Hence, these measurements allow for a much more precise comparison of temperatures with PMSE since they also show the small scale structure of the temperature profile like for example gravity wave induced local temperature minima or maxima. Such features cannot be resolved by the falling sphere technique since the typical altitude resolution of falling sphere measurements at PMSE altitudes is ∼5 km [*Schmidlin*, 1991]. Figure 14 shows a comparison of these temperature measurements with the frost point temperature for water ice (calculated from the density climatology from *Lübken* [1999] and water vapor mixing ratios from *Körner and Sonnemann* [2001]) in the altitude range where PMSE was observed during ±0.5 hours around the rocket launch. (This time interval was chosen in order to account for potential horizontal differences in the PMSE characteristics between the location of the radar and the location of the temperature measurements at a typical horizontal distance of ∼50 km). Figure 14 shows that the majority of falling sphere temperatures and ionization gauge temperatures are lower than the frost point temperature, i.e., they allow for the existence of ice particles. There are only two remarkable 'outliers', i.e., the profiles from the falling sphere flight TRS06 and the ionization gauge flight NBT05 where the temperatures reach rather large values of ∼160 K, which is at least 10 K above the frost point temperature. However, in both cases a closer inspection of the PMSE measured during these rocket flights showed in fact that the PMSE had disappeared a few minutes prior to the sounding rocket flights. This is a remarkable correlation between the appearance of PMSE and the thermal structure and provides very strong evidence that PMSE are indeed directly linked to the existence of ice particles.

Absolute volume reflectivities

Recent observations of turbulent energy dissipation rates and Schmidt-numbers around the polar summer mesopause now also allow for a quantitative comparison of observed and computed radar volume reflectivities based on the *Cho et al.* [1992]-theory [*Lübken et al.*, 1998, 2002]. In Figure 15 we have compared the measured absolute reflectivities stated in Table 1 with calculations of the volume reflectivity based on a Schmidt-number dependent turbulence model [*Driscoll and Kennedy*, 1985] (for details on the calculation of the volume reflectivity based on the *Driscoll and Kennedy*-model see *Giebeler*, 1995). Figure 15 shows

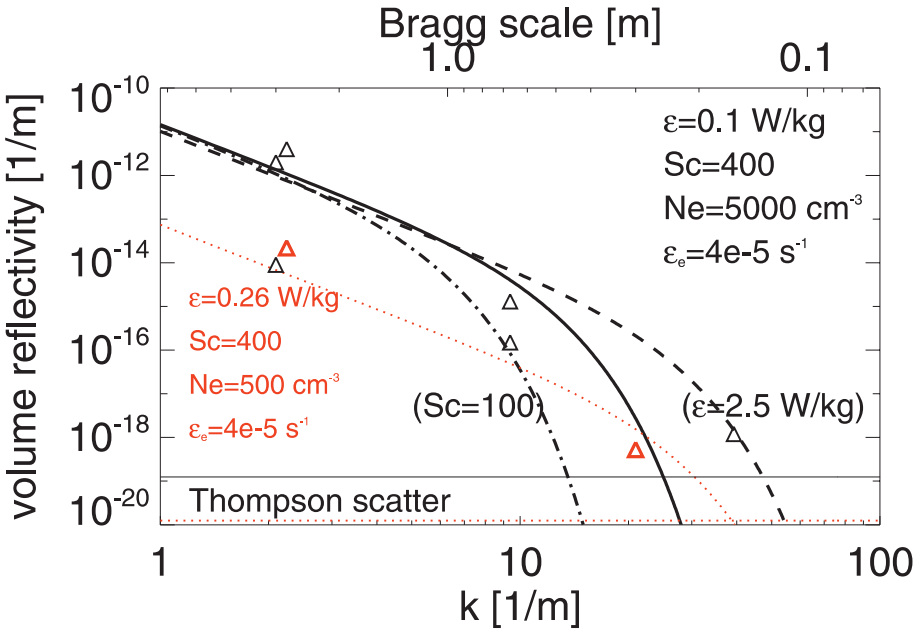

Figure 15: Measured (symbols) and calculated volume reflectivities (lines) for different radar Bragg wave numbers (lower abscissa) and Bragg scale (upper abscissa), respectively. Parameters used in the calculations for all black lines are given in the black colored insert. Parameters used in the calculations for all red lines are given in the red colored insert. The horizontal lines indicate the incoherent scatter reflectivity (Thompson scatter) for an electron number density of 5000 cm^{-3} (black) and 500 cm^{-3} (red), respectively. The two red symbols mark the observations reported by *Röttger* [2001].

that with reasonable values for the Schmidt-number [*Lübken et al.*, 1998], the turbulent energy dissipation rate [*Lübken et al.*, 2002], the electron number density N_e and the electron irregularity dissipation rate ϵ_e [*Giebeler*, 1995] the observations at 50 MHz, 224 MHz and 500 MHz can be readily explained (thick black line). It is also interesting to note that using the same parameters but $\epsilon = 2.5$ W/kg (which is the largest value that has so far been reported [*Lübken et al.*, 2002]) also allows to explain the observed reflectivity at 933 MHz (thick dashed line). Note further that the product $N_e^2 \cdot \epsilon_e$ is $\propto \frac{d}{dt}\Delta N_e$, where ΔN_e is an absolute small scale irregularity of the electron number density. Hence, $N_e^2 \cdot \epsilon_e$ is a measure of the absolute magnitude of the fluctuations in the electron gas and thus determines the absolute level of the calculated reflectivity. With this information in mind, we also see that the considerably lower values reported by *Röttger* [2001] can be directly explained in the scope of the [*Cho et al.*, 1992]-theory (red dotted line). In summary, the *Cho et al.* [1992]-theory can explain PMSE observations at all radar frequencies provided that indeed neutral

air turbulence is present.

Evidence for electron diffusivity controlling PMSE
A major step towards a deeper understanding of PMSE was achieved through the observations of *Chilson et al.* [2000] who reported the first successful artificial modulation of PMSE by heating the electron gas at PMSE altitudes with a powerful RF-heating radar. Figure 16

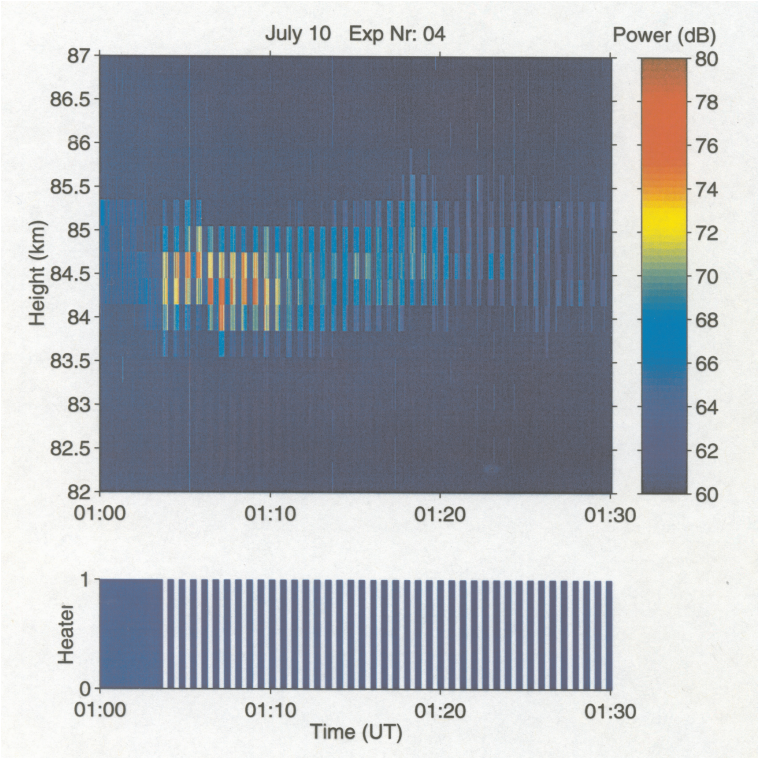

Figure 16: Upper panel: PMSE observed with the EISCAT VHF radar at Tromsø on July, 10, 1999. The lower bar code indicates when the heater was turned on (blue) and off (white), respectively. This Figure is reproduced from *Chilson et al.* [2000], copyright by the American Geophysical Union.

shows that the PMSE instantly vanished when the heater was on and returned to its undisturbed value as soon as the heater was turned off again. *Rapp and Lübken* [2000] interpreted these observations in the scope of the electron temperature dependence of the electron diffusion in the vicinity of charged aerosol particles and found that an electron temperature rise could indeed explain the observed features. Figure 17 shows calculated decay times (defined here by the demand that the irregularity amplitude decayed to 10% of its initial value) for Gaussian disturbances in the electron number density in the presence of similar disturbances in the negatively charged aerosol number density and positive ion number density for different values of $|Z_A|N_A/Ne$ and T_e/T_n, where T_e is the electron temperature and T_n the temperature of the neutral gas. Note that during heating, only the electron temperature is affected whereas the positive ion temperature and the temperatures of the neutral gas and the aerosol particles do not change [e.g., *Rietveld et al.*, 1986]. Similar to the results of *Cho et al.* [1992], Figure 17 shows that for considerably large values of $|Z_A|N_A/Ne$ and T_e/T_n=1, the decay times are much larger than without charged aerosol particles (i.e., $|Z_A|N_A/Ne \ll 1$), indicative of a significantly reduced electron diffusivity and hence the possibility to maintain fluctuations in the electron gas at the radar Bragg scale. *Belova et al.* [2001] have estimated

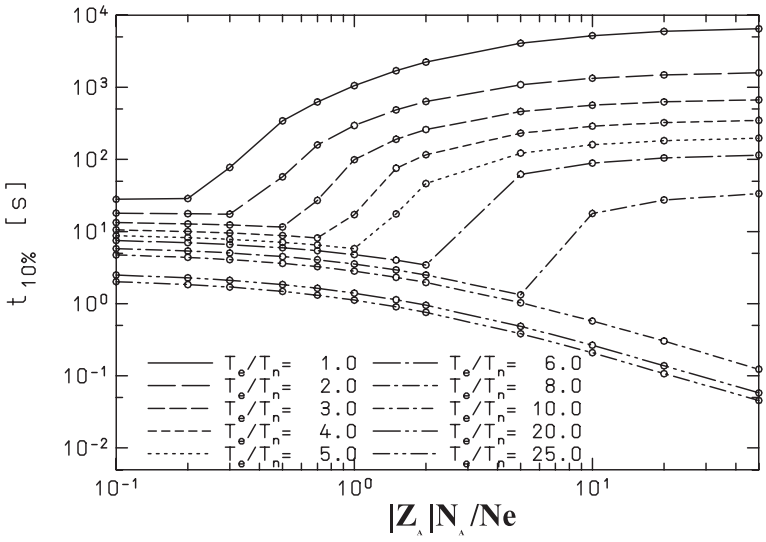

Figure 17: Decay times of a Gaussian electron perturbation (with a width = 67 cm) as a function of $|Z_A|N_A/Ne$ for the case of positive ions and singly negatively charged aerosol particles with a radius of 10 nm and different values of T_e/T_n. This Figure is reproduced from *Rapp and Lübken* [2000], copyright by the American Geophysical Union.

that during the heating pulse, the electron temperature rises by about a factor of T_e/T_n=20, i.e., to a temperature of ∼2500 K. With this T_e/T_n-ratio and for $|Z_A|N_A/Ne \geq 1$, Figure 17 predicts the decay time to decrease by several orders of magnitude leading to a fast disappearance of the PMSE. In addition, the calculations of *Rapp and Lübken* [2000] suggested that when the heater is off, the electrons immediately thermalize due to collisions with the neutral gas and diffuse back to their original positions since the disturbance in the charged aerosol particle distribution has not been affected by the heating. In a second investigation, *Rapp and Lübken* [2003b] have further shown that the PMSE decay and reappearance are expected to happen on time scales on the order of 1 ms which is also in accordance with a recent reanalysis of the original *Chilson et al.* [2000]-data by *Belova et al.* [2003]. The combined experimental and model results from *Chilson et al.* [2000] and *Rapp and Lübken* [2000, 2003b] hence provide strong evidence that the reduction of electron diffusivity due to the presence of charged aerosol particles is one of the key physical processes leading to PMSE.

3.2 Contradicting evidence

Neutral air turbulence at PMSE altitudes

Since the first observations of neutral air turbulence in the vicinity of PMSE by *Lübken et al.* [1993b] 12 additional rocket borne turbulence measurements at PMSE altitudes have been performed (2 during the NLC91 campaign, 2 during the SCALE campaign, 3 during the ECHO campaign, 1 during the DROPPS campaign, 2 during the SOLSTICE campaign and 3 during the MIDAS/MACWAVE campaign; see Table 2). The results from the first 8 launches were summarized by *Lübken et al.* [2002]. The turbulence measurements during the SOLSTICE campaign are reported in *Müllemann et al.* [2003] and results from the first sounding rocket flight during the MIDAS/MACWAVE campaign have just recently been published in *Strelnikov et al.* [2003]. Individual comparisons of PMSE observations and turbulence measurements are shown in Figure 18. It is evident from this Figure that there

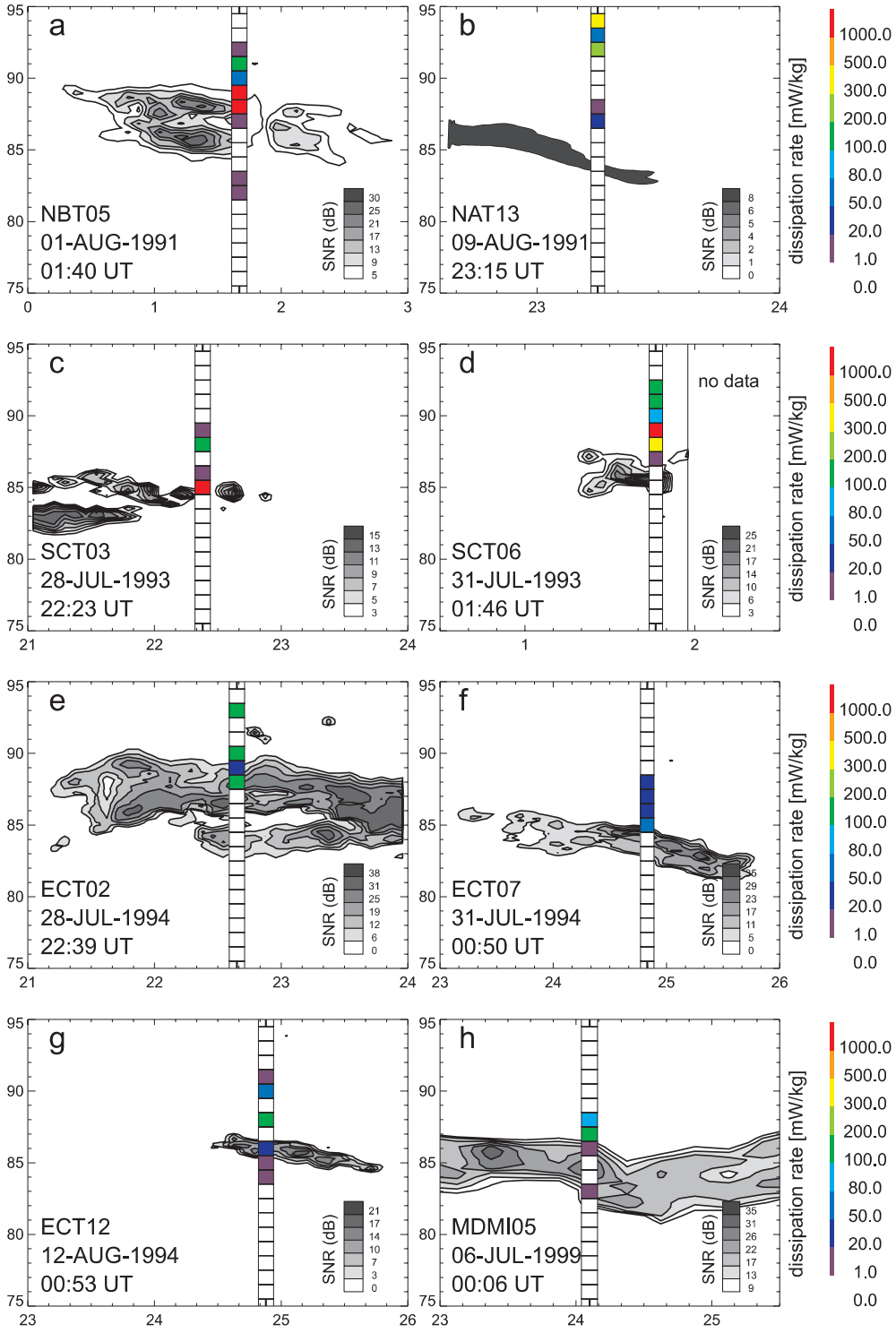

Figure 18: Comparison of turbulent energy dissipation rates ϵ (color coded) and the PMSE intensity for 8 sounding rocket flights. This Figure is reproduced from *Lübken et al.* [2002], copyright by the American Geophysical Union.

is clearly no one to one correlation between the occurrence of turbulence and the occurrence of PMSE. *Lübken et al.* [2002] performed a statistical analysis of these data and found that in more than 50 % of all altitude bins where PMSE was observed there was no neutral

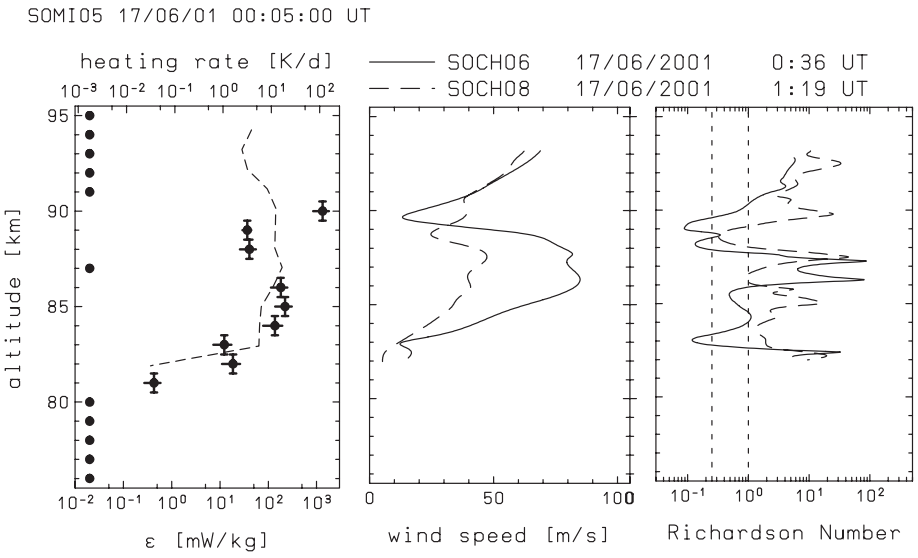

Figure 19: Left panel: Turbulent energy dissipation rates ϵ as function of altitude from sounding rocket flight SOMI05. Values for ϵ near the left ordinate were arbitrarily chosen to indicate that no turbulence was found at these altitudes. The dashed line shows a mean profile from 8 former in situ turbulence measurements [*Lübken et al.*, 2002]. Middle panel: Results of two wind measurements with chaff shortly after flight SOMI05. Right panel: Richardson numbers for the chaff measurements shown in the middle panel. The critical level of Ri=0.25 and the 'hysteresis' level of Ri=1 are marked by vertical dashed lines. This Figure is reproduced from *Müllemann et al.* [2003], copyright by COSPAR.

air turbulence present. If, however, turbulence and PMSE occurred at the same altitudes it regularly only happened in the upper portion of the PMSE layer (i.e., in flight NBT05, SCT06, ECT02, ECT07, MDMI05). In addition, it must be noted that turbulence was often observed at altitudes where no PMSE was present, i.e, normally above the PMSE layer and in one case (ECT12) also below the PMSE layer. The more recent observations by *Müllemann et al.* [2003] and *Strelnikov et al.* [2003] basically confirm this general picture of the morphology of turbulence and PMSE. One observation of *Müllemann et al.* [2003] is particularly remarkable since the authors reported the first observation of a near continuous turbulent layer between 81 and 90 km altitude. In addition, the authors analyzed high resolution wind measurements from a chaff cloud experiment [see e.g. *Widdel*, 1990] that allowed to identify a remarkably strong wind shear and hence a dynamical instability (most probably due to a breaking long period gravity wave) as the source of the observed turbulent structure (see Figure 19).
To summarize, in Figure 20 we compare the occurrence rate of PMSE with the occurrence rate of neutral air turbulence as determined from the first 10 sounding rocket flights mentioned above [see *Rapp and Lübken*, 2003a, for details how these occurrence rates were determined]. Figure 20 shows that in a climatological sense neutral air turbulence indeed occurs in the entire altitude range where PMSE is observed. At altitudes above ∼86 km the turbulence occurrence rate is even larger than the PMSE occurrence rate so that at these altitudes nothing argues against turbulence as the generating mechanism of PMSE. At lower altitudes, however, the PMSE occurrence rate is significantly larger than the turbulence occurrence rate, for example at 85 km PMSE occur with a rate of ∼65 % whereas turbulence only occurs with a rate of ∼35 %. Hence, at the lower altitudes in the PMSE altitude range, neutral air turbulence can clearly not directly account for the occurrence of PMSE.

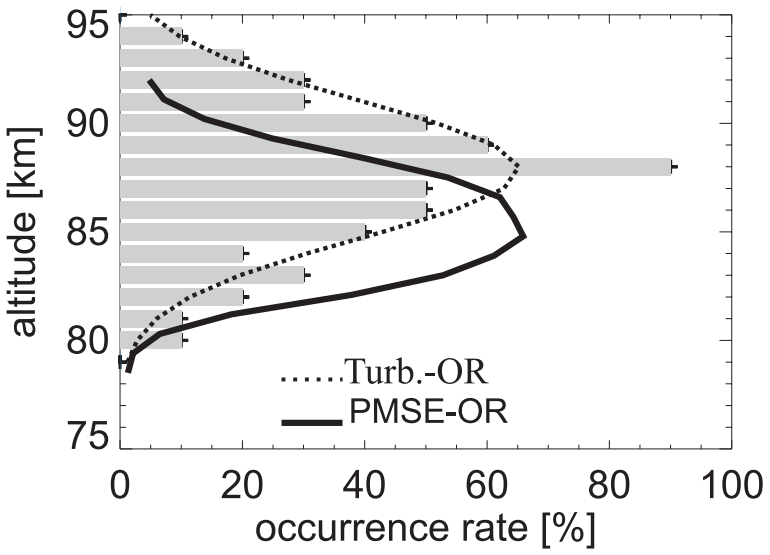

Figure 20: Occurrence rates of PMSE (solid line) and neutral air turbulence (histogram and dashed line) according to *Rapp and Lübken* [2003a].

The charge balance at PMSE altitudes

We now come to a second critical point of the theory by *Cho et al.* [1992], i.e., the requirement that the ratio between the charge number density of the aerosol particles ($|Z_A|N_A$) and the free electron number density (N_e) must be larger than a critical value of ∼1.2 in order to allow for a reduced electron diffusivity (see Figure 11).

First doubts if this condition is indeed satisfied under real PMSE conditions arose when *Havnes et al.* [2001] reported measurements of the aerosol charge number density and the electron number density from a miniaturized sounding rocket launched into a PMSE event. These measurements showed a nice correspondence between the general occurrence of charged particles and PMSE, however, *Havnes et al.* [2001] also noted that PMSE occurred in altitude regions where the ratio $|Z_A|N_A/N_e$ was as small as 0.05.

In a completely different study, *Rapp et al.* [2002a] investigated the PMSE dependence on the background electron number density during the strong solar proton event on July 14, 2000. These authors found a significant negative correlation between electron number densities determined from flux measurements of energetic protons from the geostationary GOES-8 and ACE satellites and PMSE observed with the ALWIN VHF radar at the Andøya Rocket Range (69°N) for electron number densities larger than a threshold value of $\sim 7 \cdot 10^4/\mathrm{cm}^3$ (see Figure 21). *Rapp et al.* [2002a] argued that the overall decay of the PMSE during a significant rise of the background ionization was expected on the ground of the *Cho et al.* [1992] theory since a rise in N_e would correspond to a decrease in $|Z_A|N_A/N_e$ such that at a certain threshold value the electron diffusivity should not be reduced any more. However, these authors were also puzzled by the fact that the PMSE was unaffected for a very wide range of electron number densities, i.e., between some thousand electrons/cm^3 up to $\sim 7 \cdot 10^4/\mathrm{cm}^3$ and pointed out that current knowledge about the abundance of aerosol particles at mesopause altitudes and their charging properties could not explain that $|Z_A|N_A/N_e$ remained larger than ∼1 for all these electron number densities. *Rapp et al.* [2002a] concluded that '...either our current understanding of the nucleation of ice particles in the polar summer mesopause region is incomplete or that current PMSE theories [i.e., the *Cho et al.* [1992]-theory] fail in

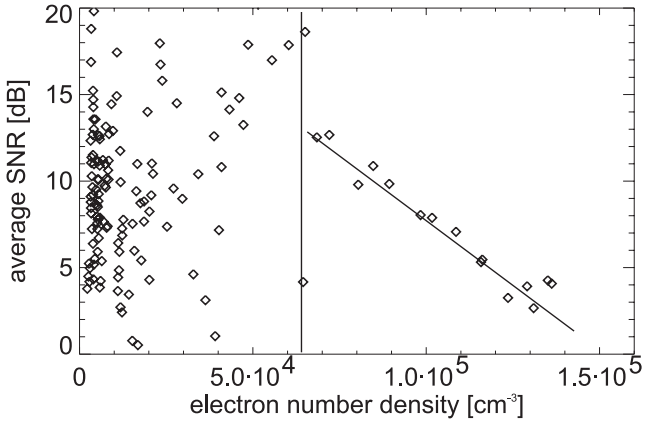

Figure 21: Scatter plot showing the dependence of the PMSE SNR values on the electron number densities at 87 km during the major solar proton event on July 14, 2000. While no correlation is detectable for electron number densities lower than $\sim 7{\cdot}10^4/\mathrm{cm}^3$ a clear anti-correlation is observed for higher electron number densities. This Figure is reproduced from *Rapp et al.* [2002a], copyright by the American Geophysical Union.

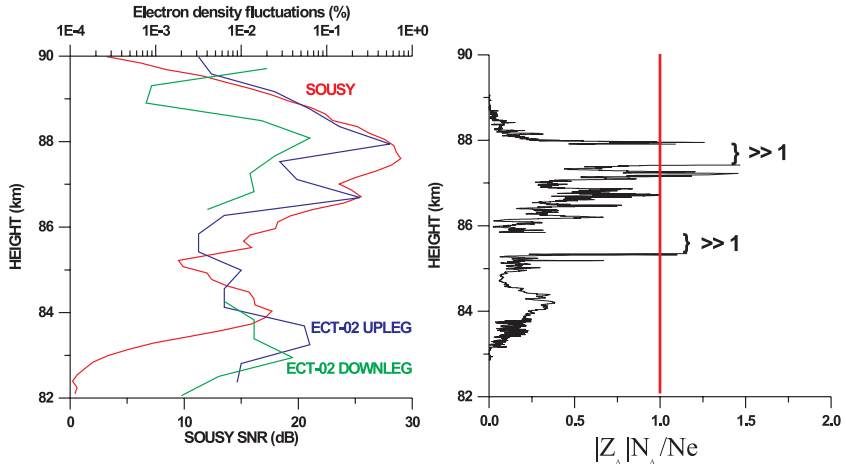

Figure 22: Left panel: Comparison of radar power in dB and electron number density fluctuations in % at 3 m scale measured on both upleg and downleg of the ECT02 flight. Right panel: Calculated ratio between aerosol charge number density ($|Z_A|N_A$) and electron density (N_e) for the upleg part of the ECT02 flight. The red vertical red lines mark ratios of $|Z_A|N_A/N_e = 1$. This Figure is reproduced from *Blix et al.* [2003c], copyright by the American Geophysical Union.

their interpretation of the role of charged aerosol particles'.
Motivated by these observations, *Blix et al.* [2003c] performed a detailed comparison of $|Z_A|N_A/N_e$- and PMSE profiles. These authors derived $|Z_A|N_A/N_e$ from in situ measurements of either positive ion and electron number densities (making use of the assumption of local charge neutrality) or directly from aerosol charge number densities and electron number densities. As an example, Figure 22 shows the comparison of the $|Z_A|N_A/N_e$- and PMSE profile as measured on sounding rocket ECT02 during the ECHO campaign (see Table 2). The comparison of electron number density fluctuations at the Bragg scale (3 m) and the power received by the ALWIN radar shown in the left panel of Figure 22 showed that the

radar echoes were indeed due to the small scale structure of the electron number density as expected. (Technically speaking, this consistency also proves that the sounding rocket indeed probed the PMSE observed with the ground based VHF radar.) The comparison of $|Z_A|N_A/N_e$-values within the PMSE layer shown in the right panel, however, showed that $|Z_A|N_A/N_e$ was smaller than 1 in almost the entire altitude range where PMSE (and strong fluctuations in the electron number density) were observed. *Blix et al.* [2003c] considered a total of four sounding rocket flights and found that only in 15 % of all altitude bins with PMSE $|Z_A|N_A/N_e$-values larger than 1 were observed and that even in ∼75 % of all altitude bins $|Z_A|N_A/N_e$ was smaller than 0.5.
Taken together, the observations by *Havnes et al.* [2001], *Rapp et al.* [2002a] and *Blix et al.* [2003c] indeed showed that *Cho et al.* [1992]'s results on the electron diffusivity in the presence of charged particles were at least quantitatively flawed and that PMSE existed in the presence of considerably smaller aerosol charge number densities as originally suspected.

3.3 Summary

In summary of this section, we stress the following points: on the one hand there is strong evidence for the significant role of (charged) ice particles and the related reduction of the electron diffusivity for the presence of PMSE. On the other hand, in situ neutral air turbulence measurements show frequent turbulent activity only in the upper part of PMSE layers and in situ measurements of the charge balance at PMSE altitudes show that the details of the electron diffusivity reduction as described in *Cho et al.* [1992] are not completely understood. The remaining part of this review will hence be dedicated to the consideration of the following questions:

1. How do electrons diffuse in the vicinity of charged aerosol particles?

2. Which physical process initially creates the small scale structures in the electron number density distribution?

4 On the microphysics of ice particles around the mesopause

Considerable progress to answer the questions raised in the preceding section has recently been made through detailed microphysical modelling of the physics of (charged) mesospheric ice particles in the mesopause region and their relation to electron diffusion characteristics and PMSE [*Rapp et al.*, 2002b, 2003c]. These results led *Rapp and Lübken* [2003a] to theoretically reconsider the physics of electron diffusivity in the presence of charged particles resulting in analytical expressions for the time development of small scale plasma irregularities in the presence of charged particles. In the following subsections we summarize the most important results from these investigations.

4.1 Ice particles in the polar summer mesopause

In order to study the microphysics of ice particles in the polar summer mesopause region, *Rapp et al.* [2002b] applied the **C**ommunity **A**erosol and **R**adiation **M**odel for **A**tmospheres (CARMA). CARMA is a further development of a multi-purpose aerosol model described by *Toon et al.* [1988]. Previous versions of CARMA have been used to investigate the physics of noctilucent clouds [*Turco et al.*, 1982; *Jensen and Thomas*, 1988; *Jensen et al.*, 1989; *Jensen and Thomas*, 1994]. While these previous model investigations were hampered by the lack of reliable knowledge on crucial parameters like mesospheric temperatures and water vapor,

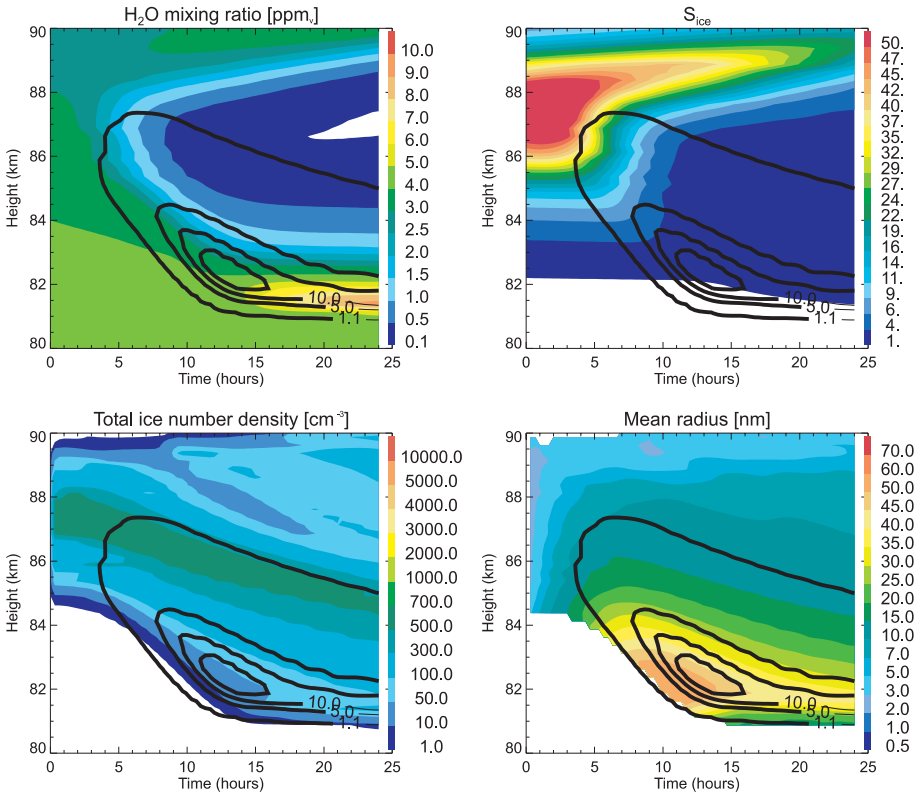

Figure 23: Time-altitude dependence of water vapor mixing ratio, saturation ratio, total ice number density and mean ice radius during the formation and growth of a noctilucent cloud. The black isolines overlayed on each plot show lines of constant backscatter ratio as it would be observed by a lidar with a laser wavelength of 532 nm [after *Rapp et al.*, 2002b, copyright by the American Geophysical Union].

the study by *Rapp et al.* [2002b] used the best available data sets to date. Temperatures were taken from the recent climatology of falling sphere measurements published by *Lübken* [1999] and water vapor profiles were taken from the 3d-model investigation by *Körner and Sonnemann* [2001] that are consistent with the best available water vapor measurements in the relevant latitude and altitude range [*Seele and Hartogh*, 1999]. Besides the water vapor profile, the model by *Körner and Sonnemann* [2001] that is based on the three dimensional general circulation model COMMA/IAP also provided input for the mean vertical wind profile [*Berger and von Zahn*, 1999]. The CARMA model treated three completely interactive constituents: meteoric smoke particles, ice particles, and mesospheric water vapor. The height profile and the size distribution of meteoric smoke particles were calculated as described in *Hunten et al.* [1980]. For the ice particles, microphysical processes like nucleation and condensational growth were treated, as well as particle sedimentation and transport. Water vapor is diminished by condensation, enhanced by evaporation of ice particles, and transported by horizontal and vertical motion. Above 85 km, water vapor is effectively photodissociated by the energetic Ly-α and Schumann-Runge radiation. A detailed description of the particular microphysical processes was given in *Turco et al.* [1982]. Optical signatures of simulated ice particles were calculated using the Mie scattering code described by *Ackermann and Toon* [1981]. Figure 23 shows the results of a microphysical model simulation performed with CARMA for an undisturbed background atmosphere for July, 1st conditions, where temperatures at the mesopause at 88 km altitude reach the lowest temperatures of the

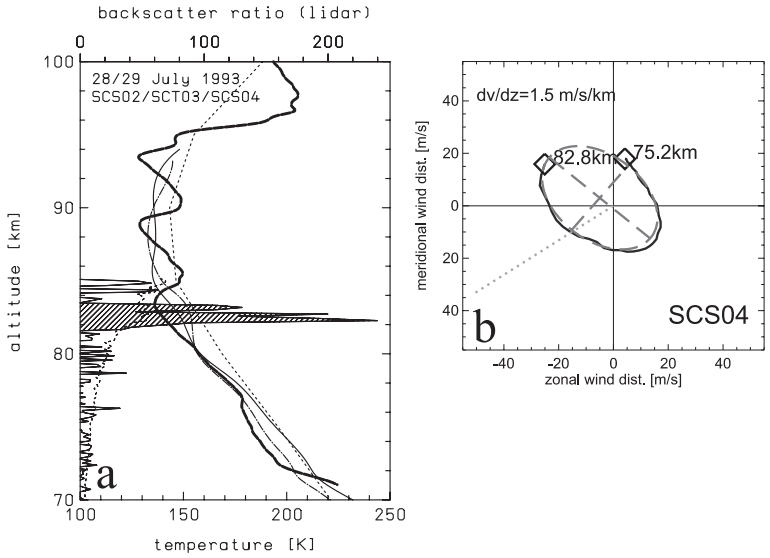

Figure 24: Panel a: Comparison of the CONE temperature profile (thick dashed line) and noctilucent cloud altitude (hatched profile, top abscissa) of flight SCT03 during the SCALE campaign in July/August 1993. In addition two falling sphere temperature profiles (labeled SCS02 and SCS04) are shown that were launched shortly before and after the sounding rocket flight. The thin dashed line indicates the reference temperature profile from *Fleming et al.* [1990] for the month August and the latitude of Andøya. Panel b: Hodograph of the wind disturbances during flight SCS04 between 75 and 82 km. The grey ellipse shows the best fit to the data resulting in an estimate of the intrinsic gravity wave period of ∼470 min. The dotted line indicates the background wind vector at 82 km altitude [after *Rapp et al.*, 2002b, copyright by the American Geophysical Union].

season, i.e., ∼129 K [*Lübken*, 1999]. Figure 23 reveals the picture of the well known growth and sedimentation scenario of mesospheric ice particles. Ice particle nucleation on meteoric smoke particles takes place at the altitudes with the lowest temperatures and hence largest saturation ratios S (=ratio between water vapor partial pressure and saturation pressure over water ice), i.e., between 84 and 90 km altitude yielding ice particle number densities of up to ∼700 cm^{-3}. The particles then sediment down due to their gravity and further grow by direct sublimation of water vapor onto their surface reaching maximum mean particle radii between 40 and 50 nm. The potential optical signature of these ice particles is indicated by the black isolines which show values of the backscatter ratio BSR that would be observed by a lidar at 532 nm wavelength (BSR=total received signal at a certain altitude divided by the signal due to pure molecular Rayleigh scattering. BSR>1 when Mie scattering due to ice particles enhance the scatter significantly over the Rayleigh background). The maximum brightness is reached at altitudes of ∼81.5 km with corresponding particle radii of ∼40 nm and number densities of 50-100 cm^{-3}. These numbers are generally consistent with values derived from multi-color lidar observations by *von Cossart et al.* [1999]. Panel a further shows that the formation and growth of the ice particles leads to significant redistribution of water vapor due to the freeze drying effect (because the ice particles 'consume' the available water vapor when they grow) and subsequent deposition of the ice contained water vapor at the bottom of the cloud. Note that recent satellite water vapor measurements indeed seem to find evidence for this local water vapor maximum at the cloud bottom height [e.g., *McHugh et al.*, 2003]. See also *von Zahn and Berger* [2003] for a more detailed discussion of the freeze

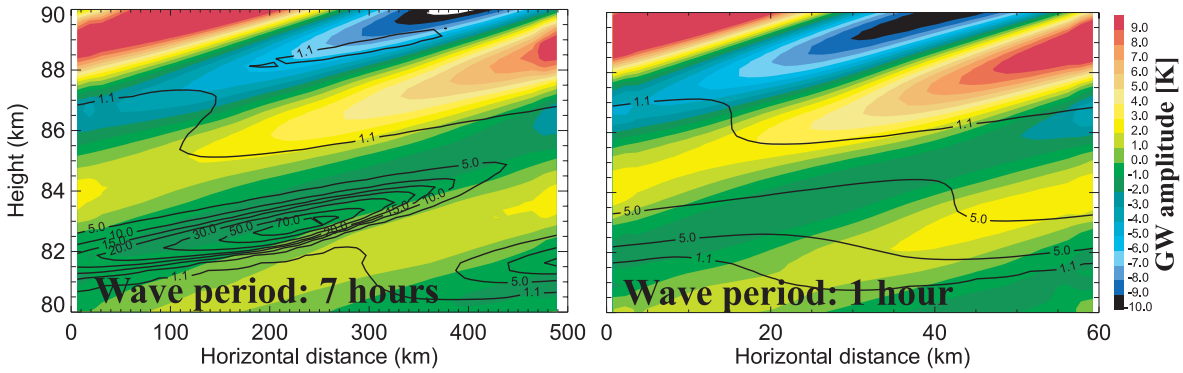

Figure 25: Altitude versus horizontal distance variation of the temperature disturbance due to a modeled gravity wave with a period of 7 hours (left panel) and 1 hour (right panel), respectively, after a simulation time of 15 hours. The black isolines show lidar backscatter ratios for a wavelength of 532 nm. [after *Rapp et al.*, 2002b, copyright by the American Geophysical Union]

drying effect due to ice particles in the summer mesopause region.
Rapp et al. [2002b] further used this model in order to interpret in situ observations of mesospheric temperatures with high spatial resolution that showed simultaneously observed NLC being located in a local gravity wave-induced temperature minimum (see an example of observations of temperatures and winds in Figure 24). *Rapp et al.* [2002b] studied the influence of such gravity wave induced disturbances on NLC with a two dimensional version of CARMA and could indeed reproduce the observed coincindence of local temperature minima and the NLC height for gravity wave parameters derived from measurements. In general, these authors further found that such a correlation is only expected for long period gravity waves with periods larger than ∼6.5 hours. In this case the time development of the particle microphysics and the temperature change along the trajectory of an ice particle are synchronized in the sense that the ice particles acquire a maximum residence time in the cold phase of the gravity wave. Model results for two different wave periods, i.e., 7 hours and 1 hour, are contrasted to each other in Figure 25. Finally, it is noteworthy that *Rapp et al.* [2002b] further found that gravity waves with periods smaller than the above mentioned 6.5 hours will tend to reduce NLC brightness whereas longer period waves should enhance brightness. Indeed, evidence for short period gravity waves reducing NLC brightness has recently been reported by *Thayer et al.* [2003]. In summary, the study by *Rapp et al.* [2002b] demonstrated the CARMA model to be a suitable tool to study ice particles in the summer mesopause environment.

4.2 An empirical proxy

As demonstrated in the previous section, the CARMA model satisfactorily describes the physics of the formation and growth of mesospheric ice particles. Subsequently, *Rapp et al.* [2003c] combined CARMA with the aerosol charging model described by *Rapp and Lübken* [2001] hence also allowing to simulate not only neutral but also charged aerosol particles. In order to test the idea that the main features of PMSE depend on microphysical properties of these charged aerosol particles, *Rapp et al.* [2003c] suggested a simple empirical proxy for PMSE that can be studied with the aid of CARMA. *Rapp et al.* [2003c] assumed that the most important physical process creating PMSE is the reduction of electron diffusivity due to the presence of charged aerosol particles. If this were the case, PMSE signal strength should be proportional to the charge number density ($|Z_A|N_A$) and the square of the radius of these

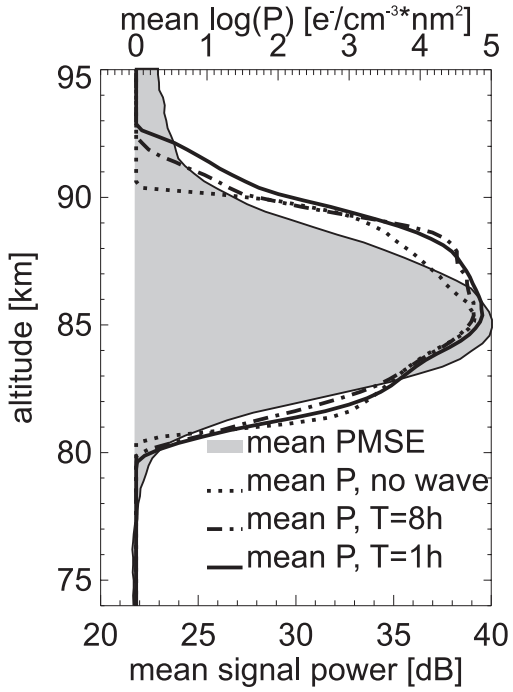

Figure 26: Grey shaded area: Mean observed PMSE signal power during the months June and July 2000. Dotted line: Mean proxy profile obtained by time averaging 24 hour CARMA model simulations. Solid, dotted, and dashed-dotted line: Mean proxy profiles obtained from CARMA simulations including gravity wave activity for wave periods of 8 hours and 1 hour, respectively. This Figure is reproduced from *Rapp et al.* [2003c], copyright by the American Geophysical Union.

particles (r_A^2) since the aerosol particle diffusion coefficient is expected to vary like ($1/r_A^2$) [e.g., *Cho et al.*, 1992]. Taken together, the proxy P was defined as

$$P = |Z_A| N_A \cdot r_A^2. \tag{1}$$

Note that such a dependence could then potentially also explain observations where strong PMSE was observed when the ratio $|Z_A| N_A / N_e$ was significantly smaller than 1 (see section 3.2).

Rapp et al. [2003c] showed that the proxy calculations indeed reproduce the observed mean PMSE profile. Figure 26 compares mean proxy profiles derived from averaging 24 hour model simulation runs for different background conditions (i.e., undisturbed and with two different gravity waves) with the mean PMSE signal strength as observed during the months June and July 2000. Evidently, the main features like altitude range and the altitude of the average PMSE maximum are nicely reproduced. In addition, the proxy calculations further suggested that individual PMSE (i.e., not averaged) should usually have their absolute maximum close to the lower edge of the layer due to the predicted dependence of the PMSE signal on the particle radius which is expected to be largest at the bottom of the ice cloud. In fact, this prediction has been confirmed by a statistical analysis of PMSE data from three complete PMSE seasons studied with the ALWIN VHF radar [see Figure 8 in *Rapp et al.*, 2003c].

Apart from the general agreement between mean proxy and PMSE profiles, the proxy also proved to be useful for the interpretation of case studies: Figure 27 compares ground based and in situ observations performed during the DROPPS campaign in July 1999 and model results [*Rapp et al.*, 2003c]. The observations show a double layer PMSE together with a weak

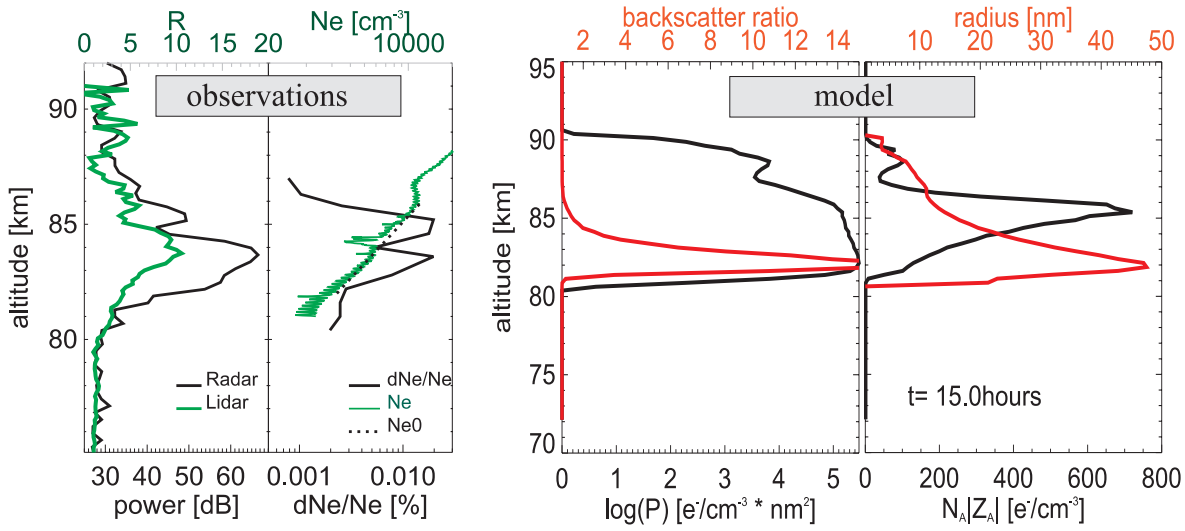

Figure 27: Left two panels: profiles of echo power received with the ALWIN VHF radar (black, left), backscatter ratio measured with the ALOMAR RMR lidar (green, left), electron number densities (green, right) and electron number density fluctuations at the radar Bragg scale (black, right) both measured in situ with the CONE instrument during sounding rocket flight MDMI05 on July, 6, 1999. The dotted line indicates an estimate of the undisturbed electron number density profile in the absence of ice particles. Right two panels: Model results of the proxy P (black,left), the calculated backscatter ratio (red, left), the charged particle number density (black, right) and the aerosol particle radius (red, right) [after *Rapp et al.*, 2003c, copyright by the American Geophysical Union].

NLC that peaks at exactly the altitude where the PMSE has its lower maximum. The in situ measurements performed at the time of these ground based observations reveal an electron number density profile that shows a significant depletion ('biteout') only in the upper part of the PMSE layer with the strongest depletion in between the two PMSE maxima. These observations are in line with the results discussed in section 3.2 showing that PMSE is observed at altitudes with only a small value of $|Z_A|N_A/N_e$. It turns out that the microphysical model calculations of the charged aerosol number densities, proxy-profiles and lidar backscatter ratios can readily reproduce these observations (right two panels in Figure 27). The proxy profile shows a double peak structure with the maximum of the calculated backscatter ratio coinciding with the lower maximum of the proxy. The model simulations further show that the lower proxy maximum is due to the presence of just a few but large particles (via the r_A^2-dependence) and that the largest amount of charged particles (corresponding to an electron number density depletion) appears exactly in between the two proxy maxima. The upper proxy maximum is created by a secondary maximum in the particle charge number density that occurs due to a second nucleation cycle of particles during their time development [*Rapp et al.*, 2003c].

At this place, it is noteworthy, that this layering effect may also be a candidate for the explanation of the frequent observation of PMSE in at least two distinct layers. *Hoffmann et al.* [2003] considered this mechanism in more detail and also investigated the influence of long period gravity waves on this layering mechanism. They ran the same microphysical model mentioned above, however, this time vertical winds and temperatures were disturbed by the influence of a long period gravity wave with a vertical wavelength of 6 km, a horizontal wavelength of 595 km and a period of 470 min. Figure 28 shows results of calculated proxy

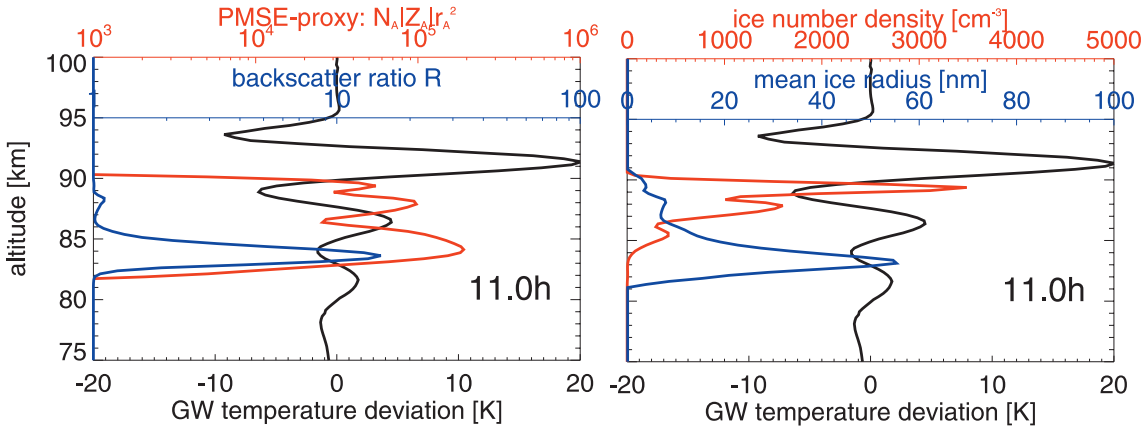

Figure 28: Left panel: altitude profiles of proxy (red line), temperature variations (black line), and lidar backscatter ratio (blue line). Right panel: altitude profiles of ice number densities (red line), temperature variations (black line), and ice particle radii (blue line) [*Hoffmann et al.*, 2003].

values and other relevant microphysical parameters. Figure 28 clearly shows that the gravity wave induced temperature variations have a strong influence on the resulting proxy profile: unlike for undisturbed conditions (Figure 27) the proxy shows three distinct layers peaking at 83, 87, and 90 km altitude. Looking at the altitude profiles of aerosol radii and number densities it becomes clear that this pronounced layering is mainly due to a structuring in the number density of the ice particles. Further analysis of the model simulations at different times (not shown here) shows that the layering occurred because of subsequent nucleation cycles of ice particles in the uppermost (and coldest) gravity wave induced temperature minimum. Subsequently, these newly created ice particles grow and sediment down which also leads to the effect that the ice particles layers are not necessarily confined to the altitude range of the temperature minimum. Based on these ideas *Hoffmann et al.* [2003] further analyzed one particularly prominent two layer PMSE event for gravity wave activity and could indeed identify an inertio gravity wave with an intrinsic period of ∼3 hours, a horizontal wavelength of ∼310 km and a vertical wavelength of ∼4 km. Hence, in the case study analyzed by *Hoffmann et al.* [2003] the idea that multi-layer PMSE are created through the action of gravity wave induced temperature minima where subsequent nucleation leads to a pronounced layering in the ice particle density is consistent with observations. However, further work is clearly needed in order to show that the simultaneous occurrence of the low frequency gravity wave and the multi-layer PMSE is not by chance but that the wave is indeed creating the layering in the PMSE.

In summary, the overall good agreement of model and PMSE properties strongly supported the view that charged aerosol particles and their influence on electron diffusivity are the key physical process for our understanding of PMSE. This triggered *Rapp and Lübken* [2003a] to reconsider the corresponding theory. Their main results are discussed in the next section.

4.3 The diffusion of electrons in the vicinity of charged particles revisited

The basic diffusion equations describing the temporal development of small scale disturbances in a three-component quasi-neutral plasma were first presented by *Hill* [1978] and may be written as

$$\frac{\partial n_e}{\partial t} = \frac{D_i - D_A}{2}\nabla^2 n_\oplus + \left[D_i + \frac{D_i + D_A}{2}(1+2\Lambda)\right]\nabla^2 n_e \tag{2}$$

$$\frac{\partial n_\oplus}{\partial t} = \frac{D_i + D_A}{2}\nabla^2 n_\oplus + \left[D_i + \frac{D_i - D_A}{2}(1+2\Lambda)\right]\nabla^2 n_e \tag{3}$$

where n_e and $n_\oplus = n_i + n_A$ are small scale disturbances of the electron number density and the total number density of positive ions and charged aerosol particles, i.e., $N_e = N_{e0} + n_e$, $N_i = N_{i0} + n_i$, $N_A = N_{A0} + n_A$ and $N_\oplus = N_{\oplus 0} + n_\oplus$. D_i and D_A are the diffusion coefficients of positive ions and charged aerosol particles [see *Cho et al.*, 1992, for appropriate expressions], respectively, and $\Lambda = |Z_A| N_A / N_e$. The underlying physical assumptions to equations 2 and 3 are: 1. quasi neutrality (i.e., outside the Debye-sphere the sum over all charges is zero), 2. zero net current, 3. no mean motion of the plasma species (i.e., due to a neutral wind or gravitational settling), and 4. no external electric and magnetic field. Equations 2 and 3 describe the diffusion of the differently charged species that is coupled through the Coulomb interaction between the constituents. Since there are Coulomb forces between the positive ions and electrons on the one hand and charged particles and electrons on the other, it turns out that the above described system possesses two distinct diffusion modes characterized by two different eigenvalues for the electron diffusion coefficient. These eigenvalues have been discussed in detail in *Rapp and Lübken* [2003a]. In short, the one diffusion coefficient (D_1^0) has the same order of magnitude as the ion diffusion coefficient but shows some dependence on the parameter Λ. The second diffusion coefficient (D_2^0) is roughly given by the aerosol diffusion coefficient and varies with the aerosol radius like $1/r_A^2$.

One of the crucial steps towards an understanding of PMSE now lies in the question for the initial condition under which the diffusion system above is to be studied. As argued in *Rapp and Lübken* [2003a], the zero net current and charge neutrality requirement lead to anticorrelated fluctuations in the charged aerosol particles and electrons as the physically most appropriate initial condition. The basic physical idea behind this is the picture that initially the charged aerosol particles are transported due to the turbulent velocity field and the accompanying shear. This transport, however, is equivalent to a charge current that must be compensated by an oppositely directed current of the electrons in oder to maintain zero net current and local charge neutrality. Note that the resulting anticorrelation between negatively charged particles and electrons is indeed in line with the available experimental evidence on small scale structures in the electron and charged particle distribution (see section 5.4). *Rapp and Lübken* [2003a] solved equations 2 and 3 analytically for the case of idealized Gaussian disturbances in the plasma species. One example of such calculations is shown in Figure 29. Concentrating first on the solutions for the electron disturbance it appears that the decay process divides into two significantly different parts: while the amplitude of the electron fluctuation decays quickly (i.e. in less than 100 s) from a value of 1 (in units of $n_A(0,0)$) to a value of $\sim$0.5, it takes $\sim$2 hours to further decay to a value of 0.1. If we look at the contributions to the electron solution due to the D_1^0- and D_2^0-eigenmode we see that the D_1^0-eigenmode (due to positive ions: $D_1^0 \approx D_i$) dominates the first period whereas the D_2^0-eigenmode (due to charged particles: $D_2^0 \approx D_A$) dominates the second period of diffusional decay (see *Rapp and Lübken* [2003a] for a thorough discussion of this behaviour). Hence, after a short initial time, the diffusion speed of the electrons is entirely determined by the diffusion speed of the charged aerosol particles. Note that unlike in *Cho et al.* [1992]'s treatment this

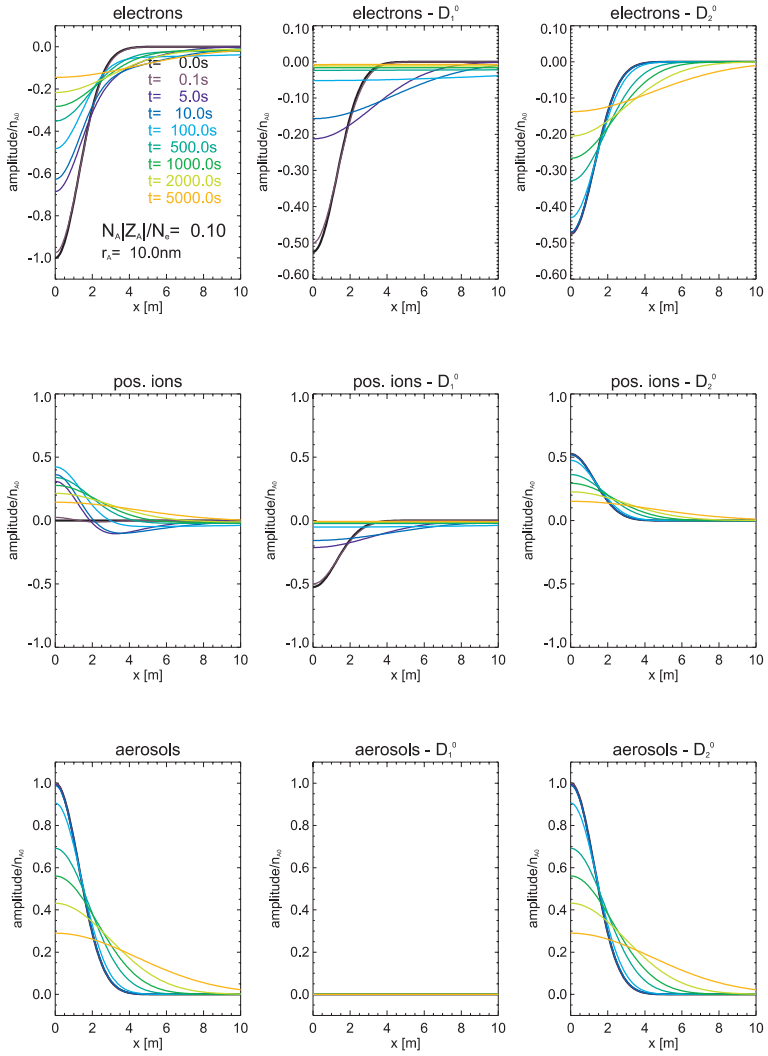

Figure 29: Temporal development of electron, positive ion and charged aerosol particle fluctuations for $|Z_A|N_A/N_e = 0.1$ and r_A=10 nm. The full width at half maximum of the Gaussians has been chosen as 3 m. Panels labeled with D_1^0 and D_2^0, respectively, show the respective contribution due to the D_1^0- and D_2^0 eigenmode. This Figure is reproduced from *Rapp and Lübken* [2003a], copyright by the American Geophysical Union.

general behaviour is almost independent of the parameter Λ, i.e, the ratio between the charge number density of aerosol particles and the free electron number density (see Figure 30)[2]. *Rapp and Lübken* [2003a] further studied the implications of these results for radio wave scattering. According to *Røyrvik and Smith* [1984] the volume reflectivity is basically proportional to the power spectral density of the (absolute) electron number density perturbation at the Bragg scale and can hence be directly calculated from the idealized disturbances shown in Figure 29. Considering only large enough decay times such that the electron diffusion is entirely determined by the diffusion of the charged aerosol particles, *Rapp and Lübken* [2003a] derived that the radar reflectivity should be proportional to $\exp(-2D_2^0 k^2 t)$ with $D_2^0 \approx D_A$ being the electron diffusion coefficient, k being the radar wavenumber, and t being the time.

[2]Closer inspection of *Cho et al.* [1992]'s work actually shows that the Λ >1.2-criterium is artificially created by an unphysical initial condition for their model calculations [see appendix B in *Rapp and Lübken*, 2003a, for a detailed discussion].

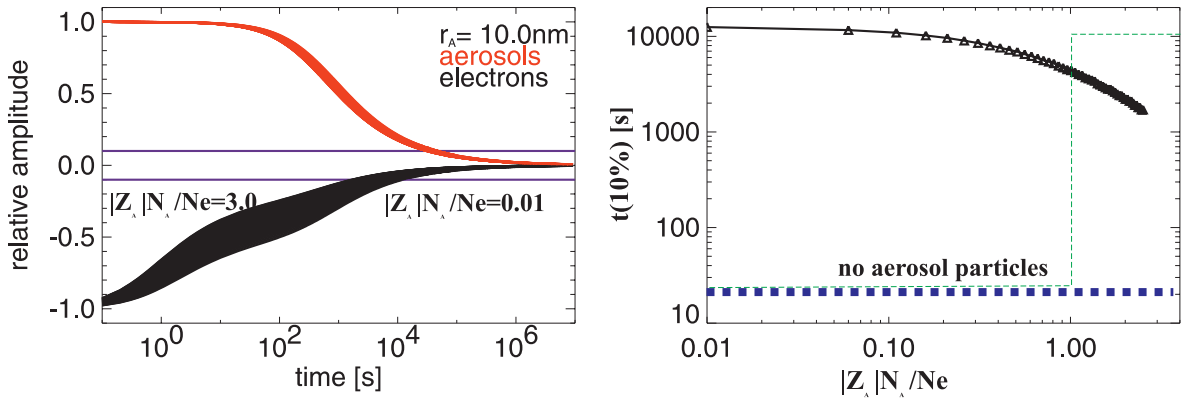

Figure 30: Left panel: Temporal development of the amplitudes of Gaussian disturbances in electrons and charged particles for different values of the parameter $|Z_A|N_A/N_e$. Right panel: Time that the electron amplitude needs to decay to 0.1 of its initial value as a function of $|Z_A|N_A/N_e$. The blue horizontal line indicates the diffusion time for electron disturbances in the absence of charged particles. The green line schematically shows the diffusion time as expected from *Cho et al.* [1992].

This dependence can also be directly used in order to determine the decay time of the radar signal. As shown in *Rapp and Lübken* [2003a] the decay time for a signal decay by Φ dB may be written as

$$\tau_{diff}^{-\Phi dB} = \frac{\Phi/10 \cdot \ln(10)}{2 \cdot D_2^0 \cdot k^2} \approx \frac{\Phi/10 \cdot \ln(10)}{2 \cdot D_A \cdot k^2} \approx 0.02 \cdot \Phi \cdot \frac{\lambda^2 \cdot r_A^2}{\nu} \tag{4}$$

where we have again used $D_2^0 \approx D_A$, the relation $\frac{\nu}{D_A} \approx 6.5 \cdot r_A^2$ [*Lübken et al.*, 1998] and $k = 2\pi/\lambda$. In the rightmost expression of equation 4, the radar wavelength λ is in m, the

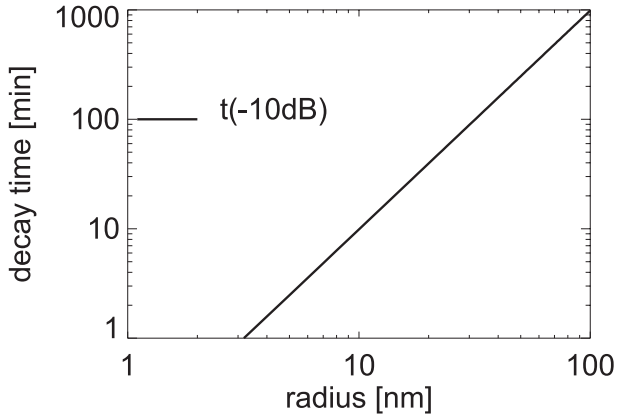

Figure 31: Radar scatter decay time for a relative reflectivity decrease by 10 dB after the PMSE generation mechanism has ceased. This Figure is reproduced from *Rapp et al.* [2003b], copyright by COSPAR.

aerosol radius r_A is in nm and the kinematic viscosity of air, ν, is given in m^2/s, resulting in τ_{diff} being given in s. Equation 4 shows that the diffusional decay time is proportional to the square of the radius of the charged particles involved and the square of radar wavelength. In Figure 31 we present this decay time for a decay by 10 dB as a function of aerosol radius.

Evidently, for particles smaller than 10 nm the decay time is rather short, i.e., only 2.5 min for particles with a radius of 5 nm and 10 min for particles with a radius of 10 nm. Due to the quadratic dependence of the decay time on the aerosol radius, the decay time is already 40 min for aerosol particles with a radius of 20 nm and even 3 hours for particles with a radius of 50 nm which exist in an NLC environment. These long decay times for particle radii larger than say 15 nm suggest that PMSE potentially are a manifestation of fossil neutral air turbulence (for details on the term 'fossil turbulence' see *Woods et al.* [1969]), an idea that was first suggested by *Cho et al.* [1996]. However, these authors estimated that the decay time of the radar echo should not exceed ∼7 min such that the repeated absence of neutral air turbulence in the lower altitude range of the echoes [*Lübken et al.*, 2002] was not likely to be explained by this effect. However, the calculations presented by *Rapp and Lübken* [2003a] strongly suggest that at low altitudes, say below 85 km, where particles are believed to have grown to sizes larger than 15-20 nm due to growth and sedimentation (see also Figure 23), the long lifetime of the structure can 'freeze in' turbulent structures for a considerable time such that the observations of *Lübken et al.* [2002] may become understandable. In the next section we discuss if these model ideas can indeed explain the statistics of PMSE observations based on available data of turbulence observations.

5 The new theory tested

5.1 Back to turbulence

In this section, we discuss if neutral air turbulence in combination with the long lifetime of plasma fluctuations due to the presence of heavy charged particles of low mobility can account for the observed statistics of PMSE observations.

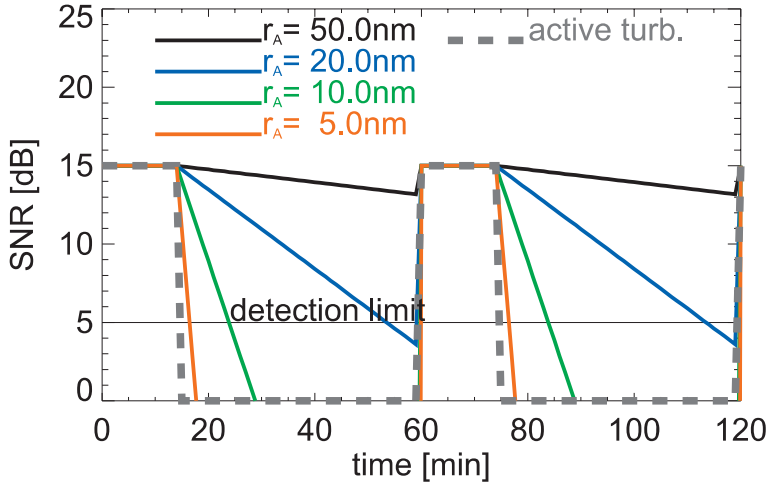

Figure 32: Temporal development of the radar SNR after regular pulses of neutral air turbulence (indicated by grey dashed lines) leading to a SNR of 15 dB. The colored lines indicate the SNR-decay for different aerosol particle radii assumed. The thin horizontal line at SNR=5 dB indicates the detection limit assumed. This Figure is reproduced from *Rapp and Lübken* [2003a], copyright by the American Geophysical Union.

Rapp and Lübken [2003a] have suggested a simple method to estimate the PMSE occurrence frequency based on observed turbulence occurrence frequencies (see Figure 32 for a schematic illustrating this idea). They started from a given occurrence frequency of neutral air turbu-

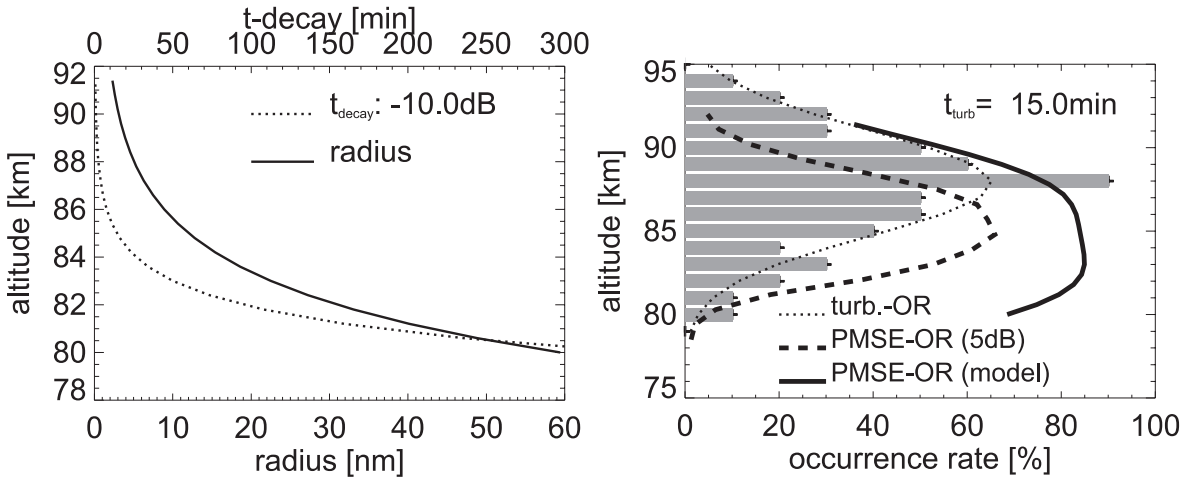

Figure 33: Left panel: assumed aerosol radii (solid lines, lower abscissa) and corresponding decay times for PMSE for a decay by 10 dB (dotted lines, upper abscissa). Right panel: Histogram of the measured turbulence occurrence rate from a total of 10 rocket soundings [*Lübken et al.*, 2002] together with a Gaussian fit to the data (dotted line). The thick dashed line shows the PMSE occurrence frequency at Andøya in the period from 1.6.2000 - 31.7.2000 (only PMSE with SNR >5 dB were counted) and the thick solid line shows our estimate of the PMSE occurrence frequency. This Figure is reproduced from *Rapp and Lübken* [2003a], copyright by the American Geophysical Union.

lence, TOR, and assumed that a turbulent event lasts τ_{turb} ∼15 minutes in accordance with model results and observations [*Andreassen et al.*, 1994; *Czechowsky and Rüster*, 1997]. Note that the actual choice of τ_{turb} is not crucial for the following arguments, see the detailed discussion by *Rapp and Lübken* [2003a]. They further assumed that the turbulent events are equally distributed over a given time interval. Then *Rapp and Lübken* [2003a] calculated the diffusional decay times for a decay by 10 dB (see equation 4) for aerosol properties (altitude profiles of radii and $N_A|Z_A|/N_e$) as determined with the CARMA microphysical aerosol model. Adding now these decay times to the time where turbulence was active and dividing this sum by the total time interval considered, they derived an estimate of the occurrence rate of PMSE, POR, as

$$POR = \begin{cases} TOR \cdot \left(1 + \frac{\tau_{diff}^{-10dB}}{\tau_{turb}}\right) & ; \; if < 100\% \\ 100\% & ; \; else \end{cases} \tag{5}$$

In Figure 33 we show the main result of the investigation of *Rapp and Lübken* [2003a]: Based on a total of 10 sounding rocket measurements of neutral air turbulence under PMSE conditions they have determined the turbulence occurrence frequency as shown by the grey shaded histograms (see also section 3.2). It turns out that turbulence is observed with a symmetrical distribution around a peak altitude of 88 km, which is the altitude of the climatological mesopause at 69°N during summer [*Lübken*, 1999]. The peak occurrence rate at this altitude is 90%, i.e., in 9 out of 10 rocket flights turbulence was observed at this altitude. Based on the observed turbulence occurrence frequency and a modeled altitude distribution of aerosol radii as shown in the left panel of Figure 33, *Rapp and Lübken* [2003a] estimated the PMSE occurrence frequency based on equation 5. The result is shown as the thick black line in Figure 33. Comparing this estimate of POR with the observed altitude

profile of POR it turns out that the general altitude distribution is well reproduced by the model approach presented here, in fact the model even overestimates the PMSE occurrence frequency at all altitudes (while formerly the problem has been to explain that PMSE can be there at all). This, however, is due to the fact that equation 5 assumes that ice particles are always there at mesopause altitudes, an assumption which is most probably not correct. The calculations show some other very interesting features: at high altitudes, i.e., above ∼88 km, POR follows TOR almost one to one. This is due to the fact that ice particles at these altitudes are rather small such that the PMSE decay time as described by equation 4 is short compared to the duration of a typical turbulence event (here assumed to be 15 min). This finding is consistent with the fact that neutral air turbulence was almost always observed in the upper part of a PMSE layer (see section 3.2). At altitudes below 85 km, however, it is striking that POR is significantly larger than TOR, which is certainly a direct consequence of the enhanced lifetime of plasma structures due to the presence of charged particles with larger radii. These findings can thus readily explain why turbulence was very seldomly observed in the lower part of a PMSE layer [*Lübken et al.*, 2002] and shows that indeed neutral air turbulence (together with the details of charged particle- and electron diffusivity discussed above) can account for all observed PMSE.

5.2 Absolute volume reflectivities

It was shown already in section 3.1 that observed volume reflectivities can be quantitatively reproduced on the basis of the neutral air turbulence with high Schmidt number idea. In this section, this question is reconsidered from a more microscopic viewpoint, i.e, we tend to determine absolute volume reflectivities based on the model ideas presented above. It was shown in *Rapp and Lübken* [2003a] that the volume reflectivity due to the idealized Gaussian disturbances introduced above (see Figure 29) may be written as

$$\eta(k) = -n\frac{k^2}{(8\pi)^3}\frac{e^4}{\epsilon_0^2 m_e^2 f^4}\cdot n_{e0}^2\cdot\sigma^2\cdot e^{-k^2\sigma^2}\cdot\left(\frac{D_i - D_2^0}{D_1^0 - D_2^0}\right)^2\cdot e^{-2D_2^0 k^2 t} \tag{6}$$

where n is the typical spectral index at the radar Bragg scale, k is the wavenumber of the radar, e is the electron charge, ϵ_0 is the permittivity of space, m_e is the electron mass, σ is the width of the Gaussian, and D_1^0 and D_2^0 are the diffusion coefficients described above. Using typical values of n=-1, k=$2\pi/6$ m, r_A=15 nm, Λ=0.1, f=50 MHz, σ =1.27 m (yielding a full width at half maximum of 3 m), n_{e0}=250 cm^{-3} and t=100 s we arrive at a volume reflectivity of $\eta \approx 9\cdot 10^{-13}$ m^{-1}. Comparing this value to the absolute reflectivities observed at ∼50 MHz stated in Table 1 we see that this value has indeed the correct order of magnitude. This estimate (together with the arguments presented in section 3.1) demonstrates that also the absolute volume reflectivities summarized in Table 1 can be readily explained in the scope of the theory by *Rapp and Lübken* [2003a].

5.3 Spectral width and aspect sensitivity

As pointed out in section 2.1.2 one of the most intriguing properties of PMSE is the often very narrow Doppler spectrum of the received signal. The Doppler spectrum is expected to be broad in the presence of active neutral air turbulence due to the turbulent velocity fluctuations. According to *Gibson-Wilde et al.* [2000] the velocity variance which is directly related to the width of the Doppler spectrum can be expressed in terms of the turbulent energy dissipation rate ϵ as

$$w_{rms} = \pm\sqrt{\frac{\epsilon}{5\cdot 0.4\ \omega_B}} \tag{7}$$

where ω_B is the mean Brunt frequency over the altitude range where the turbulent event takes place, and the factor 5 is a correction factor to an earlier formula from *Hocking* [1985] which *Gibson-Wilde et al.* [2000] derived from a direct numerical simulation of the VHF-radio scatter created by mesospheric turbulence. If we use ω_B=1.5·10^{-2} s^{-1} and a rather large value for ϵ of 0.5 m^2/s^3 (=0.5 W/kg) for the polar summer mesopause region [*Lübken et al.*, 2002] we see that ±5.8 m/s are a typically expected velocity variance due to relatively strong turbulence. Contrary to this, velocity variances derived from Doppler spectra in PMSE are often less than ± 1 m/s [*Cho and Kelley*, 1993]. However, in section 4.3 we have made the point that the electron irregularities are expected to prevail a significant time after the neutral air turbulence has ceased. Under these conditions, however, the velocity variance which determines the spectral width of the radar echo is in fact expected to be very small. For example, if we roughly estimate the 'minimum' turbulent energy dissipation rate from $\epsilon_{min} = \nu \cdot \omega_B^2$ as suggested by *Lübken* [1992] and use ν=2 m^2/s and the same Brunt frequency as before, we get ϵ_{min}=0.0005 m^2/s^3 resulting in w_{rms}=0.1 m/s which has the correct order of magnitude. These estimates indicate that the observed spectral width can be explained in the scope of the theory presented here. Furthermore, these ideas also directly explain the altitude dependence of the spectral width as described in section 2.1.2: with a higher turbulence occurrence rate at the higher altitudes and a rather low turbulence occurrence rate at the lower altitudes (see section 3.2) the spectral width is expected to be large at the upper altitudes and small at the lower altitudes, respectively. Taking it the other way round, these results imply that spectral width measured in PMSE can indeed be used to determine turbulent energy dissipation rates. It is though important to note that the information on the turbulence strength comes only from the spectral width and not from the total echo power of the observed signal since the echo power also depends on quantities that are not related to neutral air turbulence like the size of the charged aerosol particles involved.
Regarding observed aspect sensitivities (i.e., large at the bottom and low at the top of the PMSE layer) we further note that at least the low aspect sensitivities at the top of the PMSE layers are understandable in the scope of enhanced turbulent activity at these altitudes. At the lower altitudes it may be plausible to argue that the fossil structures that are frozen into the charged particle and hence electron distribution may become anisotropic for example by sedimentation effects in the ice aerosol layer. This idea has, however, not yet been quantified and will need closer inspection in the future (see also section 6).

5.4 Small scale structure of plasma species and related power spectra

Recently, *Rapp et al.* [2003a] have further checked if observed small scale fluctuations in the electrons and charged particle distribution show indeed all the features predicted by *Rapp and Lübken* [2003a]. In particular, *Rapp et al.* [2003a] checked if the small scale fluctuations of electrons and charged particles are indeed anticorrelated and if the spectra of these small scale fluctuations indeed show the spectral form as predicted from a combination of the theory by *Batchelor* [1959] (in the case of active turbulence) and *Rapp and Lübken* [2003a] (in the case that the active turbulent activity has stopped).
In Figure 34 data samples of such observed disturbances in the electron and charged aerosol number density as measured during flight ECT02 in 1994 are presented [see *Havnes et al.*, 1996b, a, for more details on this data set]. In Panels a and b, the anticorrelation between the two data sets is obvious with corresponding correlation coefficients as large as ∼-0.8. Panel c shows one example, where the instruments did not observe any fine scale structure and Panel d shows one example where in fact a strong positive correlation between electrons and negatively charged aerosol particles was observed. A possible explanation of such a

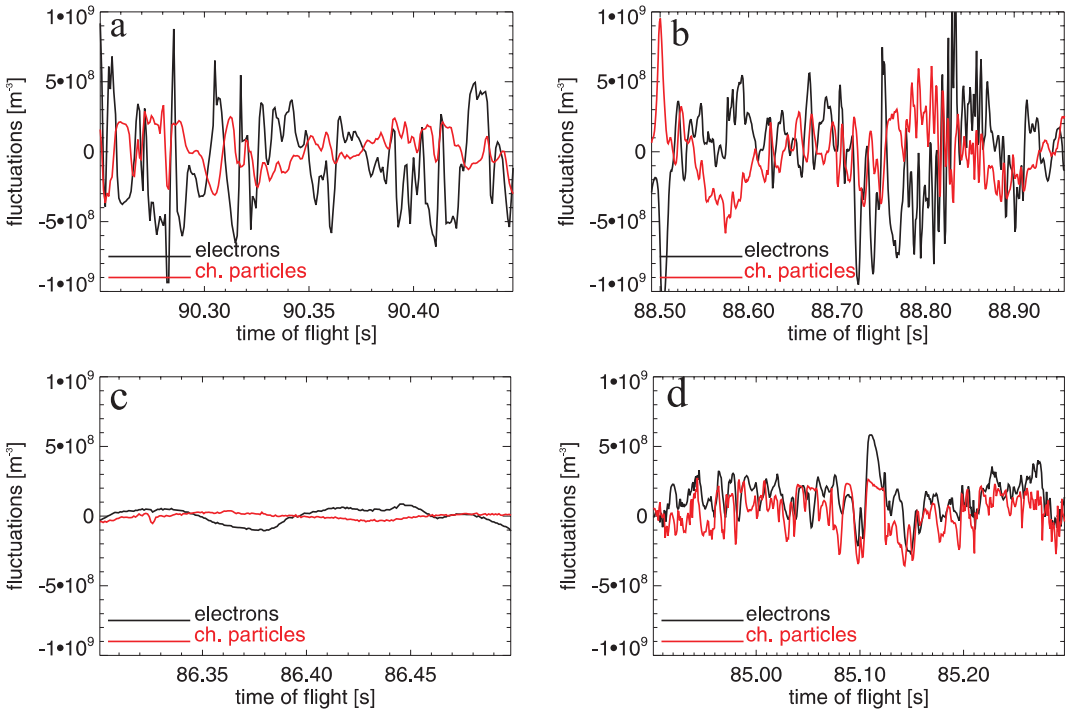

Figure 34: Perturbations of electron (black line) and aerosol charge number densities (red line) during four selected time intervals during sounding rocket flight ECT02 in July 1994. Note that the two data sets must be shifted by ∼2.5 ms for comparison since one measurement was made at the tip of the sounding rocket and the other in the rear (with a separation of 2.5 m and a rocket speed of 1000 m/s) [*Rapp et al.*, 2003a].

feature was presented in the theoretical study by *Lie-Svendsen et al.* [2003] who proposed that a positive correlation could either occur in the presence of evaporating particles or in the presence of large and hence quickly sedimenting particles. In a recent study, *Blix et al.* [2003b] analyzed similar observations together with simultaneous temperature measurements and found indeed support for the idea that evaporating ice particles are causing the observed positive correlations. In any case, such features have only been observed at the bottom of PMSE layers and must be considered as a specialty whereas the standard shows indeed the anticorrelation predicted by multipolar diffusion theory.
Rapp et al. [2003a] further considered the spectral shape of small scale disturbances in the electron and charged particle distribution. Based on the model of *Rapp and Lübken* [2003a] they found that the general spectral shape acquired during a phase of active neutral air turbulence (as described by *Batchelor* [1959]) should not change but just decay according to

$$\Gamma(k,t) = \underbrace{\frac{2\chi}{k}\sqrt{\frac{\nu}{\epsilon}} \cdot exp\left(-2l_B^2 k^2\right)}_{Batchelor,1959} \cdot e^{-D_A k^2 t} \tag{8}$$

where the underbraced part of the equation is the power spectrum at the time the neutral air turbulence stopped [*Batchelor*, 1959]. Here, χ is the rate at which fluctuations of the considered tracer are dissipated, $l_B = (\nu D^2/\epsilon)^{\frac{1}{4}}$ is the so-called Batchelor-scale, and D denotes the diffusion coefficient of the tracer. Hence, power spectra of electrons and charged particles should reveal a viscous convective subrange with its prominent k^{-1}-power law as predicted by *Batchelor* [1959] even a considerable time after the active neutral air turbulence has stopped.

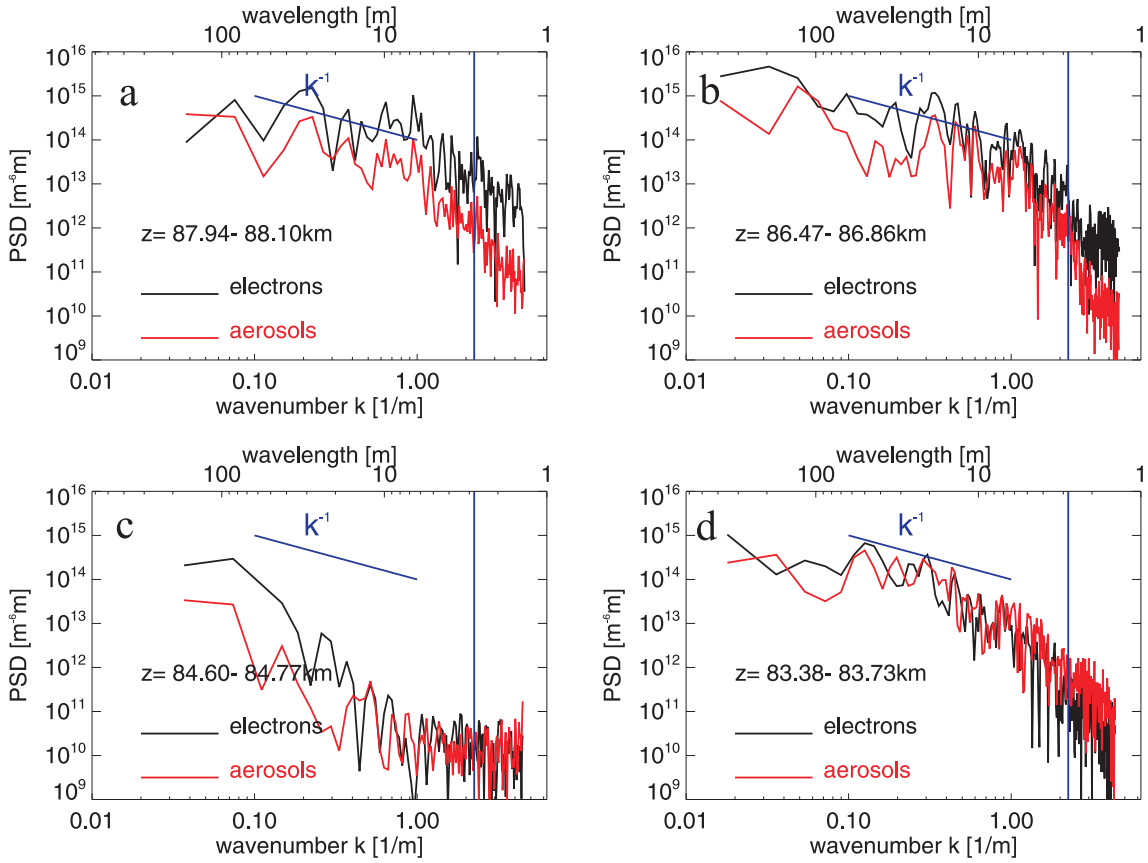

Figure 35: Power spectra of electron number density (black lines) and particle charge number density fluctuations (red lines) shown in Figures 34. The inclined line represents a spectral slope of -1 and the vertical line marks the radar Bragg scale (=2.8 m) [*Rapp et al.*, 2003a].

Indeed, the power spectra of the fluctuations shown in Figure 34 reveal indications of a viscous convective subrange and hence confirm these ideas (see Figure 35). *Rapp et al.* [2003a] also tried to classify the spectra shown in Figure 35 as 'actively turbulent' or 'fossil' based on neutral air turbulence measurements onboard the same sounding rocket and attributed spectrum (a) as 'active' whereas spectra (b) and (d) were 'fossil'. However, *Rapp et al.* [2003a] also pointed out that turbulence and plasma measurements were conducted during different parts of the rocket trajectories, i.e, the plasma measurements were made on the ascent and the turbulence measurements were made on the descent part of the rocket trajectory. Hence, this classification must be considered with some caution since the turbulent structure (as well as the structure of the plasma profiles) might be horizontally non-uniform.
In any case, all the results regarding small scale observations of plasma consituents at PMSE altitudes are consistent with the theoretical ideas by *Rapp and Lübken* [2003a] suggesting that PMSE can be explained by a combination of active and fossil neutral air turbulence acting on the large and heavy charged aerosol particles which are subsequently mirrored in the electron number density distribution that becomes visible to a VHF radar.

6 Conclusions

Polar mesosphere summer echoes are a unique geophysical phenomenon from many different points of view. Through their close relationship to ice particles, PMSE are a direct indicator for extremely low temperatures (i.e., less than ∼150 K) at mesopause altitudes. Hence, long term observations of PMSE have the potential to yield insight into the long term behaviour of the mesopause temperature, a quantity that has been suspected to change due to anthropogenic action. From a more technical point of view, the observation of PMSE allows for consistency checks with remote sensings of temperatures from satellites in an altitude range where other direct measurements of temperatures are almost unavailable (with the exception of in situ temperature measurements from sounding rockets that due to their significant costs can only be performed sporadically). In addition, these ice particles are conservative and passive tracers for the background wind field to a very good approximation, such that the observation of PMSE also allows for the derivation of winds and its short term variability induced for example by gravity waves. Owing to their usually very high signal to noise ratio (often in excess of 30 dB) PMSE observations allow to track wave motions in the atmosphere on the shortest time scales (down to a couple of minutes) that can otherwise not be accessed at all. Since these wave motions are usually excited in the troposphere, PMSE also provide a suitable tool for the study of the coupling of different atmospheric altitude regions. As described in the current manuscript, Doppler spectral width measurements in PMSE further allow for a near continuous characterization of mesospheric turbulence which is a significant contribution to the energy budget at these altitudes with corresponding heating rates in excess of the radiative input. Finally, apart from its obvious importance for the study of the Earth's middle atmosphere, PMSE further allow to study basic physical processes with significance far beyond atmospheric physics: Being caused by the turbulent advection of charged species in an ice loaded complex plasma, the study of PMSE also allow insights into the characteristics of turbulence itself and the behaviour of complex plasmas which are both areas of current intensive research.

In the current manuscript we have studied the physics of PMSE in detail: Starting from a review of the available experimental and theoretical results about polar mesosphere summer echoes we have shown that prior to this work there has been an obvious deficit in the physical understanding of the generation mechanism of these strong radar echoes.

Among the available theories, the *Cho et al.* [1992]-theory was shown to be the most promising one even though questions regarding some crucial assumptions like the requirement for the presence of neutral air turbulence were raised as early as 1993 [*Lübken et al.*, 1993b].

Consequently, the *Cho et al.* [1992]-theory was investigated in detail: on the one hand strong evidence was presented that

1. Water ice aerosol particles play a decisive role for the creation of the echoes. This evidence came from the comparison of temperatures measured in situ in the vicinity of PMSE with an unprecendented altitude resolution of ∼200 m and a relative accuracy of 2 % (paper 5).

2. Absolute volume reflectivities can be quantitatively reproduced at all radar frequencies between 50 MHz and 933 MHz based on the *Cho et al.* [1992]-theory. This could be shown on the basis of recent in situ measurements of the Schmidt number and turbulent energy dissipation rates (paper 5, this study).

3. Reduced electron diffusivity is indeed the key-physical process allowing for the existence of PMSE. This was proven through the successful interpretation of the combined PMSE/electron heating experiment [*Chilson et al.*, 2000] in the scope of the temperature dependence of electron diffusivity in the vicinity of charged aerosol particles (papers 10 and 11).

On the other hand, it was also shown that

1. Neutral air turbulence was regularly only observed in the upper altitude portion of simultaneously observed PMSE layers. This result came from the analysis of a total of ten sounding rocket flights where neutral air turbulence was measured in situ under PMSE conditions (papers 5 and 6).

2. The charge balance does not have to be dominated by the charge density of aerosol particles as required by the *Cho et al.* [1992]-theory. This was shown from the analysis of rocket borne measurements of plasma species like electrons, positive ions and charged aerosol particles at PMSE altitudes and from the analysis of observed PMSE behaviour during a major solar proton event in July 2000 (papers 2 and 3).

Taken together, these results strongly supported the idea that reduced electron diffusivity due to the presence of charged aerosol particles is one of the key physical processes for the creation of PMSE but that so far a quantitative understanding of this physical process is lacking.

Hence, the microphysics of ice particles at around the polar summer mesopause was further investigated with the aid of a microphysical model for the generation and growth of mesospheric ice particles. The model was applied to the investigation of in situ observations of gravity wave induced temperature variations and the occurrence of NLC. It was shown that the observed coincidence of local temperature minima and NLC altitude is a direct consequence of the local temperature disturbance on the ice particle microphysics (paper 1).

After having demonstrated the suitability of the microphysical model for the study of ice particles around the mesopause, the ice particle model was combined with a model for the charging of aerosol particles in the plasma of the D-region [*Rapp and Lübken*, 2001] and a microphysical proxy was proposed in order to test the idea that reduced electron diffusivity is the most important physical process for the creation of PMSE. Indeed the proxy was shown to be successful to explain ground based and in situ observations of PMSE, NLC and electron number densities and it also led to the proposal of a new mechanism that can potentially explain the occurrence of multi-layer PMSE through the layering of charged ice particles in local temperature minima due to low frequency gravity waves. In addition, the proxy provided estimates of the mean altitude range and the mean altitude of maximum PMSE signal strength in accordance with climatologically representative observations (papers 4 and 12).

These results led to a reconsideration of the theory of electron diffusion in the vicinity of charged aerosol particles. It was argued that small scale disturbances in the aerosol charge number density and the electron number density are expected to be anticorrelated because of simple charge neutrality and zero net current arguments. Based on this assumption it was shown that the electron diffusivity is expected to be reduced almost independently of the relative portion of aerosol charge number density and free electron number density. Furthermore, it was found that the lifetime of electron irregularities due to irregularities in the aerosol charge number densities depends on the square of the aerosol radius and hence varies between a couple of minutes for $\sim$5 nm particles and several hours for $\sim$50 nm particles

(papers 7 and 8).

Based on these results, it was then shown that the combination of the observed turbulence occurrence frequency with these extended lifetimes of small scale structures can resolve the observed discrepancy between observations of neutral air turbulence and PMSE. In particular at the lower altitudes where particles are expected to have grown to radii say larger than 20 nm, the extended lifetime of the small scale structures readily explains why small scale irregularities in the electron number density may exist even though turbulence generated small scale irregularities in the neutral gas may have already decayed for a long time (paper 7).

Subsequently, the theory described in paper 7 was applied in order to explain other relevant observational evidence related to PMSE: It was demonstrated that the observed spectral width of Doppler spectra in PMSE can also be directly explained in the scope of the proposed theory: the spectral width is broadened due to velocity fluctuations in the neutral gas that are only there during phases of active neutral air turbulence. In all other cases, the spectral width is expected to be narrow in accordance with observations. Given this understanding of the spectral width of PMSE Doppler spectra it is concluded that the spectral width may be used to derive the turbulent energy dissipation rate at mesospheric altitudes from PMSE observations (paper 7).

Similarly, observed aspect sensitivities can be explained by the same morphology of active and fossil neutral air turbulence: in the upper portion of the PMSE layer, neutral air turbulence is frequently there and hence leads to a reduced aspect sensitivity. At lower PMSE altitudes, however, neutral air turbulence and the existence of small scale irregularities in the electrons and charged particles are de-coupled from each other by the extended lifetime of these structures. Hence, processes like for example sedimentation of ice particles may lead to the creation of anisotropy that is observed as aspect sensitivity. At this point, however, more quantitative work is clearly needed (paper 7 and this study).

Finally, it was shown that small scale irregularities of the spatial distribution of electrons and charged particles are indeed anticorrelated as expected from the theory presented in paper 7. In addition, it was shown that the power spectra of these small scale irregularities of both species showed a spectral shape as expected on the grounds of the work by *Batchelor* [1959] and the work presented in paper 7. It was also shown that the general spectral shape described by *Batchelor* [1959] (in the particular the presence of a viscous-convective subrange with a spectral slope of -1) is not expected to change until a considerable time after the cessation of neutral air turbulence (paper 9).

In summary, the advanced understanding of PMSE presented in this manuscript has only become available because of a unique set of observational results from ground based experiments (radars and lidars), in situ experiments from sounding rockets, model results from numerical models, and rigorous theoretical investigations. Among these contributions, the in situ experiments provided observations on scales that were not accessible by any other method and proved to be highly relevant for our understanding of the physics involved. This is a strong argument in favor of continued experimental efforts applying sounding rockets to study the Earth's middle atmosphere.

Outlook
As far as future work on PMSE is concerned we see the following promising areas:

1.) Simultaneous and continuous observations of mesospheric turbulence strength (for example with a narrow beam MF radar), PMSE (observed with a VHF radar) and aerosol particles sizes (with a multi-color lidar) should be conducted in order to check the above described scenario with frequent turbulent activity and small ice particles in the upper portion of the PMSE layer and only occasional turbulent activity but large ice particles in the lower part of the layer. The same experiment could also yield useful data to check the relation between spectral width in PMSE and turbulent activity.

2.) Only very little is known so far about the degree of isotropy of mesospheric turbulence as well as its horizontal homogeneity. Indications for anisotropy and horizontal inhomogeneity come from the details of radar Doppler spectra (see section 2.1.2) and comparisons between electron number density profiles and PMSE (see paper 9). In order to study these issues, sounding rocket payloads carrying several small 'daughter' payloads should be developed that are to be ejected from the main payload during the traverse of a PMSE layer and hence yield a horizontal picture of the turbulent irregularity field. First attempts have been made before [*Blix and Thrane*, 1985], however, at that time experiments were just at the edge of feasibility. Today, the miniaturization of electronics allows for a much more robust design of such rocket probes so that the success-rate should be much better than during previous attempts.

3.) Regarding the microphysics of the involved ice particles the most important remaining open question is about the actual origin of the ice particles. It has long been assumed that the ice particles nucleate on meteoric smoke particles, however, direct experimental evidence for the existence of these particles is not available. In order to confirm the existence of these nuclei *Rapp et al.* [2003d] have recently proposed a rocket experiment that is based on the idea to charge the particles photo-electrically by the radiation of a UV-flashlamp and subsequently detect them by a sensitive electrometer. Should this attempt be successful, further work should be done in order to identify the composition of the particles and their creation through the ablation of meteorites in the mesopause region and the subsequent microphysical processes.

4.) Both from rocket borne experiments [*Mitchell et al.*, 2001; *Croskey et al.*, 2001; *Chesworth and Hale*, 1974] and from the observation of so called polar mesosphere winter echoes [*Kirkwood et al.*, 2002, 2003] evidence is emerging for the existence of aerosol particles throughout the entire mesosphere during all times of the year. At altitudes below 80 km and outside the summer season temperatures are far to warm to allow for the existence of ice particles [*Lübken*, 1999]. Hence, rocket borne experiments should be designed to identify the nature of these aerosol particles that may have influences on both the local chemistry (through the possibility for heterogeneous reactions) but also the radiative transfer and hence the energy budget of the middle atmosphere. This is particularly important for the interpretation of observed significant temperature trends in the mesosphere [*Beig et al.*, 2003].

5.) Last but not least, it should be mentioned that given the physical understanding of PMSE presented in this manuscript, these layers are a perfect tool to study the dynamics and thermal structure of the mesopause region. Actually, it turns out that the complex interplay between turbulence, ice particles, and multipolar diffusion of the plasma constituents provides us with a monitoring tool (with a typical signal to noise of $\sim$30 dB or three orders of

magnitude!) that allows to study the mesopause region almost permanently by just applying standard radar technique that is nowadays commercially available. In summary, PMSE will also in the future be an intriguing geophysical phenomenon in its own right, and a useful too in order to gather insight into the complex behaviour of the polar summer mesopause region.

Acknowledgments
I gratefully acknowledge the continous and friendly support of my long year teacher and mentor Prof. Franz-Josef Lübken who started this research many years ago. I am particularly indebted to him for his trust to let me pursue my own ideas and for the many constructive and critical scientific discussions that we had over the past years.

Among the many colleagues and friends from our scientific community I am most thankful to Dr. Tom Blix (FFI, Norway), Prof. Gary Thomas (LASP, USA), and Dr. Jörg Gumbel (MISU, Sweden). Together with Tom Blix we conducted five successful Norwegian/German sounding rocket campaigns achieving experimental results that have contributed a major part to this thesis. Gary Thomas was a generous, friendly, and inspiring host during my visit at the Laboratory for Atmospheric and Space Physics at Boulder, Colorado, in autumn 2000 where we started a collaboration on microphysical modelling of mesospheric aerosol particles with the CARMA model. Jörg Gumbel has been a good friend and inspiring colleague ever since we first met during my first sounding rocket project in winter 1998. I have stopped counting the many fruitful, inspiring, and encouraging discussions that we had ever since.

For the very good cooperation and the extremely pleasant working atmosphere at the Leibniz Institute of Atmospheric Physics here at Kühlungsborn I would like to thank all my colleagues and the technical and administrative staff of the institute. Special thanks goes to Dr. Arno Müllemann, Boris Strelnikov and Hans-Jürgen Heckl who worked with me on the sounding rocket projects. Dr. Erich Becker patiently introduced me to the mysteries of a theoretical understanding of atmospheric dynamics and Dr. Peter Hoffmann and Dr. Ralph Latteck always helped to meet my 'special' requests regarding radar data on short notice.

I would also like to thank Prof. Martin Friedrich (TU Graz, Austria) and Prof. John D. Mitchell (Pennsylvania State University, USA) for reviewing this thesis.

I gratefully acknowledge the excellent support of the sounding rocket campaigns from the following institutions: Andøya Rocket Range (Norway), DLR Mobile Raketenbasis (Germany), and the Norwegian Defence and Research Establishment (Norway). This work was funded through grants by the German Bundesmininsterium für Bildung und Forschung under DLR grants 50 OE 9802, 50 OE 9901, and through the AFO-2000 program.

Last not least, I am indebted to my wife Hoang for all her support and her patience during times of 'strong scientific enthusiasm'.

References

Ackermann, T. P., and O. B. Toon, Absorption of visible radiation in atmosphere containing mixtures of absorbing and nonabsorbing particles, *Appl. Optics*, *20*, 3661, 1981.

Andreassen, O., C. Wasberg, D. Fritts, and J. Isler, Gravity wave breaking in two and three dimensions 1. Model description and comparison of two-dimensional evolutions, *J. Geophys. Res.*, *99*, 8095–8108, 1994.

Balsley, B. B., and M. Huaman, On the relationship between seasonal occurrence of northern hemispheric polar mesosphere summer echoes and mean mesopause temperatures, *J. Geophys. Res.*, *102*, 2021–2024, 1997.

Balsley, B. B., W. L. Ecklund, and D. C. Fritts, VHF echoes form the high-latitude mesosphere and lower thermosphere: observations and interpretations, *J. Atmos. Sci.*, *40*, 2451–2466, 1983.

Balsley, B. B., R. F. Woodman, M. Sarango, J. Urbina, R. Rodriguez, E. Ragaini, and J. Carey, Southern-hemisphere PMSE: where are they ?, *Geophys. Res. Lett.*, *20*, 1983–1985, 1993.

Balsley, B. B., R. F. Woodman, M. Sarango, R. Rodriguez, J. Urbina, E. Ragaini, J. Carey, M. Huaman, and A. Giraldez, On the lack of southern-hemisphere PMSE, *J. Geophys. Res.*, *100*, 11685–11693, 1995.

Batchelor, G. K., Small-scale variation of convected quantities like temperature in a turbulent fluid, *J. Fluid Mech.*, *5*, 113–133, 1959.

Becker, E., and G. Schmitz, Energy deposition and turbulent dissipation owing to gravity waves in the mesosphere, *J. Atmos. Sci.*, *59*, 54–68, 2002.

Becker, E., and G. Schmitz, Climatological effects of orography and land-sea heating contrasts on the gravity wave driven circulation of the mesosphere, *J. Atmos. Sci.*, *60*, 103–118, 2003.

Beig, G., et al., Review of mesospheric temperature trends, *Rev. Geophys.*, *41(4), 1015, doi:10.1029/2002RG000121*, 2003.

Belova, E., P. Chilson, M. Rapp, and S. Kirkwood, Electron temperature dependence of PMSE power: experimental and modelling results, *Adv. Space Res.*, *28(7)*, 1077–1082, 2001.

Belova, E., P. B. Chilson, S. Kirkwood, and M. T. Rietveld, The response time of ionospheric heating to PMSE, *J. Geophys. Res.*, *108(D8), 8446, 10.1029/2002JD002385*, 2003.

Berger, U., and U. von Zahn, The two-level structure of the mesopause: A model study, *J. Geophys. Res.*, *104*, 22083–22093, 1999.

Blix, T. A., The importance of charged aerosols in the polar mesosphere in connection with noctilucent clouds and polar mesosphere summer echoes, *Adv. Space Res.*, *24/12*, 1645–1654, 1999.

Blix, T. A., and E. V. Thrane, Turbulence characteristics as determined by cross correlation analysis, *Proceedings of the 7th ESA Symposium on European Rocket and Balloon Programmes and Related Research, Loen, Norway (ESA SP–229)*, pp. 275–278, 1985.

Blix, T. A., J. K. Bekkeng, R. Latteck, F.-J. Lübken, M. Rapp, A. Schöch, W. Singer, B. Smiley, and B. Strelnikov, Rocket probing of PMSE and NLC - results from the recent MIDAS/MACWAVE campaign, *Adv. Space Res.*, *31*, 2061–2067, 2003a.

Blix, T. A., O. Lie-Svendsen, U. P. Hoppe, and M. Rapp, In situ observations of small scale structure in electrons, positive ions and charged aerosols in the presence of noctilucent clouds and polar mesosphere summer echoes, *Proceedings of the 16th ESA Symposium on European Rocket and Balloon Programmes and Related Research, St. Gallen, Switzerland (ESA SP–530)*, pp. 327–332, 2003b.

Blix, T. A., M. Rapp, and F.-J. Lübken, Relations between small scale electron number density fluctuations, radar backscatter and charged aerosol particles, *J. Geophys. Res.*, *108(D8), 8450, doi:10.1029/2002JD002430*, 2003c.

Bogucki, D., J. A. Domaradzki, and P. K. Yeung, Direct numerical simulations of passive scalars with Pr>1 advected by turbulent flow, *J. Fluid Mech.*, *343*, 111–130, 1997.

Bremer, J., P. Hoffmann, and T. L. Hansen, Geomagnetic control of polar mesosphere summer echoes, *Ann. Geophys.*, *18*, 202–208, 1996a.

Bremer, J., P. Hoffmann, A. Manson, C. Meek, R. Rüster, and W. Singer, PMSE observations at three different frequencies in northern Europe during summer 1994, *Ann. Geophys.*, *14*, 1317–1327, 1996b.

Bremer, J., T. L. Hansen, P. Hoffmann, and R. Latteck, Dependence of polar mesosphere summer echoes on solar and geomagnetic activity, *Adv. Space Res.*, *28*, 1071–1076, 2001.

Bremer, J., P. Hoffmann, R. Latteck, and W. Singer, Seasonal and long term variation of PMSE from VHF radar observations at Andenes, Norway, *J. Geophys. Res.*, *108(D8), 8438, doi:10.1029/2002JD002369*, 2003.

Chaxel, Y., Radar and modelling studies of polar mesospheric summer echoes, Ph.D. thesis, University College London, 1997.

Chesworth, E. T., and L. C. Hale, Ice particulates in the mesosphere, *Geophys. Res. Lett.*, *1*, 347–350, 1974.

Chilson, P. B., E. Belova, M. Rietveld, S. Kirkwood, and U.-P. Hoppe, First artificially induced modulation of PMSE using the EISCAT heating facility, *Geophys. Res. Lett.*, *27*, 3801–3804, 2000.

Chilson, P. B., T. Y. Yu, R. D. Palmer, and S. Kirkwood, Apsect sensitivity measurements of polar mesosphere summer echoes using coherent radar imaging, *Ann. Geophys.*, *20*, 213–223, 2002.

Cho, J., W. Swartz, M. Kelley, and C. Miller, CUPRI observations of PMSE during salvo B of NLC-91: evidence of both partial reflection and turbulent scatter, *Geophys. Res. Lett.*, *20*, 2291–2294, 1993.

Cho, J. Y., and M. C. Kelley, Polar mesosphere summer radar echoes, *Rev. Geophys.*, *31*, 243–265, 1993.

Cho, J. Y., C. M. Alcala, M. C. Kelley, and W. E. Swartz, Further effects of charged aerosols on summer mesospheric radar scatter, *J. Atmos. Terr. Phys.*, *58*, 661–672, 1996.

Cho, J. Y. N., and M. C. Kelley, Enhancement of Thomson scatter by charged aerosols in the polar mesosphere: measurements with a 1.29-GHz radar, *Geophys. Res. Lett.*, *19*, 1097–1100, 1992.

Cho, J. Y. N., and J. Röttger, An updated review of polar mesosphere summer echoes: Observation, theory, and their relationship to noctilucent clouds and subvisible aerosols, *J. Geophys. Res.*, *102*, 2001–2020, 1997.

Cho, J. Y. N., T. M. Hall, and M. C. Kelley, On the role of charged aerosols in polar mesosphere summer echoes, *J. Geophys. Res.*, *97*, 875–886, 1992.

Chu, X., C. S. Gardner, and R. G. Roble, Lidar studies of interannual, seasonal, and diurnal variations of polar mesospheric clouds at the South pole, *J. Geophys. Res.*, *108(D8), 8447, doi:10.1029/2002JD002524*, 2003.

Croskey, C., J. Mitchell, M. Friedrich, K. Torkar, U.-P. Hoppe, and R. Goldberg, Electrical structure of PMSE and NLC regions during the DROPPS program, *Geophys. Res. Lett.*, *28*, 1427–1430, 2001.

Czechowsky, P., and R. Rüster, VHF radar observations of turbulent structures in the polar mesopause region, *Ann. Geophys.*, *15*, 1028–1036, 1997.

Czechowsky, P., R. Rüster, and G. Schmidt, Variations of mesospheric structures in different seasons, *Geophys. Res. Lett.*, *6*, 459–462, 1979.

Czechowsky, P., I. M. Reid, and R. Rüster, VHF radar measurements of the aspect sensitivity of the summer polar mesospaus echoes over Andenes (69°N,16°E), norway, *Geophys. Res. Lett.*, *15*, 1259–1262, 1988.

Dowdy, A., R. A. Vincent, K. Igarashi, Y. Murayama, and D. J. Murphy, A comparison of mean winds and gravity wave activity in the northern and southern MLT, *Geophys. Res. Lett.*, *28*, 1475–1478, 2001.

Driscoll, R. J., and L. A. Kennedy, A model for the spectrum of passive scalars in an isotropic turbulence field, *Phys. Fluids*, *28*, 72–80, 1985.

Ecklund, W. L., and B. B. Balsley, Long-term observations of the arctic mesosphere with the MST radar at Poker Flat, Alaska, *J. Geophys. Res.*, *86*, 7775–7780, 1981.

Fleming, E. L., S. Chandra, J. J. Barnett, and M. Corney, Zonal mean temperature, pressure, zonal wind, and geopotential height as functions of latitude, *Adv. Space Res.*, *10(12)*, 11–59, 1990.

Franke, S. J., J. Röttger, C. LaHoz, and C. H. Liu, Frequency domain interferometry of polar mesosphere summer echoes with the EISCAT VHF radar: a case study, *Radio Sci.*, *27*, 417–428, 1992.

Friedrich, M., and K. M. Torkar, FIRI: A semiempirical model of the lower ionosphere, *J. Geophys. Res.*, *106(A10)*, 21,409–21,418, 2001.

Friedrich, M., K. M. Torkar, E. V. Thrane, and T. A. Blix, Common features of plasma density profiles during NLC, *Adv. Space Res.*, *14(9)*, 161–164, 1994.

Gadsden, M., The north-west europe data on noctilucent clouds: a survey, *J. Atmos. Sol. Terr. Phys.*, *60*, 1163–1174, 1998.

Gadsden, M., and W. Schröder, *Noctilucent clouds*, Springer-Verlag, New York, 1989.

Garcia, R. R., and S. Solomon, A new numerical model of the middle atmosphere 2. ozone and related species, *J. Geophys. Res.*, *99*, 12,937–12,951, 1994.

Gibson, C. H., and W. H. Schwartz, The universal equilibrium spectra of turbulent velocity and scalar fields, *J. Fluid Mech.*, *16*, 365–384, 1963.

Gibson-Wilde, D., J. Werne, D. Fritts, and R. Hill, Direct numerical simulation of VHF radar measurements of turbulence in the mesosphere, *Radio Sci.*, *35*, 783–798, 2000.

Giebeler, J., In-situ Messungen zur Untersuchung der Rolle von Turbulenz bei der Erzeugung von Radarechoes in der polaren Mesosphäre im Sommer, Ph.D. thesis, Universität Bonn, 1995.

Goldberg, R., et al., Dropps: A study of the polar summer mesosphere with rocket, radar and lidar, *Geophys. Res. Lett.*, *28*, 1407–1410, 2001.

Goldberg, R., E. Kopp, G. Witt, and W. Swartz, An overview of NLC-91: A rocket/radar study of the polar summer mesosphere, *Geophys. Res. Lett.*, *20*, 2443–2446, 1993.

Gumbel, J., and G. Witt, Cluster ions and ice particle nucleation: positive feedback at the summer mesopause, *Geophys. Res. Lett.*, *29, doi:10.1029/2002GL015146*, 2002.

Gumbel, J., D. E. Siskind, G. Witt, K. M. Torkar, and M. Friedrich, Influence of ice particles on the ion chemistry of the polar summer mesosphere, *J. Geophys. Res.*, *108(D8), 8436, doi:10.1029/2002JD002413*, 2003.

Hagfors, T., Note on the scattering of electromagnetic waves from charged dust particles in a plasma, *J. Atmos. Terr. Phys.*, *54*, 333–338, 1992.

Havnes, O., U. de Angelis, R. Bingham, C. K. Goertz, G. E. Morfill, and V. Tsytovich, On the role of dust in the summer mesopause, *J. Atmos. Terr. Phys.*, *52*, 637–643, 1990.

Havnes, O., F. Melandsø, C. L. Hoz, T. K. Aslaksen, and T. Hartquist, Charged dust in the Earth's mesopause: Effects on radar backscatter, *Phys. Scr.*, *45*, 535–544, 1992.

Havnes, O., L. I. Næsheim, T. Hartquist, G. E. Morfill, F. Melandsø, B. Schleicher, J. Trøim, T. Blix, and E. Thrane, Meter-scale variations of the charge carried by mesospheric dust, *Planet. Space Sci.*, *44*, 1191–1194, 1996a.

Havnes, O., J. Trøim, T. Blix, W. Mortensen, L. I. Næsheim, E. Thrane, and T. Tønnesen, First detection of charged dust particles in the Earth's mesosphere, *J. Geophys. Res.*, *101*, 10839–10847, 1996b.

Havnes, O., A. Brattli, T. Aslaksen, W. Singer, R. Latteck, T. Blix, E. Thrane, and J. Trøim, First common volume observations of layered plasma structures and polar mesospheric summer echoes by rocket and radar, *Geophys. Res. Lett.*, *28*, 1419–1422, 2001.

Heisenberg, W., Zur statistischen Theorie der Turbulenz, *Z. Physik*, *124*, 628–657, 1948.

Hervig, M., R. Thompson, M. McHugh, L. Gordley, J. Russell III, and M. Summers, First confirmation that water ice is the primary component of polar mesospheric clouds, *Geophys. Res. Lett.*, *28*, 971–974, 2001.

Hill, R. J., Nonneutral and quasi-neutral diffusion of weakly ionized multiconstituent plasma, *J. Geophys. Res.*, *83*, 989–998, 1978.

Hill, R. J., D. E. Gibson-Wilde, J. A. Werne, and D. C. Fritts, Turbulence-induced fluctuations in ionization and application to PMSE, *Earth Plan. Space*, *51*, 499–513, 1999.

Hocking, W., *Target parameter estimation*, pp. 228–268, in: Handbook for MAP volume 30, SCOSTEP, edited by S. Fukao, Urbana, 1989.

Hocking, W. K., Measurement of turbulent energy dissipation rates in the middle atmosphere by radar techniques: A review, *Radio Sci.*, *20*, 1403–1422, 1985.

Hocking, W. K., and J. Röttger, Studies of polar mesosphere summer echoes over EISCAT using calibrated signal strengths and statistical parameters, *Radio Sci.*, *32*, 1425–1444, 1997.

Hocking, W. K., R. Rüster, and P. Czechowsky, Absolute reflectivities and aspect sensitivities of VHF radio waves scatterers measured with the SOUSY radar, *J. Atmos. Terr. Phys.*, *48*, 131–144, 1986.

Hocking, W. K., S. Fukao, M. Yamamoto, T. Tsuda, and S. Kato, Viscosity waves and thermal-conduction waves as a cause of 'specular' reflectors in radar studies of the atmosphere, *Radio Sci.*, *26*, 1281–1303, 1991.

Hoffmann, P., W. Singer, and J. Bremer, Mean seasonal and diurnal variation of PMSE and winds from 4 years of radar observations at ALOMAR, *Geophys. Res. Lett.*, *26*, 1525–1528, 1999.

Hoffmann, P., M. Rapp, R. Latteck, A. Serafimovich, and W. Singer, Multiple layer PMSE structures: Statistical results from six years of PMSE observations and possible physical explanations of their observed properties, *Proceedings of the 16th ESA Symposium on European Rocket and Balloon Programmes and Related Research, St. Gallen, Switzerland (ESA SP–530)*, *315-320*, 2003.

Holzworth, R., et al., Large electric potential perturbations in PMSE during DROPPS, *Geophys. Res. Lett.*, *28*, 1435–1438, 2001.

Hoppe, U.-P., and D. Fritts, On the downward bias in vertical velocity measurements by VHF radars, *Geophys. Res. Lett.*, *22*, 619–622, 1994.

Hoppe, U.-P., and D. C. Fritts, High resolution measurements of vertical velocity with the european incoherent scatter VHF radar 1. motion field characteristics and measurement biases, *J. Geophys. Res.*, *100*, 16,813 – 16,825, 1995.

Hoppe, U.-P., C. Hall, and J. Röttger, First observations of summer polar mesospheric backscatter with a 224 MHz radar, *Geophys. Res. Lett.*, *15*, 28–31, 1988.

Huaman, M. M., M. C. Kelley, W. K. Hocking, and R. F. Woodman, Polar mesosphere summer echo studies at 51.5 MHz at Resolute Bay, Canada: Comparison with Poker Flat results, *Radio Sci.*, *36*, 1823–1837, 2001.

Hunten, D. M., R. P. Turco, and O. B. Toon, Smoke and dust particles of meteoric origin in the mesosphere and stratosphere, *J. Atmos. Sci.*, *37*, 1342–1357, 1980.

Inhester, B., J. Ulwick, J. Cho, M. Kelley, and G. Schmidt, Consistency of rocket and radar electron density observations: implications about the anisotropy of turbulence, *J. Atmos. Terr. Phys.*, *52*, 855–873, 1990.

Inhester, B., J. Klostermeyer, F.-J. Lübken, and U. von Zahn, Evidence for ice clouds causing polar mesosphere summer echoes, *J. Geophys. Res.*, *99*, 20,937–20,954, 1994.

Jensen, E., and G. E. Thomas, A growth-sedimentation model of polar mesospheric clouds: Comparions with SME measurements, *J. Geophys. Res.*, *93*, 2461–2473, 1988.

Jensen, E., and G. E. Thomas, Charging of mesospheric particles: implications of electron density and particle coagulation, *J. Geophys. Res.*, *96*, 18,603–18,615, 1991.

Jensen, E., and G. E. Thomas, Numerical simulations of the effects of gravity waves on noctilucent clouds, *J. Geophys. Res.*, *99*, 3421–3430, 1994.

Jensen, E., G. E. Thomas, and O. B. Toon, On the diurnal variation of noctilucent clouds, *J. Geophys. Res.*, *94*, 14,693–14,702, 1989.

Jesse, O., Auffallende Erscheinungen am Abendhimmel, *Met. Zeit.*, *2*, 311–312, 1885.

Johannessen, A., and D. Krankowsky, Positive ion composition measurement in the upper mesosphere and lower thermosphere at a high latitude during summer, *J. Geophys. Res.*, *77*, 2888–2901, 1972.

Karashtin, A. N., Y. V. S. abd V. I. Abramov, I. F. Belov, V. V. Bychkov, E. B. Eryshev, and G. P. Komrakov, First HF radar measurements of summer mesopause echoes at SURA, *Ann. Geophys.*, *15*, 935–941, 1997.

Kelley, M. C., and J. C. Ulwick, Large- and small-scale organization of electrons in the high-latitude mesosphere: implications of the STATE data, *J. Geophys. Res.*, *93*, 7001–7008, 1988.

Kelley, M. C., D. T. Farley, and J. Röttger, The effect of cluster ions on anomalous VHF backscatter from the summer polar mesosphere, *Geophys. Res. Lett.*, *14*, 1031–1034, 1987.

Kelley, M. C., M. Huaman, C. Y. Chen, C. Ramos, F. Djuth, and E. Kennedy, Polar mesosphere summer observations at HF frequencies using the HAARP Gakona Ionospheric Observatory, *Geophys. Res. Lett.*, *doi: 10.1029/2001GL013411*, 2002.

Kirkwood, S., V. Barabash, P. Chilson, A. Rechou, K. Stebel, P. Espy, G. Witt, and J. Stegman, The 1997 pmse season - its relation to wind, temperature and water vapour, *Geophys. Res. Lett.*, *25*, 1867–1870, 1998.

Kirkwood, S., V. Barabash, E. Belova, H. Nilsson, N. Rao, K. Stebel, A. Osepian, and P. B. Chilson, Polar mesosphere winter echoes during solar proton events, *Adv. Pol. Up. Atmos. Res.*, *16*, 111–125, 2002.

Kirkwood, S., E. Belova, P. Dalin, K. H. Fricke, U. Blum, F. Schmidlin, and R. A. Goldberg, Polar mesosphere winter echoes during MacWave, *Proceedings of the 16th ESA Symposium on European Rocket and Balloon Programmes and Related Research, St. Gallen, Switzerland (ESA SP–530)*, pp. 357–362, 2003.

Klostermeyer, J., A height– and time–dependent model of polar mesosphere summer echoes, *J. Geophys. Res.*, *102*, 6715–6727, 1997.

Klostermeyer, J., On the diurnal variation of polar mesosphere summer echoes, *Geophys. Res. Lett.*, *26*, 3301–3304, 1999a.

Klostermeyer, J., Comparison between observed and computed polar mesosphere summer echoes, *J. Geophys. Res.*, *104*, 11,883–11,890, 1999b.

Kopp, E., P. Eberhardt, U. Herrmann, and L. Björn, Positive ion composition of the high latitude summer D-region with noctilucent clouds, *J. Geophys. Res.*, *90*, 13041–13051, 1985.

Körner, U., and G. Sonnemann, Global 3d-modelling of the water vapor concentration of the mesosphere/mesopause region and implications with respect to the NLC region, *J. Geophys. Res.*, *106*, 9639–9651, 2001.

Latteck, R., W. Singer, and H. Bardey, The ALWIN MST radar: technical design and performance, *Proceedings of the 14th ESA Symposium on European Rocket and Balloon Programmes and Related Research, Potsdam, Germany (ESA SP–437)*, pp. 179 – 184, 1999a.

Latteck, R., W. Singer, and J. Höffner, Mesosphere summer echoes as observed by VHF radar at Kühlungsborn, *Geophys. Res. Lett.*, *26*, 1533–1536, 1999b.

Leslie, R. J., Sky glows, *Nature*, *33*, 245, 1885.

Lie-Svendsen, O., T. A. Blix, U. Hoppe, and E. Thrane, Modelling the plasma response to small-scale particle perturbations in the mesopause region, *J. Geophys. Res.*, *108(D8), 8442, doi: 10.1029/2002JD002753*, 2003.

Lübken, F., W. Hillert, G. Lehmacher, and U. von Zahn, Experiments revealing small impact of turbulence on the energy budget of the mesosphere and lower thermosphere, *J. Geophys. Res.*, *98*, 20,369–20,384, 1993a.

Lübken, F.-J., On the extraction of turbulent parameters from atmospheric density fluctuations, *J. Geophys. Res.*, *97*, 20,385–20,395, 1992.

Lübken, F.-J., Seasonal variation of turbulent energy dissipation rates at high latitudes as determined by insitu measurements of neutral density fluctuations, *J. Geophys. Res.*, *104*, 13,441–13,456, 1997.

Lübken, F.-J., Thermal structure of the Arctic summer mesosphere, *J. Geophys. Res.*, *104*, 9135–9149, 1999.

Lübken, F.-J., and M. Rapp, Modelling of particle charging in the polar summer mesosphere: Part 2 – application to measurements, *J. Atmos. Sol. Terr. Phys.*, *63*, 771–780, 2001.

Lübken, F.-J., G. Lehmacher, T. Blix, U.-P. Hoppe, E. Thrane, J. Cho, and W. Swartz, First in-situ observations of neutral and plasma density fluctuations within a PMSE layer, *Geophys. Res. Lett.*, *20*, 2311–2314, 1993b.

Lübken, F.-J., M. Rapp, T. Blix, and E. Thrane, Microphysical and turbulent measurements of the Schmidt number in the vicinity of polar mesosphere summer echoes, *Geophys. Res. Lett.*, *25*, 893–896, 1998.

Lübken, F.-J., M. J. Jarvis, and G. O. L. Jones, First insitu temperature measurements at the Antarctic summer mesopause, *Geophys. Res. Lett.*, *26*, 3581–3584, 1999.

Lübken, F.-J., M. Rapp, and P. Hoffmann, Neutral air turbulence and temperatures in the vicinity of polar mesosphere summer echoes, *J. Geophys. Res.*, *107(D15), doi:10.1029/2001JD000915*, 2002.

Lübken, F.-J., M. Zecha, J. Höffner, and J. Röttger, Temperatures, polar mesosphere summer echoes, and noctlilucent clouds over Spitsbergen (78°N), *J. Geophys. Res.*, *submitted*, 2003.

Marti, J., and K. Mauersberger, A survey and new measurements of ice vapor pressure at temperatures between 170 and 250 K, *Geophys. Res. Lett.*, *20*, 363–366, 1993.

Mauersberger, K., and D. Krankowsky, Vapor pressure above ice at temperatures below 170 K, *Geophys. Res. Lett.*, *30(3), 1121, doi:10.1029/2002GL016183*, 2003.

McHugh, M., M. Hervig, B. Magill, R. E. Thompson, E. Remsberg, J. Wrotny, and J. Russell III, Improved mesospheric temperature, water vapor and polar mesospheric cloud extinctions from HALOE, *Geophys. Res. Lett.*, *30(8), 1440, doi:10.1029/2002GL016859*, 2003.

Mitchell, J., C. Croskey, and R. Goldberg, Evidence for charged aerosol particles and associated meter-scale structure in identified PMSE/NLC regions, *Geophys. Res. Lett.*, *28*, 1423–1426, 2001.

Mitchell, J. D., C. L. Croskey, R. A. Goldberg, and M. Friedrich, Charged particles in the polar mesopause region: probe measurements from the MaCWAVE and DROPPS programs, *Proceedings of the 16th ESA Symposium on European Rocket and Balloon Programmes and Related Research, St. Gallen, Switzerland (ESA SP–530)*, pp. 351–356, 2003.

Mlynczak, M. G., A contemporary assessment of the mesospheric energy bugget, *Geophys. Monogr. Ser.*, *123*, 37–52, 2000.

Müllemann, A., M. Rapp, and F.-J. Lübken, Morphology of turbulence in the polar summer mesopause region during the MIDAS/SOLSTICE campaign 2001, *Adv. Space Res.*, *31(9)*, 2069–2074, 2003.

Natanson, G. L., On the theory of the charging of amicroscopic aerosol particles as a result of capture of gas ions, *Sov. Phys. Tech. Phys. (engl. Transl.)*, *5*, 538–551, 1960.

Nussbaumer, V., K.-H. Fricke, M. Langer, W. Singer, and U. von Zahn, First simultaneous and common-volume observations of NLC and PMSE by lidar and radar, *J. Geophys. Res.*, *101*, 19161–19167, 1996.

Pedersen, A., J. Troim, and J. Kane, Rocket measurement showing removal of electrons above the mesopause in summer at high latitudes, *Planet. Space Sci.*, *18*, 945–947, 1969.

Pfaff, R., et al., Rocket probe observations of electric field irregulatities in the polar summer mesosphere, *Geophys. Res. Lett.*, *28*, 1431–1434, 2001.

Ramaswamy, V., et al., Stratospheric temperature trends: observations and model simulations, *Rev. Geophys.*, *39*, 71–122, 2001.

Rapp, M., Capture rates of electrons and positive ions by mesospheric aerosol particles, *J. Aerosol Sci.*, *31*, 1367–1369, 2000.

Rapp, M., and F.-J. Lübken, Modelling of positively charged aerosols in the polar summer mesopause region, *Earth Plan. Space*, *51*, 799–807, 1999.

Rapp, M., and F.-J. Lübken, Electron temperature control of PMSE, *Geophys. Res. Lett.*, *27*, 3285–3288, 2000.

Rapp, M., and F.-J. Lübken, Modelling of particle charging in the polar summer mesosphere: Part 1 – general results, *J. Atmos. Sol. Terr. Phys.*, *63*, 759–770, 2001.

Rapp, M., and F.-J. Lübken, On the nature of PMSE: Electron diffusion in the vicinity of charged particles revisited, *J. Geophys. Res.*, *108(D8), 8437, doi:10.1029/2002JD002857*, 2003a.

Rapp, M., and F.-J. Lübken, Comment on "The response time of PMSE to ionospheric heating" by Belova et al., *J. Geophys. Res.*, *108(D23), 4727, doi:10.1029/2003JD003638*, 2003b.

Rapp, M., J. Gumbel, and F.-J. Lübken, Absolute density measurements in the middle atmosphere, *Ann. Geophys.*, *19*, 571–580, 2001.

Rapp, M., J. Gumbel, F.-J. Lübken, and R. Latteck, D-region electron number density limits for the existence of polar mesosphere summer echoes, *J. Geophys. Res.*, *107(D14), doi:10.1029/2001JD001323*, 2002a.

Rapp, M., F.-J. Lübken, A. Müllemann, G. E. Thomas, and E. J. Jensen, Small scale temperature variations in the vicinity of NLC: Experimental and model results, *J. Geophys. Res.*, *107(D19), doi:10.1029/2001JD001241*, 2002b.

Rapp, M., F.-J. Lübken, and T. A. Blix, Small scale density variations of electrons and charged particles in the vicinity of polar mesosphere summer echoes, *Atmos. Chem. Phys.*, *3*, 1399–1407, 2003a.

Rapp, M., F.-J. Lübken, and T. A. Blix, The role of charged ice particles for the creation of PMSE: a review of recent developments, *Adv. Space Res.*, *31(9)*, 2033–2043, 2003b.

Rapp, M., F.-J. Lübken, P. Hoffmann, R. Latteck, G. Baumgarten, and T. A. Blix, PMSE dependence on aerosol charge number density and aerosol size, *J. Geophys. Res.*, *108(D8), 8450, doi:10.1029/2002JD002650*, 2003c.

Rapp, M., B. Strelnikov, S. Wilms, F.-J. Lübken, J. Gumbel, and H. Henkel, A new detector for the in situ measurement of meteoric dust particles in the middle atmosphere, *Proceedings of the 16th ESA Symposium on European Rocket and Balloon Programmes and Related Research, St. Gallen, Switzerland (ESA SP–530)*, pp. 379–384, 2003d.

Reid, G. C., Ice particles and electron "bite-outs" at the summer polar mesopause, *J. Geophys. Res.*, *95*, 13,891–13,896, 1990.

Reid, I. M., P. Czechowsky, R. Rüster, and G. Schmidt, First VHF radar measurements of mesopause summer echoes at mid-latitudes, *Geophys. Res. Lett.*, *16*, 135–138, 1989.

Rietveld, M. T., H. Kopka, and P. Stubbe, D-region characteristics deduced from pulsed ionospheric heating under auroral electrojet conditions, *J. Atmos. Terr. Phys.*, *45*, 311–326, 1986.

Roble, R. G., and R. E. Dickinson, How will changes in carbon dioxide and methane modify the mean structure of the mesosphere and thermosphere?, *Geophys. Res. Lett.*, *16*, 1441–1444, 1989.

Röttger, J., Observations of the polar D-region and the mesosphere with the EISCAT Svalbard Radar and the SOUSY Svalbard Radar, *Mem. Nat. Inst. Pol. Res.,, 54*, 9 – 20, 2001.

Röttger, J., and C. LaHoz, Characteristics of polar mesosphere summer echoes (PMSE) observed with the EISCAT 224 MHz radar and possible explanations of their origin, *J. Atmos. Terr. Phys.*, *52*, 893–906, 1990.

Röttger, J., C. L. Hoz, M. C. Kelley, U.-P. Hoppe, and C. Hall, The structure and dynamics of polar mesosphere summer echoes observed with the EISCAT 224 MHz radar, *Geophys. Res. Lett.*, *15*, 1353–1356, 1988.

Röttger, J., M. T. Rietveld, C. LaHoz, C. Hall, M. C. Kelley, and W. Swartz, Polar mesosphere summer echoes observed with the EISCAT 933-MHz radar and the CUPRI 46.9MHz radar, their similarity to 224 MHz radar echoes and their relation to turbulence and electron density profiles, *Radio Sci.*, *25*, 671–687, 1990.

Røyrvik, O., and L. G. Smith, Comparison of mesospheric VHF radar echoes and rocket probe electron concentration measurements, *J. Geophys. Res.*, *89*, 9014–9022, 1984.

Rüster, R., P. Czechnowsky, P. Hoffmann, and W. Singer, Gravity wave signatures at mesopause heights, *Ann. Geophys.*, *14*, 1186–1191, 1996.

Rüster, R., J. Röttger, G. Schmidt, P. Czechowski, and J. Klostermeyer, Observation of mesospheric summer echoes at VHF in the polar cap region, *Geophys. Res. Lett.*, *28*, 1471–1474, 2001.

Schmidlin, F. J., The inflatable sphere: A technique for the accurate measurement of middle atmosphere temperatures, *J. Geophys. Res.*, *96*, 22,673–22,682, 1991.

Seele, C., and P. Hartogh, Water vapor of the polar middle atmosphere: Annual variation and summer mesosphere conditions as observed by ground-based microwave spectroscopy, *Geophys. Res. Lett.*, *26*, 1517–1520, 1999.

Singer, W., D. Keuer, P. Hoffmann, P. Czechowsky, and G. Schmidt, The ALOMAR-SOUSY-radar: technical design and further developments, *Proceedings of the 12th ESA Symposium on European Rocket and Balloon Programmes and Related Research, Lillehammer, Norway (ESA SP–370)*, pp. 409–415, 1995.

Siskind, D. E., S. D. Eckermann, J. P. Cormack, M. J. Alexander, and J. T. Backmeister, Hemispheric differences in the temperature of the summertime stratosphere and mesosphere, *J. Geophys. Res., 108(D2), 4051, doi:10.1029/2002JD002095*, 2003.

Smiley, B., S. Robertson, M. Horanyi, T. Blix, M. Rapp, R. Latteck, and J. Gumbel, Measurement of negatively and positively charged particles inside PMSE during MIDAS SOLSTICE 2001, *J. Geophys. Res., 108(D8), 8444, doi: 10.1029/2002JD002425*, 2003.

Strelnikov, B., M. Rapp, and F.-J. Lübken, A new technique for the analysis of neutral air density fluctuations measured in situ in the middle atmosphere, *Geophys. Res. Lett., 30(20), 2052, doi:10.1029/2003GL018271*, 2003.

Swartz, W., J. Cho, and C. Miller, CUPRI system configuration for NLC-91 and observations of PMSE during Salvo A, *Geophys. Res. Lett.*, *20*, 2287–2290, 1993.

Tatarskii, V. I., *The Effects of the Turbulent Atmosphere on Wave Propagation*, Isr. Program for Sci. Transl., Jerusalem, 1971.

Thayer, J. P., M. Rapp, A. J. Gerrard, E. Gudmundssson, and T. J. Kane, Gravity-wave influences on Arctic mesospheric clouds as determined by a rayleigh lidar at sondrestrom, greenland, *J. Geophys. Res., 108(D8), 8449, doi:10.1029/2002JD002363*, 2003.

Thomas, G. E., Mesopheric clouds and the physics of the mesopause region, *Rev. Geophys, 29*, 553–575, 1991.

Thomas, G. E., Is the polar mesosphere the miner's canary of global change?, *Adv. Space Res., 18(3)*, 149–158, 1996.

Thomas, G. E., J. J. Olivero, E. J. Jensen, W. Schröder, and O. B. Toon, Relation between increasing methane and the presence of ice clouds at the mesopause, *Nature, 338*, 490–492, 1989.

Thomas, G. E., J. J. Olivero, M. DeLand, and E. P. Shettle, A response to the article by U. von Zahn, "Are noctilucent clouds truly a miner's canary of global change?", *Eos, Transactions, American Geophysical Union, 84(36)*, 352–353, 2003.

Thomas, L., I. Astin, and I. T. Prichard, The characteristics of VHF echoes from the summer mesopause region at mid-latitudes, *J. Atmos. Terr. Phys., 54*, 969–977, 1992.

Toon, O. B., R. P. Turco, D. Westphal, R. Malone, and M. S. Liu, A multidimensional model for aerosols: description and computational analogs, *J. Atmos. Sci., 45*, 2123–2143, 1988.

Trakhtengerts, V. Y., Generation mechanism of polar mesosphere summer echoes, *J. Geophys. Res., 99*, 21,083–21088, 1994.

Trakhtengerts, V. Y., and A. G. Demekhov, Nonequilibrium electron density fluctuations and wave scattering in the mesosphere, *J. Atmos. Terr. Phys., 57*, 1153–1164, 1995.

Turco, R. P., O. B. Toon, R. C. Whitten, R. G. Keesee, and D. Hollenbach, Noctilucent clouds: Simulation studies of their genesis, properties and global influences, *Planet. Space Sci., 3*, 1147–1181, 1982.

Ulwick, J. C., K. D. Baker, M. C. Kelley, B. B. Balsley, and W. L. Ecklund, Comparison of simultaneous MST radar and electron density probe measurements during STATE, *J. Geophys. Res., 93*, 6989–7000, 1988.

Ulwick, J. C., M. C. Kelley, C. Alcala, T. Blix, and E. V. Thrane, Evidence for two different structuring and scattering mechanisms and the associated role of aerosols in the polar summer mesosphere, *Geophys. Res. Lett., 20*, 2307–2310, 1993.

von Cossart, G., J. Fiedler, and U. von Zahn, Size distributions of NLC particles as determined from 3-color observations of NLC by ground-based lidar, *Geophys. Res. Lett., 26*, 1513–1516, 1999.

von Zahn, U., Are noctilucent clouds truly a "miner's canary" of global change?, *Eos, Transactions, American Geophysical Union, 84(28)*, 261–268, 2003.

von Zahn, U., and U. Berger, Persistent ice cloud in the midsummer upper mesosphere at high latitudes: three-dimensional modeling and cloud interactions with ambient water vapor, *J. Geophys. Res., 108(D8), 8451, doi:10.1029/2002JD002409*, 2003.

von Zahn, U., and J. Bremer, Simultaneous and common-volume observations of noctilucent clouds and polar mesosphere summer echoes, *Geophys. Res. Lett.*, *26*, 1521–1524, 1999.

von Zahn, U., G. von Cossart, J. Fiedler, and D. Rees, Tidal variations of noctilucent clouds measured at 69° latitude by groundbased lidar, *Geophys. Res. Lett.*, *25*, 1289–1292, 1998.

von Zahn, U., G. von Cossart, J. Fiedler, K. Fricke, G. Nelke, G. Baumgarten, D. Rees, A. Hauchecorne, and K. Adolfsen, The ALOMAR Rayleigh/Mie/Raman lidar: Objectives, configuration, and performance, *Ann. Geophys.*, *18*, 815 – 833, 2000.

Widdel, H. U., Foil chaff clouds as a tool for in-situ measurements of atmospheric motions in the middle atmosphere: their flight behaviour and implications for radar tracking, *J. Atmos. Terr. Phys.*, *52*, 89–101, 1990.

Woodman, R. F., and A. Guillen, Radar observations of winds and turbulence in the stratosphere and mesosphere, *J. Atmos. Sci.*, *31*, 493–505, 1974.

Woodman, R. F., B. B. Balsley, F. Aquino, L. Flores, E. Vazquez, M. Sarango, M. Huaman, and H. Soldi, First observations of pmse in antarctica, *J. Geophys. Res.*, *104*, 22,577–22,590, 1999.

Woods, J. D., V. Högström, P. Misme, H. Ottersten, and O. M. Phillips, Fossil turbulence, *Radio Sci.*, *4*, 1365–1367, 1969.

Zadorozhny, A. M., A. A. Tyutin, G. Witt, N. Wilhelm, U. Wälchli, J. Cho, and W. E. Swartz, Electric field measurements in the vicinity of noctilucent clouds and PMSE, *Geophys. Res. Lett.*, *20*, 2299–2302, 1993.

Zadorozhny, A. M., A. A. Vostrikov, G. Witt, , O. A. Bragin, D. Y. Dubov, V. G. Kazakov, V. N. Kikhtenko, and A. A. Tyutin, Laboratory and in situ evidence for the presence of ice particles in a PMSE region, *Geophys. Res. Lett.*, *24*, 841–844, 1997.

Zecha, M., J. Röttger, W. Singer, P. Hoffmann, and D. Keuer, Scattering properties of PMSE irregularities and refinement of velocity estimates, *J. Atmos. Sol. Terr. Phys.*, *63*, 201–214, 2001.

Zecha, M., J. Bremer, R. Latteck, and W. Singer, Properties of midlatitude mesosphere summer echoes after three seasons of VHF radar observations at 54°N, *J. Geophys. Res.*, *108(D8), 8439, doi:10.1029/2002JD002442*, 2003.

A List of included publications

This thesis summarizes the following publications:

- **Paper 1** (Appendix B: page 1)
  Rapp, M., F.-J. Lübken, A. Müllemann, G. E. Thomas, and E. J. Jensen, Small scale temperature variations in the vicinity of NLC: Experimental and model results, *J. Geophys. Res.*, *107(D19), doi:10.1029/2001JD001241*, 2002

- **Paper 2** (Appendix B: page 22)
  Rapp, M., J. Gumbel, F.-J. Lübken, and R. Latteck, D-region electron number density limits for the existence of polar mesosphere summer echoes, *J. Geophys. Res.*, *107(D14), doi:10.1029/2001JD001323*, 2002

- **Paper 3** (Appendix B: page 38)
  Blix, T. A., M. Rapp, and F.-J. Lübken, Relations between small scale electron number density fluctuations, radar backscatter and charged aerosol particles, *J. Geophys. Res.*, *108(D8), 8450, doi:10.1029/2002JD002430*, 2003

- **Paper 4** (Appendix B: page 49)
  Rapp, M., F.-J. Lübken, P. Hoffmann, R. Latteck, G. Baumgarten, and T. A. Blix, PMSE dependence on aerosol charge number density and aerosol size, *J. Geophys. Res.*, *108(D8), 8450, doi:10.1029/2002JD002650*, 2003

- **Paper 5** (Appendix B: page 62)
  Lübken, F.-J., M. Rapp, and P. Hoffmann, Neutral air turbulence and temperatures in the vicinity of polar mesosphere summer echoes, *J. Geophys. Res.*, *107(D15), doi:10.1029/2001JD000915*, 2002

- **Paper 6** (Appendix B: page 73)
  Müllemann, A., M. Rapp, and F.-J. Lübken, Morphology of turbulence in the polar summer mesopause region during the MIDAS/SOLSTICE campaign 2001, *Adv. Space Res.*, *31(9)*, 2069–2074, 2003

- **Paper 7** (Appendix B: page 80)
  Rapp, M., and F.-J. Lübken, On the nature of PMSE: Electron diffusion in the vicinity of charged particles revisited, *J. Geophys. Res.*, *108(D8), 8437, doi:10.1029/2002JD002857*, 2003

- **Paper 8** (Appendix B: page 94)
  Rapp, M., F.-J. Lübken, and T. A. Blix, The role of charged ice particles for the creation of PMSE: a review of recent developments, *Adv. Space Res.*, *31(9)*, 2033–2043, 2003

- **Paper 9** (Appendix B: page 106)
  Rapp, M., F.-J. Lübken, and T. A. Blix, Small scale density variations of electrons and charged particles in the vicinity of polar mesosphere summer echoes, *Atmos. Chem. Phys.*, *3*, 1399–1407, 2003

- **Paper 10** (Appendix B: page 116)
  Rapp, M., and F.-J. Lübken, Electron temperature control of PMSE, *Geophys. Res. Lett.*, *27*, 3285–3288, 2000

- **Paper 11** (Appendix B: page 121)
  Rapp, M., and F.-J. Lübken, Comment on "The response time of PMSE to ionospheric heating" by Belova et al., *J. Geophys. Res.*, *108(D23), 4727, doi:10.1029/2003JD003638*, 2003

- **Paper 12** (Appendix B: page 126)
  Hoffmann, P., M. Rapp, R. Latteck, A. Serafimovich, and W. Singer, Multiple layer PMSE structures: Statistical results from six years of PMSE observations and possible physical explanations of their observed properties, *Proceedings of the 16th ESA Symposium on European Rocket and Balloon Programmes and Related Research, St. Gallen, Switzerland (ESA SP–530)*, *315-320*, 2003

B Copies of included publications